



Energy Fuels Resources (USA) Inc.  
225 Union Blvd. Suite 600  
Lakewood, CO, US, 80228  
303 974 2140  
[www.energyfuels.com](http://www.energyfuels.com)

December 7, 2012

**VIA PDF AND OVERNIGHT DELIVERY**

Mr. Rusty Lundberg  
Division of Radiation Control  
Utah Department of Environmental Quality  
195 North 1950 West  
P.O. Box 144850  
Salt Lake City, UT 84114-4820

**Re: Transmittal of Pyrite Investigation Report  
White Mesa Mill Utah Ground Water Quality Discharge Permit UGW370004**

Dear Mr. Lundberg:

Enclosed are two copies of Energy Fuels Resources (USA) Inc.'s ("EFRI's") Investigation of Pyrite in the Perched Zone, White Mesa Mill (the "Report"). The pyrite investigation and this Report were prepared in accordance with the Pyrite Analysis Plan described in Section 3.2 of EFRI's *Plan to Investigate pH Exceedances in Perched Groundwater Monitoring Wells, White Mesa Mill*, to address dual exceedances in pH at 10 monitoring wells at the site and to explain the overall decline in pH observed at the Mill site.

This transmittal includes two hard copies and two CDs each containing a word searchable electronic copy in pdf format of the report.

If you should have any questions regarding this report please contact me.

Yours very truly,

A handwritten signature in blue ink that reads "Jo Ann Tischler".

**ENERGY FUELS RESOURCES (USA) INC.**  
Jo Ann Tischler  
Director, Compliance

cc: Dan Erskine, INTERA  
David C. Frydenlund  
Dan Hillsten  
Harold R. Roberts  
David E. Turk  
Katherine A. Weinell  
Central Files



**INVESTIGATION OF PYRITE IN THE PERCHED ZONE  
WHITE MESA URANIUM MILL SITE**

**BLANDING, UTAH**

December 7, 2012

*Prepared for:*

**ENERGY FUELS RESOURCES (USA) INC.**

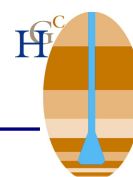
225 Union Boulevard, Suite 600  
Lakewood, Colorado 80228  
(303) 974-2140

*Prepared by:*

**HYDRO GEO CHEM, INC.**

51 W. Wetmore, Suite 101  
Tucson, Arizona 85705-1678  
(520) 293-1500

Project Number 7180000.00-02.0



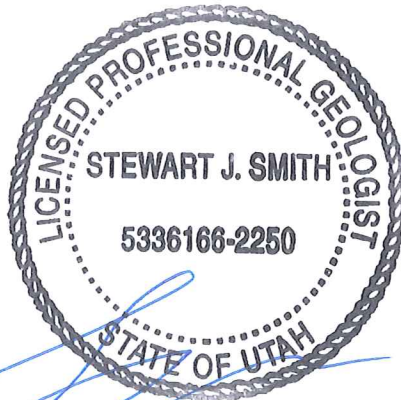


**INVESTIGATION OF PYRITE IN THE  
PERCHED ZONE  
WHITE MESA URANIUM MILL SITE  
  
BLANDING, UTAH**

Prepared for:  
**ENERGY FUELS RESOURCES (USA) INC.**  
225 Union Boulevard, Suite 600  
Lakewood, Colorado 80228

(303) 974-2140

Prepared by:



Stewart J. Smith, R.G.

Utah Registration Number 5336166-2250

December 7, 2012



# TABLE OF CONTENTS

1.	INTRODUCTION .....	1
2.	BACKGROUND .....	5
2.1	Pyrite Occurrence as Described in Site Boring Logs.....	5
2.2	Site Geology and Pyrite Occurrence in the Dakota and Burro Canyon Formations Near the Site .....	5
2.2.1	Overview of Site Geology .....	6
2.2.2	Burro Canyon Formation .....	7
2.2.3	Dakota Sandstone.....	7
2.2.4	Mancos Shale .....	7
2.2.5	Pyrite Occurrence in the Dakota Sandstone and Burro Canyon Formation .....	9
2.3	Pyrite Oxidation as a Potential Mechanism for Decreasing pH .....	10
2.3.1	Pyrite Oxidation in the Perched Zone at the Site .....	11
2.3.2	Pyrite (and Other Sulfide) Oxidation in Other Aquifers.....	14
3.	METHODOLOGY .....	15
3.1	Sample Collection and Screening Procedures .....	15
3.1.1	Sample Collection.....	15
3.1.2	Sample Screening.....	16
3.2	Laboratory Analysis.....	17
3.2.1	Visual Identification.....	17
3.2.2	Quantitative Analysis.....	17
4.	RESULTS .....	19
4.1	Visual Identification and Analysis.....	19
4.2	Quantitative Analysis.....	19
4.3	Implications for Pyrite Oxidation as the Mechanism for Decreasing pH in the Perched Zone at the Site.....	20
4.3.1	Calculation of Pyrite Concentrations Over the Saturated Thicknesses ....	21
4.3.2	Screening Level Calculations .....	22
4.3.2.1	MW-3A .....	23
4.3.2.2	MW-24.....	24
4.3.2.3	MW-27.....	25
4.3.3	Effect of Dissolved Carbonate Species on pH Change.....	26
4.3.4	Preliminary PHREEQC Simulations .....	28
4.3.4.1	MW-3A .....	29
4.3.4.2	MW-24.....	30
4.3.4.3	MW-27.....	30
4.3.5	Impact of Carbonate Species .....	30
4.4	Implications for Natural Attenuation of Nitrate via Reduction by Pyrite.....	31

## TABLE OF CONTENTS (Continued)

5.	CONCLUSIONS.....	33
6.	REFERENCES .....	39
7.	LIMITATIONS STATEMENT .....	43

### TABLES

1	Tabulation of Presence of Pyrite, Iron Oxide, and Carbonaceous Fragments in Drill Logs
2	Results of Sample Screening Using Portable XRF
3	Sulfide Analysis by Optical Microscopy
4	Results of XRD and Sulfur Analysis in Weight Percent
5	Summary of Pyrite in Drill Cuttings and Core

### FIGURES

1	Kriged 3 <sup>rd</sup> Quarter, 2012 Water Levels, White Mesa Site
2	Lithologic Column
3	Extent of the Western Interior Sea (Cretaceous)
4	White Mesa Site Plan Showing Pyrite Occurrence in Perched Borings

### APPENDICES

A	Photographs of Samples Submitted for Analysis
B	Laboratory Analytical Reports
C	PHREEQC Output Tables 1 through 6

## 1. INTRODUCTION

This report describes an investigation into the occurrence of pyrite in the perched water zone at the White Mesa Uranium Mill (the Mill or the site) located near Blanding, Utah, based on the Pyrite Analysis Plan (the Plan) described in Section 3.2 of HGC (2012). HGC (2012) was prepared to address dual exceedances of pH in ten perched groundwater monitoring wells at the Mill and to provide information related to the overall decline in groundwater pH that has been observed in site wells. The “Source Assessment Report”, INTERA (2012a), addresses parameters other than pH in out-of-compliance status based on two successive exceedances of their respective GWCLs, as committed to in Section 3.1 of HGC (2012), and proposes revised GWCLs for these parameters. The “pH Report White Mesa Uranium Mill”, INTERA (2012b) analyzes trends in pH and other site indicator parameters and proposes revised pH GWCLs for wells in out of compliance status for pH.

As discussed in both of the preceding reports, the evaluations of exceedances of GWCLs indicate they are:

1. due to a number of contributing factors unrelated to Mill operations, and
2. may be expected to continue due to those factors in a number of wells.

As discussed in the preceding reports and in this document, the contributing factors may be expected to affect additional wells in the near future.

This document evaluates and quantifies the presence of pyrite throughout the Mill site, and identifies and quantifies the mechanism by which it contributes to the sitewide decline in pH, and, therefore, concentrations of pH-sensitive analytes in perched groundwater.

As discussed in the Plan and INTERA (2012b) the pH decline has been noted in perched wells located upgradient, cross-gradient, and downgradient of the millsite and tailings cells. Factors that may affect wells that are out of compliance (“OOC”) for pH include:

1. The generally low rates of groundwater movement due to the generally low permeability of the perched zone,
2. The generally low productivity of perched wells due to the low permeability of the perched zone,
3. Rising water levels in the northeastern portion of the site resulting from seepage from the wildlife ponds, and

4. The presence of pyrite in the perched zone, combined with the introduction of oxygen into the vadose and/or saturated zones as a result of the introduction of surface water from the wildlife ponds into the perched zone, rising water levels in the perched zone, and activities (well installation, redevelopment and increased monitoring frequency) associated with the groundwater monitoring program.

The generally low productivity of perched wells at the site results in large fluctuations in water levels within and near the wells during routine purging and sampling activities. The overall impact of purging and sampling increased in 2005 when sampling activities at the site increased due to the addition of monitoring wells, increased purging activity, and the acceleration of monitoring in a number of wells from quarterly to monthly. Low productivity exacerbated water level fluctuations resulting from the recent redevelopment effort during the latter half of 2010 and first half of 2011 (HGC, 2011). The redevelopment effort was aggressive and included surging, bailing, and overpumping of the wells.

The pH decline may have any number of causes; however, the widespread nature of the declining pH indicates that, whether recent or longer-term, it results from a natural phenomenon unrelated to Mill operations. This conclusion is supported by findings discussed in Section 4.

Oxidation of pyrite by dissolved oxygen within the Dakota Sandstone and Burro Canyon Formations, which host the perched water at the site, is a likely mechanism for the decreasing pH measured in perched zone wells because it releases acid and sulfate. The widespread occurrence of visible pyrite in the Burro Canyon Formation and Dakota Sandstone (upgradient, cross-gradient, and downgradient of the millsite and tailings cells) makes this mechanism plausible both for the reduction of pH and the increasing trends in sulfate in some wells observed at the Mill site.

Perched water will be made more acidic by oxidation of pyrite within the saturated zone in the presence of oxygen. Sources of oxygen include 1) diffusion through the vadose zone aided by barometric pumping and the generally dry condition of the vadose zone, 2) transport of oxygen from the surface directly to the formation via perched monitoring well casings (also aided by barometric pumping), 3) infiltration of water containing dissolved oxygen and 4) groundwater rising into a relatively oxygen-rich vadose zone and mixing with oxygen-rich pore waters.

Perched water will also become more acidic if it mixes with vadose pore waters made acidic by pyrite oxidation. The correlation of pH decline with rising water levels (INTERA, 2012b) could result from three mechanisms: 1) mixing of perched groundwater with relatively acidic vadose pore waters, 2) oxygen transport via groundwater to relatively anoxic vadose areas containing pyrite, or 3) increased oxygen transport to perched groundwater as it rises into a relatively oxygen-rich vadose zone.

Oxygen transport to groundwater in the vicinities of perched wells is enhanced by fluctuations in the perched water table caused by routine purging and sampling of wells, the aggressive well redevelopment effort during the latter half of 2010 and the first half of 2011, and changes in pumping at chloroform extraction wells MW-4, MW-26, TW4-4, TW4-19, and TW4-20. Increasing the number of monitoring wells and increasing the sampling frequency of MW-series wells in 2005, as a result of the expansion of the groundwater monitoring program associated with the Mill's Groundwater Discharge Permit (and resulting accelerated monitoring in a number of wells), increased oxygen transport to groundwater. Each time a well is purged for sampling purposes the water column in the well and the water level in the formation near the well will fluctuate, increasing the mixing of air containing oxygen into the groundwater. Therefore, oxygen transport in the vicinities of older wells at the site is expected to have increased since 2005 as a result of increased sampling frequency. Increased oxygen transport will also have resulted from the recent redevelopment effort which resulted in large fluctuations in water levels in and near the wells as a consequence of surging, bailing, and overpumping.

Significant sources of infiltrating water containing oxygen include the wildlife ponds. Another (past) source of potentially oxygen-laden infiltration is the historic pond (discussed in INTERA, 2009.) The persistence of chloroform and nitrate in the chloroform plume originating from two former leach fields (described in HGC, 2007) and the persistence of nitrate in a nitrate/chloride plume associated with the historic pond (described in INTERA, 2009) are consistent with primarily oxidizing conditions.

Enhanced oxygen transport into the vadose zone in the vicinities of perched wells having screens extending above the water table is also an important mechanism. Oxygen-laden air within the well casings will diffuse into the vadose zone via the unsaturated portions of the screens and move radially in all directions away from the well screens including upgradient with respect to perched groundwater flow. The process will be aided by barometric pumping and the fact that the diffusion coefficient for oxygen in air is approximately four orders of magnitude higher than its diffusion coefficient in water (on the order of 0.1 centimeters squared per second ( $\text{cm}^2/\text{s}$ ) in air vs  $10^{-5}$   $\text{cm}^2/\text{s}$  in water). The resulting enhanced vadose concentrations of oxygen near the wells will be available to react with the vadose formation and pore waters and to dissolve in groundwater near and upgradient of the wells. The generally low rates of perched water movement increase the residence time of groundwater in contact with oxygenated vadose areas near the wells, increasing oxygen transport to groundwater. The availability of air supplying oxygen in the vadose zone is particularly important because the oxygen content of air on a mass basis is approximately 30 times higher than the maximum amount of oxygen that can be dissolved in groundwater. Therefore vadose oxygen constitutes a large reservoir of oxygen available to dissolve in groundwater.

Furthermore, the correlation between pH decrease and increasing water levels in many of the site wells (INTERA, 2012b) is consistent with pH decline resulting from pyrite oxidation via one of three mechanisms. The first mechanism involves the rise of oxygen-bearing groundwater into relatively anoxic vadose pyritic materials resulting in increased pyrite oxidation and a decrease in pH. This is expected to be particularly important near the wildlife ponds where seepage of oxygen-laden water into the perched zone is occurring and increases in water levels due to seepage are large. The second and more important mechanism involves the rise of groundwater into vadose pore waters that have been made acidic as a result of pyrite oxidation. Oxidation of pyrite in the vadose zone (where oxygen is likely to be more abundant than in the saturated zone) is consistent with Shawe (1976) who noted that most detected pyrite was below the water table and the vadose zone contained iron oxide after pyrite. The third mechanism involves the rise of perched groundwater into an oxygen-rich vadose zone. The rise of groundwater into an oxygen-rich vadose zone will also increase oxygen content of the groundwater thereby increasing pyrite oxidation. Diffusion of oxygen into the vadose zone, where it is available to react with pyrite and pore waters, is expected to be enhanced in the vicinities of perched wells having screens extending above the water table, thereby enhancing the above mechanisms. All wells that are out of compliance (OOC) for pH have screens extending above the water table (wells MW-3, MW-3A, MW-12, MW-14, MW-23, MW-24, MW-25, MW-26, MW-28, MW-29, and MW-32).

The primary purpose of the Plan and this evaluation and Report is to verify the presence of pyrite as one of the possible causes of the decrease in pH. Existing drill cuttings and/or core samples stored at the site were used for this purpose. The data quality objectives are as follows.

- a) To confirm the validity of the observations of the apparently ubiquitous presence of pyrite as identified during initial well logging, specifically, to verify the existence of pyrite reported in existing boring logs, by visual inspection and/or quantitative analysis by an independent laboratory, from a sample of site borings. The sample includes borings located across the entire site (upgradient, cross-gradient, and downgradient of the millsite and tailings cells).
- b) To verify the existence of and analyze for pyrite in MW-series wells which are in accelerated monitoring for pH or OOC for pH and which have drill cuttings and/or core stored onsite, by visual inspection and/or quantitative analysis by an independent laboratory.

## 2. BACKGROUND

As discussed in the Plan, pyrite has been noted in approximately  $\frac{2}{3}$  of the site borings having detailed lithologic logs. This includes all borings drilled into the Dakota Sandstone and Burro Canyon Formation for perched zone well installation since 1999. Pyrite has been described as occurring in disseminated form, as cement filling the interstices between grains, and as aggregates.

The oxidation of pyrite will be enhanced in the vicinities of perched wells because they provide a direct conduit for oxygen to dissolve in the perched water and to react with any pyrite present in the formation near the wells. This is a likely mechanism for the decreasing trends in pH measured in most of the wells at the site, including up-gradient, cross-gradient, and downgradient wells. Figure 1 is a water level contour map of the site showing perched well and piezometer locations and third quarter, 2012 perched water levels.

The following Sections describe the occurrence of pyrite as described in boring logs at the site, the occurrence of pyrite in the Dakota and Burro Canyon Formations in nearby areas, and the mechanism for decreasing pH in site perched zone wells that is consistent with most of the site data.

### 2.1 Pyrite Occurrence as Described in Site Boring Logs

Table 1 summarizes the occurrence of pyrite, iron oxides, and carbonaceous material in site boring logs. As discussed in the Plan pyrite has been noted in approximately  $\frac{2}{3}$  of site borings having detailed lithologic logs. These borings are located upgradient, cross-gradient and downgradient of the millsite and tailings cells. In addition, carbonaceous material has been noted at many locations which is consistent with reduced conditions and the existence of pyrite (Table 1).

### 2.2 Site Geology and Pyrite Occurrence in the Dakota and Burro Canyon Formations Near the Site

Site geology is discussed in Sections 2.2.1 through 2.2.4. The occurrence of pyrite in the Dakota Sandstone and Burro Canyon Formations in the vicinity of the site has been documented in various publications including United States Geological Survey (USGS) publications and State of Utah documents. Based on these documents, a discussion of the occurrence of pyrite is provided in Sections 2.2.5 and 2.3.1.

As will be discussed in Section 2.2.5, (Shawe, 1976) describes the Burro Canyon Formation and Dakota Sandstone as “altered-facies” rocks that “contain only sparse black opaque minerals but

appreciable pyrite”. As will be discussed in Section 2.3.1, UDEQ Groundwater Discharge Permit Modification No. UGW370005 for the Lisbon Valley Mining Company, LLC (located approximately 45 miles north-northeast of the site), considers the Dakota Sandstone and Burro Canyon Formation to be acid generating.

### 2.2.1 Overview of Site Geology

The White Mesa Uranium Mill is located within the Blanding Basin of the Colorado Plateau physiographic province. Typical of large portions of the Colorado Plateau province, the rocks underlying the site are relatively undeformed (TITAN, 1994).

Bedrock units exposed in the Blanding Basin include Upper Jurassic through Cretaceous sedimentary rocks (Figure 2, from Doelling, 2004). The general succession, in ascending order, is the Upper Jurassic Brushy Basin Member of the Morrison Formation, the Lower Cretaceous Burro Canyon Formation, and the Upper Cretaceous Dakota Sandstone and Mancos Shale.

The Upper Jurassic Morrison Formation is the youngest Jurassic unit in the Basin. In many places an unconformity separates the Morrison Formation from underlying Middle Jurassic strata. The Morrison was deposited in a variety of depositional environments, ranging from eolian to fluvial and lacustrine. Much of the Morrison is composed of fluvial sandstone and mudstone that have sources to the west and southwest of the Basin (Peterson and Turner-Peterson, 1987). An upper member, the Brushy Basin Member (primarily a shale), was deposited in a combination of lacustrine and marginal lacustrine environments (Turner and Fishman, 1991).

The contact between the Morrison Formation and overlying strata has been the subject of much discussion. In the southeastern part of the Basin, the Lower Cretaceous Burro Canyon Formation overlies the Morrison Formation. The contact between the Burro Canyon Formation and the Morrison Formation has been interpreted as a disconformity (Young, 1960); however, Tschudy *et al.*, (1984) indicated that the Burro Canyon Formation may be a continuation of deposition of the Morrison Formation. Recent studies by Aubrey (1992) also suggest interfingering between the Morrison Formation and overlying units.

Kirby (2008) indicates that the contact between the Morrison Formation and the Burro Canyon Formation (between the Brushy Basin Member of the Morrison and the Burro Canyon Formation) near Blanding, Utah is disconformable with “local erosional relief of several feet”. Data collected from perched borings at the site are consistent with a disconformable, erosional contact in agreement with Kirby (2008).

### 2.2.2 Burro Canyon Formation

As defined by Stokes and Phoenix (1948), the Burro Canyon Formation at its type locality near Slick Rock, Colorado, consists of alternating conglomerate, sandstone, shale, limestone and chert ranging in thickness from 150 to 260 feet. In the Blanding Basin the Burro Canyon Formation consists of deposits of alluvial and floodplain materials up to about 100 feet thick consisting of medium to coarse grained sandstone, conglomerate, pebbly sandstone, and claystone. At several horizons in the formation are persistent, widely traceable, conglomeratic sandstones interpreted as deposits of a braided channel subenvironment. Sandwiched between these sandstones are variegated mudstone units with some sandstone and siltstone lenses, the products of interchannel and meandering channel subenvironments. Fossils collected from the Burro Canyon Formation at various localities include freshwater invertebrates, dinosaur bones and plants. None are truly diagnostic but all suggest an Early Cretaceous (Aptian) age.

### 2.2.3 Dakota Sandstone

The Dakota Sandstone, named by Meek and Hayden (1862) for exposures in northeastern Nebraska, is also present in the Blanding Basin. Where the Burro Canyon Formation is present the Dakota Sandstone rests disconformably upon it. In many localities a three-fold lithologic sequence is present, consisting of a basal conglomeratic sandstone with an underlying disconformity, a middle unit of carbonaceous shale and coal, and an upper unit of evenly-bedded sandstone which intertongues with the overlying Mancos Shale. These strata have been described as deposits of transitional environments which accompanied the westward transgressing Mancos Sea (Young, 1973).

The basal conglomerate represents floodplain braided channel deposits which continue into the adjacent paludal environment. The carbonaceous shales are partly marshy but most formed in lagoon ponds, tidal flats and tidal channels of the lagoonal environment just seaward of the marsh belt. The evenly-bedded sandstone was formed at the shoreline as a mainland or barrier beach deposit of the littoral marine environment. Faunal evidence summarized by O'Sullivan *et al.*, (1972) indicates that the lower part of the Dakota Sandstone is of Early Cretaceous age and the upper part is of Late Cretaceous age.

### 2.2.4 Mancos Shale

Conformably overlying the Dakota Sandstone is the Upper Cretaceous Mancos Shale. The Mancos Shale was deposited in the Western Interior Cretaceous seaway (Figure 3) and is primarily composed of uniform, dark-gray mudstone, shale, and siltstone. It was deposited in nearshore and offshore neritic subenvironments of the Late Cretaceous Sea during its overall southwestern transgression and subsequent northeastward regression.

The Mancos Shale was named by Cross and Purington (1899) from exposures near Mancos, Colorado. Outcrops of the Upper Cretaceous Mancos Shale occur as hills and slopes generally near or directly beneath overlying Quaternary pediment remnants across portions of the Blanding Basin. Mancos Shale is absent in most of the Blanding Basin (due to erosion) where rocks of the Dakota Sandstone and Burro Canyon Formation are either exposed or mantled by thin unconsolidated deposits.

The Mancos Shale in the Blanding Basin consists of marine shale and interbeds of thin (less than 2 feet) sandstone and siltstone beds. Various pelecypod fossils are common in Mancos Shale outcrop areas (Huff and Lesure, 1965; Haynes *et al.*, 1972). Total thickness is estimated at 30 to 40 feet, but is generally negligible to 20 feet, a small erosional remnant of its original thickness of approximately 2,000 feet. The Mancos Shale was deposited during transgression and highstand of the Cretaceous Interior Seaway during the Late Cretaceous (Elder and Kirkland, 1994). Where present, the Mancos Shale may act as an important impermeable layer reducing the amount of potential infiltration and recharge to the underlying Dakota-Burro Canyon perched aquifer (Avery, 1986; Goodknight and Smith, 1996).

The Mancos Shale belongs to the group of thick marine organic muds (or black shales) generally thought of as deposited in geosynclinal areas. Bentonitic volcanic ash layers are abundant in the Mancos Shale (Shawe *et al.*, 1968). An abundance of pyrite in the layers may indicate that iron was an important constituent of the ash, possibly being liberated by devitrification of glass and redeposited with the diagenetic development of pyrite. Hydrogen sulfide was abundant in the organic rich sediments accumulating at the bottom of the Mancos Sea, if it was a typical sapropelic marine environment, as seems likely, and may have been especially abundant in the volcanic ash (Fenner, 1933).

Trapped sea water that is buried in the mud of the Mancos Shale likely had a high content of organic material consistent with the abundance of diagenetic pyrite. Chemical reduction resulting from hydrogen sulfide generated in carbon-rich sediments is characteristic of stagnant sea bottoms.

In the Early Tertiary, the original clay and silt deposited in the Mancos Shale became compacted to about a third to a tenth of its original water saturated volume by the time it was buried to a depth of about 10,000 feet. Pore water throughout the Colorado Plateau, driven from compacting mud, moved largely upward into younger sediments (Yoder, 1955), but much water must have moved into the lower more porous strata because of local conditions of rock structure (Hedberg, 1936), because of the relatively high water density, and because of abnormally high fluid pressures. Expulsion of water likely occurred throughout the deposition of the Mancos Shale in

the Late Cretaceous and during deposition of younger sediments in the Early Tertiary. Therefore expulsion occurred during a period of many millions of years and at depths ranging from near-surface to nearly maximum depths of burial.

Faulting occurred in many places on the Colorado Plateau, including the Blanding Basin during the Late Cretaceous and Early Tertiary when the Mancos was being deeply buried by younger strata, and this provided numerous avenues to allow water movement into underlying porous strata. It seems likely therefore that the Dakota Sandstone at the base of the Mancos Shale and the dominantly sandy underlying Burro Canyon Formation contained pore water which was expelled from the Mancos and was under abnormally high fluid pressures.

Compaction of bedding around pyrite crystals shows the early development of part of the diagenetic pyrite, and indicates that pore fluids were being squeezed out of the Mancos Shale during the period of diagenesis. As pore fluids became trapped in the Mancos Shale following deposition of sediment in the Late Cretaceous, they immediately began to react with black opaque minerals, with magnetite deposited with the abundant ash fall material and possibly with volcanic glass and other iron-bearing material to form pyrite. Faulting that occurred on the Colorado Plateau in the Late Cretaceous and Early Tertiary facilitated movement of the Mancos pore water into underlying beds, causing removal of hematite coating on sand grains, destruction of detrital black opaque minerals, and growth of iron sulfide minerals.

#### 2.2.5 Pyrite Occurrence in the Dakota Sandstone and Burro Canyon Formation

As discussed above, downward movement of the Mancos Shale pore water into underlying beds of the Dakota Sandstone and Burro Canyon Formations caused removal of hematite coatings on sand grains, destruction of detrital black opaque minerals, and the growth of iron sulfide minerals. Shawe (1976) classifies the Dakota Sandstone and Burro Canyon Formations as “altered-facies” rocks primarily as a result of the invasion of pore waters expelled from the overlying Mancos Shale during compaction. He states that “altered facies rocks that developed by solution attack are notable for their almost complete loss of black opaque minerals and gain of significant pyrite.” He further states that “altered-facies rocks contain only sparse black opaque minerals but appreciable pyrite” and later that “alteration caused destruction of most detrital black opaque minerals, precipitation of substantial pyrite, and recrystallization of carbonate minerals that took up much of the iron liberated from the solution of black opaque minerals.”

According to Shawe (1976), “altered-facies sandstone is light gray or, where weathered, also light buff to light brown. It contains only a small amount of black opaque heavy minerals and may or may not contain carbonaceous material. The light buff to light brown colors are imparted by limonite formed from oxidation of pyrite in weathered rock.”

Furthermore Shawe (1976) states “In weathered rocks as observed in thin sections pyrite has been replaced by ‘limonite’, but preservation of original pyrite crystal forms and lack of abundant limonite ‘wash’ or dustlike limonite suggest that the forms of most limonite are indicative of the original forms of pyrite before oxidation. Pyrite (or limonite) in sandstone occurs as isolated interstitial patches as much as 2 millimeters (mm) in diameter enclosing many detrital grains, or as cubes 1 mm across and smaller that are mainly interstitial but that also partially replace detrital grains.” Also “limonite pseudomorphs after marcasite have been recognized in vugs in altered-facies sandstone of the Burro Canyon Formation.” Shawe (1976) also notes that pyrite is more common below the water table and iron oxides (likely formed by oxidation of pyrite) are more common in the vadose zone. These observations are consistent with the occurrence of and oxidation of pyrite in the formations hosting the perched water at the site.

### **2.3 Pyrite Oxidation as a Potential Mechanism for Decreasing pH**

As discussed in Shawe (1976), pyrite is common in “altered-facies” rocks that include the Dakota Sandstone and Burro Canyon Formations which host the perched water at the site. When exposed to oxygen (and water), the pyrite in these “altered facies” rocks oxidizes to limonite, releasing acid and sulfate in the process. Typically, oxidation occurs where rocks are exposed to weathering, but oxidation is expected to occur anywhere a source of oxygen (and water) is available.

As discussed in Section 1, sources of oxygen include 1) diffusion through the vadose zone aided by barometric pumping and the generally dry condition of the vadose zone, 2) transport of oxygen from the surface directly to the formation via perched monitoring well casings (also aided by barometric pumping), 3) infiltration of water containing dissolved oxygen from the wildlife ponds, and 4) groundwater rising into a relatively oxygen-rich vadose zone and mixing with oxygen-rich pore waters.

Perched water will also become more acidic if it mixes with vadose pore waters made acidic by pyrite oxidation. The correlation of pH decline with rising water levels (INTERA, 2012b) could result from three mechanisms: 1) mixing of perched groundwater with relatively acidic vadose pore waters, 2) oxygen transport via groundwater to relatively anoxic vadose areas containing pyrite, or 3) increased oxygen transport to perched groundwater as it rises into a relatively oxygen-rich vadose zone.

Oxygen transport to groundwater in the vicinities of perched wells is enhanced by fluctuations in the perched water table caused by routine purging and sampling of wells, the increased number of monitoring wells, increased purging activity resulting from the increased sampling frequency since 2005 (due to accelerated monitoring in a number of wells), the aggressive well

redevelopment effort during the latter half of 2010 and the first half of 2011, and changes in pumping at chloroform extraction wells MW-4, MW-26, TW4-4, TW4-19, and TW4-20. Enhanced oxygen transport into the vadose zone in the vicinities of perched wells having screens extending above the water table is also an important mechanism.

### 2.3.1 Pyrite Oxidation in the Perched Zone at the Site

Oxidation of pyrite within the Dakota Sandstone and Burro Canyon Formations, which host the perched water at the site, is a likely mechanism for the decreasing pH measured in perched zone wells and is consistent with most of the site data. Pyrite ( $\text{FeS}_2$ ) oxidizes in the presence of oxygen according to the following equation, producing Iron (II), hydrogen ions and sulfate in the process:



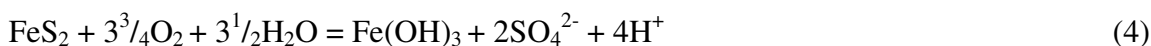
Iron(II) then reacts with oxygen and hydrogen ion according to the following reaction:



Iron(III) then reacts with water according to the following reaction:



Combining the above yields the following reaction (Hartog et al 2001; HGC, 1989):



Oxidation of 1 mole of pyrite therefore yields 4 moles of hydrogen ions. The resulting increase in hydrogen ions lowers the pH (defined as the negative log of the concentration [or activity] of hydrogen ion in moles per liter). As will be discussed in Section 4.3, the laboratory measured concentrations of pyrite in drill cuttings and/or core samples from three representative wells (MW-3A, MW-24, and MW-27) is more than sufficient to account for measured pH declines and increases in sulfate concentrations at these wells. The pH declines will also result in changes in concentrations of analytes sensitive to pH such as metals.

Oxidation of pyrite (and other sulfides) is the same mechanism that results in acidic drainage from mine tailings or waste rock piles containing pyrite and other sulfides. Oxygen transported into the piles reacts with the pyrite (in the presence of water) releasing acid and sulfate. As an example, UDEQ Groundwater Discharge Permit Modification No. UGW370005 for the Lisbon Valley Mining Company, LLC (located approximately 45 miles north-northeast of the site), considers the Dakota Sandstone and Burro Canyon Formation to be acid generating. Discharge

Permit No. UGW370005 states “The potentially acid producing rock will come from the Burro Canyon and Dakota formations and can be identified by color. Acid generating waste rock from beds 6 through 10 of these formations will be encapsulated in acid neutralizing material within the waste dumps.”

As discussed in Section 1, the widespread occurrence of visible pyrite in the Burro Canyon Formation and Dakota Sandstone (upgradient, cross-gradient, and downgradient of the millsite and tailings cells) makes pyrite oxidation a plausible mechanism for pH decrease. Sources of oxygen include 1) diffusion through the vadose zone aided by barometric pumping and the generally dry condition of the vadose zone, 2) transport of oxygen from the surface directly to the formation via perched monitoring well casings (also aided by barometric pumping), 3) infiltration of water containing dissolved oxygen, and 4) perched groundwater rising into an oxygen-rich vadose zone.

Oxygen transport to groundwater in the vicinities of perched wells is enhanced by fluctuations in the perched water table caused by routine purging and sampling of wells, the aggressive well redevelopment effort during the latter half of 2010 and the first half of 2011, and changes in pumping at chloroform extraction wells MW-4, MW-26, TW4-4, TW4-19, and TW4-20. Increasing the number of monitoring wells and the sampling (therefore purging) frequency of MW-series wells since 2005 (due to accelerated monitoring of a number of wells), as a result of the expansion of the groundwater monitoring program under the Mill’s Groundwater Discharge Permit, increased oxygen transport to groundwater. Each time a well is purged for sampling purposes the water column in the well and the water level in the formation near the well will fluctuate, increasing the mixing of air containing oxygen into the groundwater. Therefore, oxygen transport in the vicinities of older wells at the site is expected to have increased since 2005 as a result of increased sampling frequency. Increased oxygen transport will also have resulted from the recent redevelopment effort which resulted in large fluctuations in water levels in and near the wells as a consequence of surging, bailing, and overpumping.

Significant sources of infiltrating water containing oxygen include the wildlife ponds. Another (past) source of potentially oxygen-laden infiltration is the historic pond (discussed in INTERA, 2009.) The persistence of chloroform and nitrate in the chloroform plume originating from two former leach fields (described in HGC, 2007), the relatively low concentrations of chloroform degradation products, and the persistence of nitrate in a nitrate/chloride plume associated with the historic pond (described in INTERA, 2009) are consistent with oxidizing conditions. As discussed in HGC (2007) chloroform daughter products, such as dichloromethane (DCM), have been detected but at low concentrations. The persistence of chloroform and the low concentrations of daughter products imply relatively low rates of chloroform degradation. Owing

to its relatively high oxidation state, chloroform would be expected to degrade relatively rapidly, yielding higher concentrations of daughter products such as DCM, under primarily anaerobic conditions. Likewise, under anaerobic conditions, nitrate is expected to be reduced to nitrogen gas.

Enhanced oxygen transport into the vadose zone in the vicinities of perched wells having screens extending above the water table is also an important mechanism. Oxygen-laden air within the well casings will diffuse into the vadose zone via the unsaturated portions of the screens and move radially in all directions away from the well screens including upgradient with respect to perched groundwater flow. The process will be aided by barometric pumping and the fact that the diffusion coefficient for oxygen in air is approximately four orders of magnitude higher than its diffusion coefficient in water (on the order of 0.1 centimeters squared per second ( $\text{cm}^2/\text{s}$ ) in air vs  $10^{-5}$   $\text{cm}^2/\text{s}$  in water). The resulting enhanced vadose concentrations of oxygen near the wells will be available to react with the vadose formation and pore waters and to dissolve in groundwater near and upgradient of the wells. The generally low rates of perched water movement increase the residence time of groundwater in contact with oxygenated vadose areas near the wells, increasing oxygen transport to groundwater. The availability of air supplying oxygen in the vadose zone is particularly important because the oxygen content of air on a mass basis is approximately 30 times higher than the maximum amount of oxygen that can be dissolved in groundwater. Therefore vadose oxygen constitutes a large reservoir of oxygen available to dissolve in groundwater.

Furthermore, the correlation between pH decrease and increasing water levels in many of the site wells (as discussed in INTERA, 2012b) is consistent with pH decline resulting from pyrite oxidation via one of three mechanisms. The first mechanism involves the rise of oxygen bearing groundwater into relatively anoxic pyritic vadose materials, resulting in increased pyrite oxidation and a decrease in pH. This is expected to be particularly important near the wildlife ponds where seepage of oxygen-laden water into the perched zone is occurring and increases in water levels resulting from seepage are large. The second and more important mechanism involves the rise of groundwater into vadose pore waters that have been made acidic as a result of pyrite oxidation. Oxidation of pyrite in the vadose zone (where oxygen is likely to be more abundant than in the saturated zone) is consistent with Shawe (1976) who noted that most detected pyrite was below the water table and the vadose zone contained iron oxide after pyrite. The third mechanism involves the rise of perched groundwater into an oxygen-rich vadose zone. The rise of groundwater into an oxygen-rich vadose zone will also increase oxygen content of the groundwater thereby increasing pyrite oxidation. Diffusion of oxygen into the vadose zone, where it is available to react with pyrite and pore waters, is expected to be enhanced in the vicinities of perched wells having screens extending above the water table, which includes all

wells OOC for pH (wells MW-3, MW-3A, MW-12, MW-14, MW-23, MW-24, MW-25, MW-26, MW-28, MW-29, and MW-32).

### 2.3.2 Pyrite (and Other Sulfide) Oxidation in Other Aquifers

Pyrite oxidation has been identified at numerous other sites as a mechanism for reduction in pH. Pyrite oxidation has been identified as one mechanism that has decreased the total reduction capacity of aquifers in the Netherlands (Hartog et al, 2001). Acidification of groundwater resulting from several factors including oxidation of sulfide compounds in the soil is discussed in Knutsson (1994). Knutsson (1994) discusses decreases in alkalinity and pH (by 1 to 2 units) in shallow sandy aquifers in Belgium between 1959 and 1984; significant decreases in alkalinity and pH in wells drilled in southwest Denmark from 1950 to 1986; and decreases in alkalinity and pH with corresponding increases in  $\text{Al}^{3+}$ ,  $\text{Ca}^{2+}$ , and  $\text{SO}_4^{2-}$  in shallow wells in Finland during the 1970s and 1980s. The ranges of pH decrease discussed in Knutsson are similar to those detected in perched wells at the Mill.

### **3. METHODOLOGY**

Existing samples of drill cuttings and core from perched borings installed at the site were selected, screened, and analyzed as discussed in the following Sections. Work was performed substantially in accordance with HGC (2012).

#### **3.1 Sample Collection and Screening Procedures**

Sample collection and screening (described in Sections 3.1.1 and 3.1.2) was performed by Mr. Stewart Smith of HGC. Mr. Thomas Rushing III of the State of Utah Division of Radiation Control (DRC) was on-site during the sample screening process and provided helpful input to the process.

During sample collection unexpectedly small cuttings sample volumes were available for many of the desired intervals (for example intervals from MW-26). Although sample volumes were adequate (except for two depth intervals at MW-26 as discussed in Section 3.2), the small sample volumes may reduce the representativeness of some of the samples analyzed for pyrite. The likelihood is that the small sample volumes (which represent subsamples of cuttings produced during drilling) bias the analyses toward lower detected concentrations of pyrite, that is, the actual pyrite concentration is likely larger than indicated by the small sample. This occurs because pyrite is not uniformly distributed throughout any particular drilled depth interval. The smaller the subsample of cuttings from the interval the more likely the subsample contains none of the pyrite that may be present at discrete locations within that interval. Furthermore, oxidation of pyrite within the samples during storage will reduce detected pyrite concentrations, and possibly lead to non-detections in samples that originally contained small amounts of pyrite.

##### **3.1.1 Sample Collection**

All samples submitted for pyrite analysis consisted of existing drill cuttings or drill core samples that were bagged or boxed at the time of drilling and stored on-site in a core storage area. Bagged cuttings samples were stored in boxes labeled with the boring ID. Each cuttings sample, which represented a 2.5 foot interval, was stored in a resealable plastic bag labeled with the boring ID and the depth interval at the time of collection. Each bagged sample identified for analysis was placed in a new resealable plastic bag also labeled with the boring ID and the depth interval. This reduced the possibility that the original sample bag would be damaged and possibly leak during shipping.

All core samples were stored in cardboard core boxes sized to store up to 10 feet of core in five parallel 2-foot long sections. At the time of collection, each core box was labeled with the boring

ID and the 10-foot depth interval represented. Core subsamples selected for analysis were placed in resealable plastic bags labeled with the boring ID and the depth represented.

Samples were identified, selected, photographed, and stored in a cooler on August 14, 2012. Appendix A contains photographs of bagged cuttings and core samples submitted for analysis. At the time of collection, it was not known which of several laboratories were to be contracted to analyze the samples so the samples were transported to HGC's Tucson office prior to shipping. The delay in selecting the contract laboratory was due to the originally identified laboratory's inability to guarantee an acceptable turn around time. By August 16, an alternate contract laboratory was confirmed (Pittsburgh Mineral and Environmental Technology, Inc [PMET]), and samples were shipped on August 17, 2012. The shipment contained two quality control samples that consisted of "play sand".

Two additional samples and a quality control sample were shipped to the contract laboratory on October 9, 2012. These samples were to replace the samples initially sent for TWN-16 and TWN-19 as specified in the Plan. As will be discussed in Section 3.2.1, the initial samples sent for TWN-16 and TWN-19 were actually from AWN-X2 and TWN-16, respectively.

### 3.1.2 Sample Screening

The majority of the samples submitted for analysis were from depth intervals having pyrite noted in the lithologic logs. However, borings MW-3A, MW-23, MW-24, MW-28, and MW-29 had no pyrite noted in the lithologic logs. As will be discussed in Section 4.2, pyrite was directly detected or detected based on iron and total sulfur in samples from all of these borings. The lack of detection at the time of drilling may have been due to an absence of pyrite in the subsamples of the drill cuttings examined by the field geologist, or more likely, to pyrite that was too fine-grained to be detected visually in the field.

As discussed in the Plan, core or cuttings material from the above borings was screened to identify intervals likely to have pyrite. The screening was performed visually and with the aid of a portable Innov-X Alpha Series X-Ray Fluorescence (XRF) meter. Based on the Plan, the XRF meter was to have the capability to measure major elements (including iron) as well as a suite of light elements that included sulfur. The instrument that was ordered was to have the capability to measure sulfur; however the instrument that was shipped did not have this capability. As there was no meter with this capability available on short notice, the planned procedure to use the instrument to identify samples anomalous in both iron and sulfur was modified. Sample screening consisted of using the portable XRF to measure the iron contents of samples having a greenish or grayish to white color consistent with reduced conditions. The samples having the highest iron were then selected for analysis.

The results of the sample screening procedure are provided in Table 2. As indicated, the sample selected from MW-23 had a strong sulfide odor even though pyrite was not detected. The sulfide odor is consistent with the presence of pyrite, and the presence of pyrite is also supported by the analysis of iron, and total sulfur (the components of pyrite) in this sample (Table 4, Section 4.2).

## **3.2 Laboratory Analysis**

Samples submitted for laboratory analysis were analyzed for pyrite using visual (microscopic) methods as well as quantitative methods, as described in Sections 3.2.1 and 3.2.2. Because of the small amounts of sample material available from MW-26, the laboratory combined samples from depth intervals 92.5'-95' and 95'-97.5' in order to perform a visual analysis. This was appropriate because both samples were from the same boring and adjacent depth intervals.

### **3.2.1 Visual Identification**

In accordance with the Plan, existing drill cuttings and core samples from depth intervals noted to have pyrite in the lithologic logs were sent to the contract laboratory for visual (microscopic) verification of the existence of, estimated abundance of, and estimated grain sizes of pyrite and any other visible sulfides. Samples to be sent for visual analysis were listed in Table 4 of the Plan. These samples were from a subset of site borings located upgradient, downgradient, and cross-gradient of the millsite and tailings cells at the site as shown in Figure 2 of the Plan. The sample from TW4-16 in the depth interval 95' – 97.5' was not available so the sample from the depth interval 92.5' – 95' was sent for analysis. Likewise, no sample was available for TW4-22 in the depth interval 102.5' – 105' so only the cuttings sample from 90' – 92.5' was submitted.

The samples initially submitted from TWN-16 and TWN-19 were actually from AWN-X2 and TWN-16. There were originally 22 TWN-series borings and three were abandoned. The abandoned borings were re-named AWN-X1 (originally TWN-11), AWN-X2 (originally TWN-16), and AWN-X3 (originally TWN-17). TWN-19 was renamed TWN-16 and TWN-22 was renamed TWN-19. To meet the intent of the Plan, the 87.5' – 90' sample from TWN-19 (re-named TWN-16) and the 82.5' – 85' sample from TWN-22 (re-named TWN-19) were also submitted to the contract laboratory.

Due to the small amount of material available from MW-26, samples from depth intervals 92.5'-95' and 95'-97.5' were combined by the laboratory for visual analysis as discussed above.

### **3.2.2 Quantitative Analysis**

In accordance with Table 5 of the Plan, existing samples from MW-3A, MW-23, MW-24, MW-25, MW-26 (TW4-15), MW-27, MW-28, MW-29, MW-30, MW-31, and MW-32

(TW4-17) were submitted to the contract laboratory for quantitative analysis of pyrite. These wells are also located upgradient, downgradient, and cross-gradient of the millsite and tailings cells at the site as shown in Figure 3 of the Plan. Samples were from depth intervals noted to have pyrite in the lithologic logs or from intervals likely to have pyrite based on the screening process (Section 3.1.2). X-ray Diffraction (XRD) analysis was performed by PMET using a Bruker D-500 X-ray Diffractometer with Rietveld Whole Pattern refinement and an internal standard. Total sulfur was also analyzed using a Leco-type analyzer with an induction heater and infrared sulfur detector.

Although sample volumes for some of the borings were small (for example at MW-26) they were adequate for quantitative analysis. As discussed in Section 3.1, the small sample volumes (which represent subsamples of drill cuttings produced) likely bias the analyses toward lower detected concentrations of pyrite, that is, had larger sample volumes been available, the pyrite concentrations detected by the laboratory would likely have been higher than reported in this document. As discussed earlier, pyrite is not uniformly, distributed within any particular depth interval, and the smaller the subsample of cuttings from the interval, the more likely the subsample does not contain any of the discretely distributed pyrite within that interval. Furthermore, even though sample volumes from MW-26 were small, the detection of pyrite both visually and quantitatively confirms the presence of pyrite in that boring.

## 4. RESULTS

The results of the visual (microscopic) and quantitative (XRD) analyses for pyrite and other sulfides are provided in Tables 3 and 4, respectively. Copies of the contract laboratory reports are provided in Appendix B. Table 5 and Figure 4 summarize the occurrence of pyrite in site borings based on lithologic logs and laboratory analysis.

### 4.1 Visual Identification and Analysis

The results of the visual analysis to verify the existence of, estimate the abundance of, and estimate the grain sizes of pyrite and any other microscopically detectable sulfides is provided in Table 3. The laboratory reports provided in Appendix B contain color photographs depicting the detected sulfides in samples submitted for visual (microscopic) analysis.

Pyrite (the cubic crystalline form of  $\text{FeS}_2$ ) and/or marcasite (the orthorhombic crystalline form of the same compound,  $\text{FeS}_2$ ) were detected in all samples submitted for visual analysis that had pyrite noted in their respective lithologic logs. Small amounts of sulfide (pyrite and chalcopyrite) were also detected in the quality control samples consisting of “play sand”. The amounts detected in these samples were smaller than the amounts detected in the cuttings samples identified to have pyrite in the lithologic logs. As seen in the photographs provided in the laboratory reports (Appendix B), pyrite occurs primarily as individual grains and as a cementing material, and more rarely as inclusions in quartz grains.

The results of the visual analysis verify and confirm the existence of pyrite in the perched zone at the site at locations upgradient, cross-gradient, and downgradient of the millsite and tailings cells, and the validity of the observations of the apparently ubiquitous presence of pyrite as identified during initial well logging. Pyrite and/or marcasite were detected at volume percents ranging from approximately 0.05 to 25. Grain sizes ranged from approximately one micrometer to nearly 2,000 micrometers. Small grain sizes suggest that much of the pyrite present in the formation may not be detectable during lithologic logging of boreholes and that more pyrite is present than the lithologic logs would indicate. The presence of marcasite is an important result because it is more reactive than pyrite.

### 4.2 Quantitative Analysis

The results of the XRD and total sulfur analyses are provided in Table 4. Table 4 also shows other mineral phases detected by XRD. As shown, pyrite was detected by XRD in samples from MW-3A, MW-24, MW-26, MW-27, MW-28, and MW-32 at concentrations ranging from 0.1% to 0.8% by weight. Based on the iron content via XRD analysis and the total sulfur analysis,

pyrite is likely present in samples from MW-23, MW-25, and MW-29 at concentrations ranging from 0.1% to 0.3% (“equivalent FeS<sub>2</sub>” in Table 4). Pyrite was not detected in quality control samples that consisted of “play sand”.

The presence of pyrite at MW-23 is consistent with the sulfide odor detected during sample screening as shown in Table 2. The presence of pyrite is not indicated in MW-30 or MW-31 by either method of analysis although pyrite was noted in the lithologic logs for these borings suggesting that the samples submitted for analysis (which are subsamples of cuttings produced during drilling) were not representative of the subsamples examined in the field. As of the fourth quarter of 2012, MW-30 and MW-31 are not in out-of-compliance or accelerated monitoring status for pH.

Although pyrite was not directly detected by XRD in samples from MW-23, MW-25, or MW-29, the detected iron and sulfur in these samples is consistent with the presence of pyrite. While at least a portion of the detected sulfur may result from the gypsum or anhydrite detected in some of these samples, iron not in the form of pyrite would be expected to exist primarily in the form of iron oxides or perhaps iron carbonates. The absence of detected iron oxides or carbonates in samples from these borings suggests iron in the form of pyrite.

As shown in Table 5, pyrite was either directly detected or possibly detected based on the presence of iron and sulfur in samples from MW-3A, MW-23, MW-24, MW-28, and MW-29 which were the borings screened for pyrite, indicating that the screening procedure was successful. The detection of pyrite in samples from these borings, which did not have pyrite noted in the associated lithologic logs, indicates that the absence of pyrite in a log does not necessarily mean pyrite is not present in the associated boring.

The results of the XRD analyses verify and confirm the existence of pyrite in the perched zone at the site at locations upgradient, cross-gradient, downgradient and within the area of the tailings cells.

### **4.3 Implications for Pyrite Oxidation as the Mechanism for Decreasing pH in the Perched Zone at the Site**

Screening-level calculations and preliminary geochemical modeling to determine the feasibility of pyrite oxidation as a mechanism for decreasing pH at wells MW-3A, MW-24, and MW-27 are presented in Sections 4.3.1 through 4.3.4. The calculations and modeling performed for these three wells is representative of other wells currently in out-of-compliance status for pH.

MW-3A, MW-24, and MW-27 are located far downgradient, immediately downgradient, and immediately upgradient, respectively, of the tailings cells and were chosen as representative of

MW-series wells at the site experiencing decreasing pH. MW-3A and MW-24 are OOC for pH and MW-27 is in accelerated monitoring for pH. MW-27 is affected by the chloride/nitrate plume (INTERA, 2012b) but changes in pH and sulfate concentrations may be unrelated to the plume.

MW-3A can be considered a “worst case” example because of the relatively low detected pyrite concentrations in this well boring, a change in sulfate concentrations (hundreds of milligrams per liter) which implies a relatively large mass of pyrite has been oxidized, and because of the presence of calcite which will buffer pH changes (and which is taken into account in the preliminary geochemical modeling [Section 4.3.4]). That the calculations and modeling described below demonstrate that pyrite exists in sufficient quantity to explain changes in pH and sulfate concentrations for a “worst case” example implies that the mechanism will be valid for other wells at the site.

Some of the assumptions used in the screening-level calculations and preliminary modeling include:

- Oxygen is not limited in the screening level calculations (Section 4.3.2).
- Oxygen diffuses into the vadose zone via the unsaturated portions of the well screens, aided by barometric pumping, moving radially in all directions (including upgradient). Because the relevant reactions occur upgradient, and affect water moving into a particular well, groundwater flow and the potential resulting dilution from unaffected upgradient water can be ignored.
- Pyrite occurs only in the depth interval represented by the sample submitted for analysis.

#### 4.3.1 Calculation of Pyrite Concentrations Over the Saturated Thicknesses

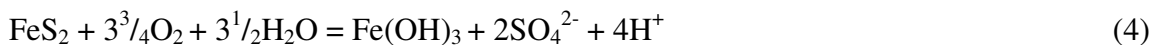
Pyrite was detected in core and cuttings samples within the screened intervals of MW-3A, MW-24, and MW-27 at concentrations of 0.1%, 0.8%, and 0.4% by weight, respectively (Table 4). Pyrite was detected in approximately 6-inch length subsamples of core from MW-3A and MW-24 based on the screening analysis discussed in Section 3.1, and in a cuttings sample from a 2<sup>1</sup>/<sub>2</sub> foot thick interval from MW-27. Pyrite is likely present within other portions of the screened intervals of these wells but this has not been confirmed by laboratory analysis. The likelihood that additional pyrite exists in MW-3A and MW-24 is based on the iron detected within reduced-appearing core material outside the depth interval selected for analysis (Table 2). The interval selected for sampling was based on the highest iron detection but other intervals with detectable iron are also likely to have pyrite.

To be conservative the pyrite concentrations assigned over the saturated thicknesses of the wells for purposes of calculation were made assuming that pyrite existed only in the interval

corresponding to the sample analyzed. Therefore, the pyrite concentration of 0.1% reported for the MW-3A sample was divided by 18 (the approximate thickness of the sample [6-inches] divided by the saturated thickness of 9 feet) to yield a conservatively low concentration of 0.0056%. Likewise, the pyrite concentration of 0.8% reported for the MW-24 sample was divided by 10 (the approximate thickness of the sample [6-inches] divided by the saturated thickness of 5 feet) to yield a conservatively low concentration of 0.08%; and the pyrite concentration of 0.4% reported for the sample from MW-27 was divided by 15.6 (the 2<sup>1</sup>/<sub>2</sub> foot thickness of the sample divided by the saturated thickness of 39 feet) to yield a conservatively low concentration of 0.026%. It should be noted that this approach has the potential to underestimate the quantity of pyrite in the saturated thickness because it assumes that the concentration in any part of the saturated thickness, other than the sampled portion, is zero.

#### 4.3.2 Screening Level Calculations

As discussed in Section 2.3, oxidation of 1 mole of pyrite (FeS<sub>2</sub>) releases 1 mole of iron hydroxide, 2 moles of sulfate, and 4 moles of hydrogen ions:



Sulfate is expected to be relatively conservative once generated but hydrogen ions are expected to react with other species in the water and with the formation. Therefore, most of the sulfate generated from the oxidation of pyrite is expected to be retained in solution, raising the concentration accordingly, but not all hydrogen ion generated will act to lower the pH. Much of the hydrogen ion generated is expected to react with carbonate species in the water thereby buffering the pH. The more carbonate species present the more pyrite will need to be oxidized to produce a given change in pH.

Carbonate species will have an impact on the ratio of the change in sulfate concentration to the change in pH resulting from pyrite oxidation. The more carbonate species present the larger this ratio will be. Therefore, because of the carbonate species known to exist in perched water at the site, relatively small changes in pH may be accompanied by relatively large changes in sulfate concentrations at some locations.

Screening-level calculations can be performed to estimate the mass of pyrite that would have to be oxidized to result in a particular increase in sulfate concentration. Similar calculations can be performed to estimate the amount of pyrite that would have to be oxidized to result in a particular decrease in pH, assuming the hydrogen ion generated did not react with other species. The latter assumption will result in an overestimation of the actual pH decrease; however, if the

amount of pyrite is insufficient to lower pH by a particular amount under these ideal conditions, pyrite oxidation can be ruled out as the sole mechanism for pH decrease.

In performing the calculations, a conservatively high porosity of 0.2 (rather than 0.18) is used. Using a porosity of 0.2 and assuming a density of solids of 2.6 kilograms per liter (Kg/L), 1 liter (L) of the formation has a mass of approximately 2 kilograms (Kg). This implies the following:

- The weight fraction of water in the perched aquifer is approximately 0.1.
- There are approximately 200 grams(g) of water per L of aquifer.
- There are approximately 100 g of water ( $\frac{1}{10}$  L of water) per Kg of aquifer.

#### 4.3.2.1 MW-3A

The change in pH at MW-3A from approximately 7.1 at the initial sampling in 2005 to approximately 6.1 in the first quarter of 2011 is approximately 1 pH unit. Since the first quarter of 2011, the pH at MW-3A has been on an upward trend and is about 6.7 based on the second quarter, 2012 sampling, a change of only 0.4 pH units. Based on the trendline applied by INTERA (INTERA, 2012b) the change in pH is approximately 0.55 pH units. To be conservative, the larger change of 1 pH unit will be used in the calculations.

The pyrite concentration of 0.0056% calculated for MW-3A is equivalent to a concentration of  $5.6 \times 10^{-5}$  g/g of the formation (0.056 g/Kg of the formation) or 0.56 g pyrite/L of water. 0.56 g pyrite/L of water is 0.0047 moles pyrite/L of water assuming a gram molecular weight of 120 for pyrite.

Based on equation (4) the total number of moles of hydrogen ion available from degradation of 0.0047 moles of pyrite is 0.019 moles, yielding a maximum possible increase in hydrogen ion concentration in solution of 0.019 moles/L.

Assuming initial and final pH values of 7.1 and 6.1, respectively, the initial and potential maximum final concentrations of hydrogen ion are calculated as:

$$\begin{aligned} \text{Initial: } [\text{H}^+] &= 10^{-7.1} \text{ moles/L} = 7.9 \times 10^{-8} \text{ moles/L} \\ \text{Final: } [\text{H}^+] &= 10^{-6.1} \text{ moles/L} = 7.9 \times 10^{-7} \text{ moles/L} \end{aligned}$$

The difference between initial and final hydrogen ion concentrations is approximately  $7.1 \times 10^{-7}$  moles/L, approximately 4 orders of magnitude lower than the amount of hydrogen ion that can potentially be generated by pyrite oxidation.

The change in sulfate concentration at MW-3A from the initial value of 3,380 milligrams per liter (mg/L) in the third quarter of 2005 to the value of 3,730 mg/L in the first quarter of 2011 is approximately 350 mg/L. Since the first quarter of 2011, the sulfate concentrations at MW-3A appear to be on a generally downward trend. Based on the trendline applied by INTERA (INTERA, 2012b) the change in sulfate concentration is approximately 180 mg/L. To be conservative, the larger change of 350 mg/L will be used in the calculations.

Based on equation (4) the total number of moles of sulfate available from degradation of 0.0047 moles of pyrite is 0.0094 moles, yielding a maximum possible increase in sulfate concentration in solution of 0.0094 moles/L or 900 mg/L assuming a gram molecular weight of 96 for sulfate. This is approximately  $2^{1/2}$  times more sulfate than needed to account for the measured increase. The measured increase implies that only about 39% of the available pyrite is oxidized, suggesting that trends in pH and related parameters may be expected to continue.

Screening level calculations for both pH and sulfate support pyrite oxidation as the mechanism for measured pH decrease and sulfate increase at MW-3A.

#### 4.3.2.2 MW-24

The change in pH at MW-24 from approximately 6.8 at the initial sampling in 2005 to approximately 5.7 in the first quarter of 2011 is approximately 1.1 pH units. Since the first quarter of 2011, the pH at MW-24 appears to be on an upward trend and is about 6.2 based on the second quarter, 2012 sampling, a change of only 0.6 pH units. Based on the trendline applied by INTERA (INTERA, 2012b) the change in pH is approximately 1.4 pH units (from approximately 7.3 to 5.9 pH units). To be conservative, the larger change of 1.4 pH units will be used in the calculations.

The pyrite concentration of 0.08% is equivalent to a concentration of  $8 \times 10^{-4}$  g/g of the formation (0.8 g/Kg of the formation) or 8 g pyrite/L of water. 8 g pyrite/L of water is 0.067 moles pyrite/L of water assuming a gram molecular weight of 120 for pyrite.

Based on equation (4) the total number of moles of hydrogen ion available from degradation of 0.067 moles of pyrite is 0.27 moles, yielding a maximum possible increase in hydrogen ion concentration in solution of 0.27 moles/L.

Assuming initial and final pH values of 7.3 and 5.9, respectively, the initial and final potential maximum concentrations of hydrogen ion are calculated as:

$$\text{Initial: } [\text{H}^+] = 10^{-7.3} \text{ moles/L} = 5.0 \times 10^{-8} \text{ moles/L}$$

$$\text{Final: } [\text{H}^+] = 10^{-5.9} \text{ moles/L} = 1.3 \times 10^{-6} \text{ moles/L}$$

The difference between initial and final hydrogen ion concentrations is approximately  $1.2 \times 10^{-6}$  moles/L, approximately 5 orders of magnitude lower than the amount of hydrogen ion that can potentially be generated by pyrite oxidation.

The change in sulfate concentration at MW-24 from the initial value of 2,450 mg/L in the second quarter of 2005 to the value of 2,760 mg/L in the fourth quarter of 2010 is approximately 310 mg/L. Since the fourth quarter of 2010, the sulfate concentrations at MW-24 appear to be on a generally downward trend. Based on the trendline applied by INTERA (INTERA, 2012b) the change in sulfate concentration is approximately 60 mg/L. To be conservative, the larger change of 310 mg/L will be used in the calculations.

Based on equation (4) the total number of moles of sulfate available from degradation of 0.067 moles of pyrite is 0.13 moles, yielding a maximum possible increase in sulfate concentration in solution of 0.13 moles/L or approximately 12,500 mg/L assuming a gram molecular weight of 96 for sulfate. This is approximately 40 times more sulfate than needed to account for the measured increase. The measured increase implies that only about 3% of the available pyrite is oxidized, suggesting that trends in pH and related parameters may be expected to continue.

Screening level calculations for both pH and sulfate support pyrite oxidation as the mechanism for measured pH decrease and sulfate increase at MW-24.

#### 4.3.2.3 MW-27

The change in pH at MW-27 from approximately 7.3 at the initial sampling in 2005 to approximately 6.7 in the first quarter of 2011 is approximately 0.6 pH units. Since the first quarter of 2011, the pH at MW-24 appears to be on a generally upward trend and is about 7 based on the second quarter, 2012 sampling, a change of only 0.3 pH units. Based on the trendline applied by INTERA (INTERA, 2012b) the change in pH is approximately 0.4 pH units (from approximately 7.3 to 6.9 pH units). To be conservative, the larger change of 0.6 pH units will be used in the calculations.

The pyrite concentration of 0.026% is equivalent to a concentration of  $2.6 \times 10^{-4}$  g/g of the formation (0.26 g/Kg of the formation) or 2.6 g pyrite/L of water. 2.6 g pyrite/L of water is 0.022 moles pyrite/L of water assuming a gram molecular weight of 120 for pyrite.

Based on equation (4) the total number of moles of hydrogen ion available from degradation of 0.022 moles of pyrite is 0.088 moles, yielding a maximum possible increase in hydrogen ion concentration in solution of 0.088 moles/L.

Assuming initial and final pH values of 7.3 and 6.7, respectively, the initial and potential maximum final concentrations of hydrogen ion are calculated as:

$$\text{Initial: } [\text{H}^+] = 10^{-7.3} \text{ moles/L} = 5.0 \times 10^{-8} \text{ moles/L}$$

$$\text{Final: } [\text{H}^+] = 10^{-6.7} \text{ moles/L} = 2.0 \times 10^{-7} \text{ moles/L}$$

The difference between initial and final hydrogen ion concentrations is approximately  $1.5 \times 10^{-7}$  moles/L, approximately 5 orders of magnitude lower than the amount of hydrogen ion that can potentially be generated by pyrite oxidation.

The change in sulfate concentration at MW-27 from the initial value of approximately 400 mg/L in the second quarter of 2005 to the value of approximately 470 mg/L in the second quarter of 2010 is approximately 70 mg/L. Since the second quarter of 2010, the sulfate concentrations at MW-24 appear to be on a generally downward trend. Based on the trendline applied by INTERA (INTERA, 2012b) the change in sulfate concentration is approximately 65 mg/L. To be conservative, the larger change of 70 mg/L will be used in the calculations.

Based on equation (4) the total number of moles of sulfate available from degradation of 0.022 moles of pyrite is 0.044 moles, yielding a maximum possible increase in sulfate concentration in solution of 0.044 moles/L or approximately 4,200 mg/L assuming a gram molecular weight of 96 for sulfate. This is approximately 60 times more sulfate than needed to account for the measured increase. The measured increase implies that only about 2% of the available pyrite is oxidized, suggesting that trends in pH and related parameters may be expected to continue.

Screening level calculations for both pH and sulfate support pyrite oxidation as the mechanism for measured pH decrease and sulfate increase at MW-27.

#### 4.3.3 Effect of Dissolved Carbonate Species on pH Change

The screening level calculations in Section 4.3.2 were conducted to establish whether pyrite concentrations in the perched zone hosted by the Dakota Canyon and Burro Canyon Formations at the site are sufficient to have caused the increases in sulfate concentrations and decreases in pH observed in the perched zone groundwater. The calculations were based on the simplifying assumption that all of the hydrogen ions released by pyrite oxidation (Equation 4) contribute to the change in pH, whereas it is well known that the pH change will be reduced by the released acid's interaction with the aquifer's dissolved carbonate species, including dissolved  $\text{CO}_2$  ( $\text{H}_2\text{CO}_3^0$ ), bicarbonate ( $\text{HCO}_3^-$ ), and carbonate ( $\text{CO}_3^{2-}$ ). This system property of resistance to pH change is called its "buffer capacity". (Langmuir, 1997, Sec. 5.10).

This section discusses the buffering capacity associated with dissolved  $\text{HCO}_3^-$ . Based on equation (4), 1 mole of pyrite (95.825 g) can react to consume  $3 \frac{3}{4}$  moles of oxygen (119.99 g) and release 2 moles of sulfate (192.122 g) and 4 moles of  $\text{H}^+$  (4 g).

The following mass conversion factors can be derived from equation (4):

- 1.2522g  $\text{O}_2$  per g of  $\text{FeS}_2$  oxidized
- 3.75 moles  $\text{O}_2$  per mole  $\text{FeS}_2$  oxidized
- 1 mole of  $\text{SO}_4^{2-}$  per 1.875 moles of  $\text{O}_2$  consumed
- 0.22476 g  $\text{O}_2$  per g of  $\text{SO}_4^{2-}$  produced
- 4 moles of  $\text{H}^+$  per mole of  $\text{FeS}_2$  oxidized
- 2 moles of  $\text{H}^+$  per mole  $\text{SO}_4^{2-}$  produced
- 0.02082 moles of  $\text{H}^+$  per g  $\text{SO}_4^{2-}$  produced

Buffering capacity resulting from carbonate species is described as follows:

$\text{H}_2\text{CO}_3^0$  dissociates according to Equation



The equilibrium dissociation constant  $K_1$  (at a temperature assumed to be 25° C) is

$$K_1 = [\text{H}^+] [\text{HCO}_3^-] / [\text{H}_2\text{CO}_3^0] = 10^{-6.35} \quad (6)$$

where the activities of the constituents, in moles/L, are bracketed. We assume for simplicity that we can ignore activity coefficients and employ molar concentrations instead.

Taking logs of (6),

$$\log 10^{-6.35} = \log [\text{H}^+] + \log ([\text{HCO}_3^-] / [\text{H}_2\text{CO}_3^0]) \quad (7)$$

and rearranging

$$\text{pH} = 6.35 + \log ([\text{HCO}_3^-] / [\text{H}_2\text{CO}_3^0]) \quad (8)$$

Solving for  $[\text{H}_2\text{CO}_3^0]$ ,

$$\begin{aligned} \log [\text{H}_2\text{CO}_3^0] &= 6.35 - \text{pH} + \log [\text{HCO}_3^-] \\ [\text{H}_2\text{CO}_3^0] &= 10^{(6.35 - \text{pH} + \log [\text{HCO}_3^-])} \end{aligned} \quad (9)$$

Example: Assuming pH = 7 and  $[\text{HCO}_3^-] = 0.001$  moles/L,

$$\log \text{H}_2\text{CO}_3^0 = 6.35 - \text{pH} + \log [\text{HCO}_3^-] = 6.35 - 7.0 - 3.0 = -3.65$$

$$\text{H}_2\text{CO}_3^0 = 10^{-3.65} = 2.2 \times 10^{-4} \text{ moles/L}$$

Addition of strong acid to a bicarbonate solution will reduce the solution's concentration of  $\text{HCO}_3^-$  and increase its concentration of  $\text{H}_2\text{CO}_3^0$  by the same molar amount. Once the concentration of  $\text{H}_2\text{CO}_3^0$  is calculated, Equation (9) could be used to predict the pH change. Assuming that  $\alpha$  is an amount of acid (moles) added to a bicarbonate solution, the new pH would be given by

$$(\text{pH} + \Delta\text{pH}) = 6.35 + \log (([\text{HCO}_3^-] - \alpha) / ([\text{H}_2\text{CO}_3^0] + \alpha)) \quad (10)$$

Alternatively, if alkalinity (bicarbonate) is increased, the formula would be

$$(\text{pH} + \Delta\text{pH}) = 6.35 + \log (([\text{HCO}_3^-] + \alpha) / ([\text{H}_2\text{CO}_3^0] - \alpha)) \quad (11)$$

Where  $\alpha$  is the moles of bicarbonate added.

Equations 10 and 11 could be used to predict the pH changes resulting from the release of hydrogen ion via the oxidation of pyrite as discussed in Section 4.3.2. However, the water in the formation is also expected to react with solid phase species, such as calcite (where present), in addition to dissolved carbonate species. A more accurate way to account for pH changes resulting from pyrite oxidation is to use a model that can account for the interaction between solid and dissolved species as discussed in the following Section (Section 4.3.4)

#### 4.3.4 Preliminary PHREEQC Simulations

Preliminary geochemical modeling was performed using PHREEQC (Parkhurst and Appelo, 1999), a chemical speciation code developed by the USGS, to simulate the impact of pyrite on perched aquifer chemistry. The simulations use the pyrite concentrations calculated for MW-3A, MW-24, and MW-27 as described in Section 4.3.1, account for the mineral species that were determined by the contract laboratory using XRD (Table 4), and are constrained by measured pH and sulfate concentrations.

For each well, two simulations were run. The first set of simulations represented conditions in the 25 years prior to well installation in 2005 and assumed anoxic conditions. The second set of simulations represented years 25 to 30 (approximately years 2005 to 2010) and assumed oxygen was available. For simulation purposes, oxygen at MW-3A and MW-24 was limited to the

amount contained in 10 L of air (10 L of air/L of soil) and at MW-27, 0.1 L of air (0.1 L of air/L of soil) which were determined to be adequate based on a number of trial runs. The amount supplied to MW-3A, which has the lowest permeability of the three wells, is less than the amount of oxygen that would be delivered via groundwater flow, assuming groundwater contains 8 mg/L oxygen (the approximate solubility of oxygen in water). This suggests that oxygen delivery via mechanism 2 (as discussed in Section 2.3.1) is more important than delivery simply via flow of oxygenated water from surface sources (at least at some wells). Output from the model runs is provided in Appendix C.

Pyrite consumptions predicted by the second (oxic) set of simulations range from approximately 3% at MW-27 to 33% at MW-3A, similar to the values calculated in Section 4.3.2. Based on these and other trial simulations that have been performed, most mineral species remain relatively stable or tend to change from unhydrated to hydrated forms. For example, anhydrite tends to convert to gypsum and kaolinite tends to convert to pyrophyllite.

As described in the following Sections, the preliminary simulations predict changes in pH and sulfate concentrations that are similar to the measured changes and support pyrite oxidation as a mechanism for pH decrease and sulfate increase in site wells. The simulations also suggest that only a portion of the available pyrite has been consumed (consistent with the screening level calculations in Section 4.3.2) and that the trends in pH and sulfate may continue in the future.

#### *4.3.4.1 MW-3A*

The pH and sulfate values estimated from the first (anoxic) run, which represented initial conditions for the second (oxic) run, were approximately 6.8 and 3,410 mg/L, respectively. Pyrite was stable in this (anoxic) simulation.

The pH and sulfate values estimated from the second run (oxic conditions over a 5-year period) were approximately 6.4 and 3,740 mg/L respectively. The pH decreased by approximately 0.4 pH units and the sulfate increased by approximately 330 mg/L. The decrease in pH is approximately equal to the change in pH suggested by the trendline in INTERA (2012b) and the change in sulfate is similar to that used in the screening level calculation presented in Section 4.3.2.1. Approximately 33% of the available pyrite was consumed in the simulation.

The preliminary simulation results for both pH and sulfate support pyrite oxidation as the mechanism for measured pH decrease and sulfate increase at MW-3A.

#### 4.3.4.2 MW-24

The pH and sulfate values estimated from the first (anoxic) run, which represented initial conditions for the second (oxic) run were approximately 7.4 and 2,580 mg/L, respectively. Pyrite was stable in this (anoxic) simulation.

The pH and sulfate values estimated from the second run (oxic conditions over a 5-year period) were approximately 6.2 and 2,800 mg/L respectively. The pH decreased by approximately 1.2 pH units and the sulfate increased by approximately 225 mg/L. The decrease in pH is similar to that used in the screening level calculation presented in Section 4.3.2.2 and the change in sulfate is within the range of 60 mg/L to 310 mg/L as discussed in Section 4.3.2.2. Approximately 6% of the available pyrite was consumed in the simulation.

The preliminary simulation results for both pH and sulfate support pyrite oxidation as the mechanism for measured pH decrease and sulfate increase at MW-24.

#### 4.3.4.3 MW-27

The pH and sulfate values estimated from the first (anoxic) run, which represented initial conditions for the second (oxic) run, were approximately 7.2 and 390 mg/L, respectively. Pyrite was stable in this (anoxic) simulation.

The pH and sulfate values estimated from the second run (oxic conditions over a 5-year period) were approximately 6.8 and 450 mg/L respectively. The pH decreased by approximately 0.4 pH units and the sulfate increased by approximately 60 mg/L. The decrease in pH is similar to that suggested by the trendline provided in INTERA (2012b) and the change in sulfate is similar to the value of 70 mg/L used in the screening level calculations provided in Section 4.3.2.3. Approximately 3% of the available pyrite was consumed in the simulation.

The preliminary simulation results for both pH and sulfate support pyrite oxidation as the mechanism for measured pH decrease and sulfate increase at MW-27.

### 4.3.5 Impact of Carbonate Species

Using the changes in sulfate and pH derived from the preliminary modeling (Sections 4.3.4.1 through 4.3.4.3) the ratios of the change in sulfate concentrations in mg/L to change in pH units at each well can be calculated. These ratios are approximately 825 for MW-3A, approximately 188 for MW-24, and approximately 150 for MW-27.

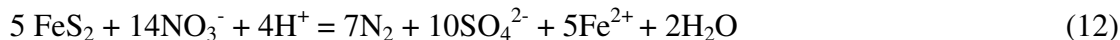
The ratio for MW-3A is much larger than the ratios for MW-24 and MW-27 which are similar to each other. The primary reason for the large ratio at MW-3A is the presence of calcite (Table 4)

accounted for in the simulations. MW-3A is an example of a location where carbonate species reacting with acid produced by pyrite oxidation can result in a relatively large change in sulfate for a given change in pH. Areas of the site having relatively little carbonate and relatively large changes in pH resulting from pyrite oxidation can be expected to have relatively large changes in concentrations of pH-sensitive analytes such as metals.

The complex interaction of the various naturally occurring factors identified at the site, including the presence of pyrite at varying concentrations, variable oxygen transport, and variable carbonate species concentrations, is expected to result in relatively large background variations in pH, sulfate (and therefore total dissolved solids [TDS]) concentrations, as well as variations in background concentrations of pH-sensitive analytes such as metals. The expected impact of these various factors on pH and analyte concentrations, all of which are unrelated to Mill operations, is generally consistent with site analytical results, suggesting that pyrite oxidation plays a significant role in perched water chemistry at the site.

#### **4.4 Implications for Natural Attenuation of Nitrate via Reduction by Pyrite**

Just as pyrite can be oxidized by dissolved oxygen, pyrite can also be oxidized by nitrate according to the following reaction (Tesfay, 2006):



which indicates that 14 moles of nitrate will be reduced to nitrogen gas by oxidizing 5 moles of pyrite. Thus pyrite in the perched zone at the site has the potential to enhance natural attenuation of and reduce the downgradient rate of migration of nitrate in the nitrate/chloride plume.

As discussed in the Nitrate Corrective Action Plan (HGC, 2012b), natural attenuation of nitrate was expected to be primarily the result of hydrodynamic dispersion and dilution. Decomposition of nitrate by either biologically mediated or abiotic means was not considered important at that time. However, the confirmation of pyrite in the perched zone as a result of the present investigation indicates that reduction of nitrate by pyrite is an important mechanism to be considered, and may help explain the apparent stability of the downgradient edge of the plume.



## 5. CONCLUSIONS

The results of the visual and quantitative analysis verify the site-wide, apparently ubiquitous existence of pyrite in the perched zone at the site. The existence of pyrite is confirmed at locations upgradient, cross-gradient, and downgradient of the millsite and tailings cells. The results are consistent with Shawe's (1976) description of the Dakota Sandstone and Burro Canyon Formations as "altered-facies" rocks within which pyrite formed as a result of invasion by pore waters originating from compaction of the overlying Mancos Shale.

Pyrite and/or marcasite were detected in all samples submitted for visual (microscopic) analysis (Table 3) having pyrite noted in their respective lithologic logs. Pyrite occurs primarily as individual grains and as a cementing material, and more rarely as inclusions in quartz grains. Pyrite and/or marcasite were detected at volume percents ranging from approximately 0.05 to 25. Grain sizes ranged from approximately one micrometer to nearly 2,000 micrometers. Small grain sizes suggest that much of the pyrite present in the formation may not be detectable during lithologic logging of boreholes and that the actual abundance of pyrite is larger than indicated by the lithologic logs. The detection of marcasite (orthorhombic crystalline  $\text{FeS}_2$ ), which is more reactive than pyrite (cubic crystalline  $\text{FeS}_2$ ), is an important result of the investigation because its reaction rate with either oxygen or nitrate will likely be higher. The visual (microscopic) analysis confirms the visual observations made during initial well logging.

Pyrite was detected by quantitative (XRD) analysis in samples from MW-3A, MW-24, MW-26, MW-27, MW-28, and MW-32 at concentrations ranging from 0.1% to 0.8% by weight (Table 4). Based on the iron content via XRD analysis and the total sulfur analysis, pyrite may also be present in samples from MW-23, MW-25, and MW-29 at concentrations ranging from 0.1% to 0.3%. The presence of pyrite is not indicated in MW-30 or MW-31 by either method of analysis, although it was noted in the lithologic logs. This suggests that the samples submitted for analysis from these borings may not have been representative, or that pyrite degraded over time during storage. Except for MW-30 and MW-31, the quantitative analysis confirms the visual observations made during initial well logging.

Although pyrite was not directly detected by XRD in samples from MW-23, MW-25, or MW-29, the detected iron and sulfur in these samples is consistent with the presence of pyrite. While at least a portion of the detected sulfur may result from the gypsum or anhydrite detected in some of these samples (Table 4), iron not in the form of pyrite would be expected to exist primarily in the form of iron oxides or perhaps iron carbonates. The absence of detected iron oxides or carbonates in samples from these borings suggests iron in the form of pyrite. Therefore, pyrite

has been directly detected, or detected based on iron and total sulfur, in all OOC wells having samples analyzed by the laboratory.

Furthermore, pyrite was either directly detected or possibly detected based on the presence of iron and sulfur in samples from MW-3A, MW-23, MW-24, MW-28, and MW-29, which did not have pyrite noted in the associated lithologic logs. These results are consistent with the small grain sizes noted via the visual (microscopic) analysis indicating the absence of pyrite in a lithologic log does not necessarily mean pyrite is not present in the associated boring, and that pyrite occurrence at the site has been underestimated based on the lithologic logs.

Pyrite reacts with oxygen to yield sulfate and acid according to equation (4). Perched water will be made more acidic by oxidation of pyrite within the saturated zone in the presence of oxygen. Sources of oxygen include 1) diffusion through the vadose zone aided by barometric pumping and the generally dry condition of the vadose zone, 2) transport of oxygen from the surface directly to the formation via perched monitoring well casings (also aided by barometric pumping), 3) infiltration of water containing dissolved oxygen, and 4) groundwater rising into a relatively oxygen-rich vadose zone and mixing with oxygen-rich pore waters.

Perched water will also become more acidic if it mixes with vadose pore waters made acidic by pyrite oxidation. The correlation of pH decline with rising water levels (INTERA, 2012b) could result from three mechanisms: 1) mixing of perched groundwater with relatively acidic vadose pore waters, 2) oxygen transport via groundwater to relatively anoxic vadose areas containing pyrite, or 3) increased oxygen transport to perched groundwater as it rises into a relatively oxygen-rich vadose zone.

Factors affecting wells having dual exceedances for pH that have implications with regard to oxygen transport include:

1. The generally low rates of groundwater movement due to the generally low permeability of the perched zone,
2. The generally low productivity of perched wells due to the low permeability of the perched zone,
3. Rising water levels in the northeastern portion of the site resulting from seepage from the wildlife ponds, and
4. The presence of pyrite in the perched zone.

Oxygen transport to groundwater in the vicinities of perched wells is enhanced by fluctuations in the perched water table caused by routine purging and sampling of wells, the aggressive well redevelopment effort during the latter half of 2010 and the first half of 2011 (HGC, 2011), and changes in pumping at chloroform extraction wells MW-4, MW-26, TW4-4, TW4-19, and TW4-20. Increasing the number of monitoring wells and the sampling (and purging) frequency, of MW-series wells in 2005 (due to accelerated monitoring in a number of wells), as a result of the expansion of the groundwater monitoring program associated with the Mill's Groundwater Discharge Permit, increased oxygen transport to groundwater. Each time a well is purged for sampling purposes the water column in the well and the water level in the formation near the well will fluctuate, increasing the mixing of air containing oxygen into the groundwater. Therefore, oxygen transport in the vicinities of older wells at the site is expected to have increased since 2005 as a result of increased sampling frequency and monitoring activities. Increased oxygen transport will also have resulted from the recent redevelopment effort which resulted in large fluctuations in water levels in and near the wells as a consequence of surging, bailing, and overpumping.

Significant sources of infiltrating water containing oxygen include the wildlife ponds. Another (past) source of potentially oxygen-laden infiltration is the historic pond (discussed in INTERA, 2009.)

Enhanced oxygen transport into the vadose zone in the vicinities of perched wells having screens extending above the water table is also an important mechanism. Oxygen-laden air within the well casings will diffuse into the vadose zone via the unsaturated portions of the screens and move radially in all directions away from the well screens including upgradient with respect to perched groundwater flow. The process will be aided by barometric pumping and the fact that the diffusion coefficient for oxygen in air is approximately four orders of magnitude higher than its diffusion coefficient in water (on the order of 0.1 centimeters squared per second ( $\text{cm}^2/\text{s}$ ) in air vs  $10^{-5}$   $\text{cm}^2/\text{s}$  in water). The resulting enhanced vadose concentrations of oxygen near the wells will be available to react with the vadose formation and pore waters and to dissolve in groundwater near and upgradient of the wells. The generally low rates of perched water movement increase the residence time of groundwater in contact with oxygenated vadose areas near the wells, increasing oxygen transport to groundwater. The availability of air supplying oxygen in the vadose zone is particularly important because the oxygen content of air on a mass basis is approximately 30 times higher than the maximum amount of oxygen that can be dissolved in groundwater. Therefore vadose oxygen constitutes a large reservoir of oxygen available to dissolve in groundwater.

Furthermore, the correlation between pH decrease and increasing water levels in many of the site wells (as discussed in INTERA, 2012b) is consistent with pH decline resulting from pyrite oxidation via one of three mechanisms. The first mechanism involves the rise of oxygen bearing groundwater into relatively anoxic pyritic vadose materials, resulting in increased pyrite oxidation and a decrease in pH. This is expected to be particularly important near the wildlife ponds where seepage of oxygen-laden water into the perched zone is occurring and increases in water levels resulting from seepage are large. The second and more important mechanism involves the rise of groundwater into vadose pore waters that have been made acidic as a result of pyrite oxidation. Oxidation of pyrite in the vadose zone (where oxygen is likely to be more abundant than in the saturated zone) is consistent with Shawe (1976) who noted that most detected pyrite was below the water table and the vadose zone contained iron oxide after pyrite. The third mechanism involves the rise of perched groundwater into an oxygen-rich vadose zone. The rise of groundwater into an oxygen-rich vadose zone will also increase oxygen content of the groundwater thereby increasing pyrite oxidation. Diffusion of oxygen into the vadose zone, where it is available to react with pyrite and pore waters, is expected to be enhanced in the vicinities of perched wells having screens extending above the water table, which includes all wells OOC for pH (wells MW-3, MW-3A, MW-12, MW-14, MW-23, MW-24, MW-25, MW-26, MW-28, MW-29, and MW-32).

Screening level calculations and preliminary geochemical modeling using PHREEQC as discussed in Section 4.3 demonstrate that pyrite exists in sufficient quantity in the perched zone to explain changes in pH and sulfate concentrations at three representative wells (MW-3A, MW-24, and MW-27) located far downgradient, immediately downgradient, and immediately upgradient of the tailings cells at the site, respectively. The calculations and simulations suggest that only a portion of the available pyrite has been consumed near these wells and that trends in pH and associated parameters may continue in the future as more pyrite is oxidized.

MW-3A can be considered a “worst case” example because of relatively low detected pyrite concentrations, a change in sulfate concentrations (hundreds of mg/L) which implies a relatively large mass of pyrite has been oxidized, and because of the presence of calcite (Table 4) which will buffer pH changes (a mechanism taken into account in the preliminary geochemical modeling [Section 4.3.4]). That the screening-level calculations and preliminary modeling demonstrate that pyrite exists in sufficient quantity to explain changes in pH and sulfate concentrations for a “worst case” example implies that the mechanism will be valid for other wells at the site.

Overall, the results of the investigation support pyrite oxidation as the most likely mechanism to explain decreases in pH and increases in sulfate concentrations in site wells and indicates that

pyrite must be considered in assessing perched water chemistry in the future. The complex interaction of the various naturally occurring factors identified at the site, including the presence of pyrite at varying concentrations, variable oxygen transport, and variable carbonate species concentrations, is expected to result in relatively large background variations in pH, sulfate (and therefore TDS) concentrations, as well as variations in background concentrations of pH-sensitive analytes such as metals. The expected impact of these various factors on pH and analyte concentrations, all of which are unrelated to Mill operations, is generally consistent with site analytical results, suggesting that pyrite oxidation plays a significant role in perched water chemistry at the site.

Specifically, it can be concluded that:

1. Pyrite oxidation explains the decreasing trends in pH observed in a number of wells at the site because acid is released in the reaction. The decreases in pH predicted for MW-3A, MW-24, and MW-27 by the preliminary geochemical modeling discussed in Section 4.3.4, which closely correspond to the actual decreases observed in these wells, support pyrite oxidation as the mechanism for pH decrease.
2. Pyrite oxidation explains some of the increasing trends in sulfate and TDS observed at the site because sulfate is also released in the reaction and is a significant component of TDS. The increases in sulfate predicted for MW-3A, MW-24, and MW-27 by the preliminary geochemical modeling, which closely correspond to the actual increases observed in these wells, support pyrite oxidation as the mechanism for sulfate increase.

Furthermore, as discussed in Section 4.5, reduction of nitrate by pyrite will be an important enhancement to natural attenuation of the nitrate in the nitrate/chloride plume that must be taken into account in the corrective action.



## 6. REFERENCES

- Aubrey, W. M. 1992. Stratigraphy and Sedimentology of Latest Jurassic to Mid-Cretaceous Rocks, Four Corners Area, in Semken, S. C., ed., Field Guide to a Geologic Excursion in the Northeastern Navajo Nation: Shiprock, New Mexico, Navajo Community College, p. 33-40.
- Avery, C., 1986. Bedrock Aquifers of Eastern San Juan County, Utah: Utah Department of Natural Resources Technical Publication no. 86, 114 p.
- Cross, C. W., and Purington, C. W. 1899. Description of the Telluride Quadrangle (Colorado): U.S. Geological Survey Geological Atlas, Folio 57, 19 p.
- Doelling, H. H. 2004. Geologic Map of the La Sal 30' x 60' Quadrangle, San Juan, Wayne, and Garfield Counties, Utah, and Montrose and San Miguel Counties, Colorado: Utah Geological Survey Map 205, scale 1:100,000.
- Elder, W. P., and Kirkland, J. I. 1994. Cretaceous Paleogeography of the Southern Western Interior Region, in Caputo, M.V., Peterson, J. A., and Franczyk, K. J. editors, Mesozoic Systems of the Rocky Mountain Region, USA: Denver, Colorado, Rocky Mountain Section, SEPM (Society for Sedimentary Geology), p. 415- 440.
- Tesfay, T., and Korom.S. 2006. Modeling Groundwater Denitrification by Ferrous Iron using PHREEQC. Technical Report No: ND06-03, North Dakota Water resources Research Institute, North Dakota State University, Fargo, North Dakota.
- Fenner, C. N. 1933. Pneumatolytic Processes in the Formation of Minerals and Ores, in Ore Deposits of the Western States (Lindgren Volume): American Institute Mining & Metallurgical Engineers, p. 58-106
- Goodknight, C. S., and Smith, G. M., 1996. Influences of Geologic and Hydrogeologic Conditions on the Uranium Mill Tailings Repository Design, Monticello, Utah, in Huffman, A. C., Jr., Lund, W.R., and Godwin, L.H., editors, Geology and Resources of the Paradox Basin: Utah Geological Association Guidebook 25, p. 377-388
- Hartog, N., Griffionen, J., Van Bergen, P., and Van Der Weidjen, C. 2001. Determining The Reactivity of Reduced Components in Dutch Aquifer Sediments. Proceedings of a Symposium Held During the Sixth IAHS Scientific Assembly at Maastricht, the Netherlands, July 2001).
- Haynes, D. D., Vogel, J. D., and Wyant, D. G. 1972. Geology, Structure, and Uranium Deposits of the Cortez [1° x 2°] Quadrangle, Colorado and Utah: U.S. Geological Survey Miscellaneous Investigations Series Map I-629, 2 sheets, scale 1:250,000.
- Hedberg, H. D. 1936. Gravitational Compaction of Clays and Shales: American Association of Petroleum Geologists Bulletin v. 10, no. 11, p. 241-287.
- Huff, L.C., and Lesure, F. G. 1965. Geology and Uranium Deposits of Montezuma Canyon area, San Juan County, Utah: U.S. Geological Survey Bulletin 1190, 102 p.

- Hydro Geo Chem, Inc. 1989. Remedial Investigatio Report and remedial Action Pan for the Pinal Creek WQARF Site, Gila County, Arizona, November 29, 1989.
- Hydro Geo Chem, Inc. 2007. Preliminary Contamination Investigation Report. White Mesa Uranium Mill Site Near Blanding, Utah. November 20, 2007.
- Hydro Geo Chem, Inc. 2011. Redevelopment of Existing Perched Monitoring Wells. White Mesa Uranium Mill Near Blanding, Utah. September 30, 2011.
- Hydro Geo Chem, Inc. 2012. Plan to Investigate pH Exceedances in Perched Groundwater Monitoring Wells, White Mesa Uranium Mill, Blanding, Utah. April 13, 2012.
- Hydro Geo Chem, Inc. 2012b. Corrective Action Plan for Nitrate, White Mesa Uranium Mill Near Blanding, Utah. May 7, 2012.
- INTERA 2009. Nitrate Contamination Investigation Report, White Mesa Uranium Mill Site, Blanding Utah.
- INTERA 2012a. Source Assessment Report, White Mesa Uranium Mill, Blanding Utah. October 10, 2012.
- INTERA 2012b. pH Report, White Mesa Uranium Mill, Blanding Utah. November 9, 2012.
- Kirby, S. 2008. Geologic and Hydrogeologic Characterization of the Dakota-Burro Canyon Aquifer Near Blanding, San Juan County, Utah. Utah Geological Survey Special Study 123.
- Knutsson, G. 1994. Trends in the Acidification of Groundwater. Groundwater Quality Management (Proceedings of the GQM 93 Conference Held at Tallinn, September 1993)
- Langmuir, D. 1977. Aqueous Environmental Geochemistry, Prentice Hall, NJ 07458
- Meek, F. B., and Hayden, F. V. 1862. Descriptions of New Cretaceous Fossils from Nebraska Territory: Acad. National Science, Philadelphia Proc., p. 21-28.
- O'Sullivan, R. B., Repenning, C. A., Beaumont, E. C., and Page, Fl. G. 1972. Stratigraphy of the Cretaceous Rocks and the Tertiary Ojo Alamo Sandstone, Navajo and Hopi Indian Reservations, Arizona, New Mexico and Utah: U.S. Geological Society Professional Paper 521-E, 61 p.
- Parkhurst, D. L., and C. A. J. Appelo. 1999. User's Guide to PHREEQC (Version 2) - A Computer Program for Speciation, Batch Reaction, One-Dimensional Transport, and Inverse Geochemical Calculations. US Department of the Interior, USGS, Water-Resources Investigations Report 99-4259, 1999.
- Peterson, Fred, and Turner-Peterson, C. E. 1987, The Morrison Formation of the Colorado Plateau-Recent Advances in Sedimentology, Stratigraphy, and Paleotectonics: North American Paleontological Conference, 4th, Proceedings, Hunteria, v. 2, no. 1, p. 1-18.
- Shawe, D. R. 1968. Petrography of Sedimentary Rocks in the Slick Rock District, San Miguel and Dolores Counties, Colorado. U.S. Geological Survey Professional Paper 576-B., 34 p.

- Shawe, D. R. 1976. Sedimentary Rock Alteration in the Slick Rock District, San Miguel and Dolores Counties, Colorado. U.S. Geological Survey Professional Paper 576-D., 51 p.
- Stokes, W. L. and Phoenix, D. A. 1948. Geology of the Egnar-Gypsum Valley Area, San Miguel and Montrose Counties, Colorado: U.S. Geological Survey Oil and Gas Preliminary Map 93.
- TITAN. 1994. Hydrogeological Evaluation of White Mesa Uranium Mill. Submitted to Energy Fuels Nuclear.
- Turner, C. E., and Fishman, N. S. 1991, Jurassic Lake T'oo'dichi' - A Large Alkaline, Saline Lake, Morrison Formation, Eastern Colorado Plateau: Geological Society of America Bulletin, v. 103, p. 538-558.
- Tschudy, R.H., Tschudy, B.D., and Craig, L.C. 1984, Palynological Evaluation of Cedar Mountain and Burro Canyon Formation, Colorado Plateau: U.S. Geological Survey Professional Paper 1281, 24 p.
- Yoder, H. S., Jr., 1955. Role of Water in Metamorphism, in Poldevaart, Arie, Crust of the Earth: Geological Society of America Special Paper 62, p. 505-523.
- Young, R. G., 1960. Dakota Group of Colorado Plateau: American Association of Petroleum Geologists Bulletin, v. 44, no. 2, p. 156-194.
- Young, R. G., 1973. Depositional Environments of Basal Cretaceous Rocks of Colorado Plateau. Geological Society Memorandum.



## 7. LIMITATIONS STATEMENT

The opinions and recommendations presented in this report are based upon the scope of services and information obtained through the performance of the services, as agreed upon by HGC and the party for whom this report was originally prepared. Results of any investigations, tests, or findings presented in this report apply solely to conditions existing at the time HGC's investigative work was performed and are inherently based on and limited to the available data and the extent of the investigation activities. No representation, warranty, or guarantee, express or implied, is intended or given. HGC makes no representation as to the accuracy or completeness of any information provided by other parties not under contract to HGC to the extent that HGC relied upon that information. This report is expressly for the sole and exclusive use of the party for whom this report was originally prepared and for the particular purpose that it was intended. Reuse of this report, or any portion thereof, for other than its intended purpose, or if modified, or if used by third parties, shall be at the sole risk of the user.



## **TABLES**

**TABLE 1**  
**Tabulation of Presence of**  
**Pyrite, Iron Oxide, and Carbonaceous Fragments in Drill Logs**

Well	Pyrite	C Fragments	Iron Oxide
MW-3A			X
<sup>a</sup> MW-16			X
<sup>a</sup> MW-17			X
<sup>a</sup> MW-18			X
<sup>a</sup> MW-19			X
<sup>a</sup> MW-20			X
<sup>a</sup> MW-21	X		X
<sup>a</sup> MW-22			X
MW-23			X
MW-24			X
MW-25	X		X
MW-26	X		X
MW-27	X		X
MW-28			X
MW-29			X
MW-30	X		X
MW-31	X		X
MW-32	X		X
MW-33			X
MW-34	X	X	X
MW-35	X	X	X
MW-36	X		X
MW-37	X		X
Piez-2			X
Piez-4	X		X
Piez-5	X		X
DR-2	X		X
DR-5	X		X
DR-6	X		X
DR-7			X
DR-8			X
DR-9	X		X
DR-10			X
DR-11	X		X
DR-12	X		X
DR-13			X
DR-14	X		X
DR-15	X		X
DR-16	X		X
DR-17			
DR-18	X		X
DR-19			X
DR-20	X		X
DR-21			X
DR-22			
DR-23	X		X
DR-24	X		X
DR-25	X		X
TW4-1			X
TW4-2	X		X
TW4-3	X	X	X
TW4-4			

**TABLE 1**  
**Tabulation of Presence of**  
**Pyrite, Iron Oxide, and Carbonaceous Fragments in Drill Logs**

Well	Pyrite	C Fragments	Iron Oxide
TW4-5	X	X	
TW4-6	X	X	X
TW4-7	X	X	X
TW4-8			X
TW4-9	X	X	X
TW4-10	X	X	
TW4-11		X	
TW4-12	X	X	X
TW4-13	X	X	X
TW4-14			X
TW4-15	X		X
TW4-16	X		X
TW4-17	X		X
TW4-18		X	X
TW4-19			X
TW4-20			X
TW4-21	X		X
TW4-22	X		
TW4-23	X	X	X
TW4-24			X
TW4-25	X		X
TW4-26			X
TW4-27	X		X
TWN-1			X
TWN-2	X		X
TWN-3	X		X
TWN-4			X
TWN-5	X		X
TWN-6	X		X
TWN-7			X
TWN-8	X		X
TWN-9			X
TWN-10			X
TWN-11	X		X
TWN-12	X		X
TWN-13	X		X
TWN-14	X		X
TWN-15	X		X
TWN-16	X		X
TWN-17			X
TWN-18	X		X
TWN-19	X		X

*Notes:*

*C Fragments = particles of carbonaceous material (plant remains, etc)*

<sup>a</sup> = only moderately detailed log available

**TABLE 2**  
**Results of Sample Screening Using Portable XRF**

Boring	Type	Depth (feet)	Fe (ppm)	Color	Sample Selected?	Comment
MW-3A	core	79.5	796	lt gray	no	
MW-3A	core	89.5	2,544	lt brown	yes	
MW-23	core	98.5	1,620	lt gray	no	above screen/filter pack
MW-23	core	108	1,256	lt gray	yes	strong sulfide odor
MW-23	core	119	763	lt gray	no	
MW-23	core	126	1,009	lt gray	no	
MW-24	core	118	1,514	lt gray	no	
MW-24	core	118.2	2,002	lt gray	no	
MW-24	core	118.5	9,771	gray-red br	yes	at Brushy Basin contact
MW-28	core	78.5	1,983	lt yellowish-gray	no	
MW-28	core	88.5	3,237	lt yellowish-gray	yes	
MW-28	core	92.5	1,515	lt reddish brown	no	disseminated hematite
MW-28	core	95	2,131	lt yellowish brown	no	
MW-28	core	99	2,297	lt reddish brown	no	
MW-29	cuttings	95 - 97.5	263	white	no	
MW-29	cuttings	97.5 - 100	456	white	no	
MW-29	cuttings	100 - 102.5	676	white	no	
MW-29	cuttings	102.5 - 105	1,466	white	yes	
MW-29	cuttings	105 - 107.5	1,431	lt yellowish white	no	
MW-29	cuttings	107.5 - 110	706	white	no	
MW-29	cuttings	110 - 112.5	827	white	no	
MW-29	cuttings	112.5 - 115	735	lt yellowish white	no	
MW-29	cuttings	115 - 117.5	1,318	lt yellowish white	no	
MW-29	cuttings	120 - 122.5	761	lt reddish yellow	no	
MW-29	cuttings	122.5 - 125	23,281	reddish yellow	no	Brushy Basin/pyrite noted

*Note: Depth of core sample represents approximate midpoint of 4 to 6 inch sample to within 1/2 foot*

**TABLE 3**  
**Sulfide Analysis by Optical Microscopy**

Sample	Depth (feet)	Mineral	Volume%	Grain size (micrometers)		
				Minimum	Maximum	Mean
MW-26 (TW4-15) <sup>1</sup>	92.5' - 97.5'	pyrite	4.30	5.6	44.4	128.9
MW-34	67.5' - 70'	pyrite	0.30	1.1	177.8	71.1
MW-36	87.5' - 90'	pyrite	5.20	5.6	88.9	52.2
MW-36	87.5' - 90'	marcasite	0.50	22.2	488.8	121.2
MW-36	112.5' - 115'	pyrite	2.20	16.7	577.7	188.9
MW-36	112.5' - 115'	marcasite	0.20	22.2	333.3	177.8
MW-37	110' - 112.5'	pyrite	9.80	11.1	1666.5	131.1
TW4-16 <sup>2</sup>	92.5' - 95'	pyrite	0.10	11.1	105.5	47.8
TW4-22	90' - 92.5'	pyrite	0.30	5.6	66.7	26.7
TWN-5	110' - 112.5'	pyrite	15.80	5.6	1377.6	208.9
TWN-5	112.5' - 115'	pyrite	0.50	5.6	266.6	70
TWN-5	112.5' - 115'	marcasite	0.50	22.2	55.6	36.7
TWN-5	112.5' - 115'	chalcopyrite	0.02	ND	ND	6
TWN-8	117.5' - 120'	pyrite	12.00	5.6	455.1	137.8
TWN-8	117.5' - 120'	marcasite	0.60	66.6	288.9	155.5
AWN-X2 <sup>3</sup>	87.5' - 90'	pyrite	2.40	5.6	33.3	17.8
AWN-X2 <sup>3</sup>	87.5' - 90'	marcasite	0.60	66.6	288.9	155.5
TWN-16 <sup>4</sup>	82.5' - 85'	pyrite	0.10	1.1	11.1	6.1
TWN-16 <sup>4</sup>	87.5' - 90'	pyrite	0.16	7	168	35.5
TWN-16 <sup>4</sup>	87.5' - 90'	marcasite	0.05	ND	129.5	ND
TWN-19 <sup>5</sup>	82.5' - 85'	pyrite	1.18	3.5	434	42.1
TWN-19 <sup>5</sup>	82.5' - 85'	marcasite	0.06	21	42	36.4
DR-9	105' - 107.5'	pyrite	17.00	2.2	677.7	136.7
DR-12	87.5' - 90'	pyrite	0.30	11.1	111.1	52.2
DR-12	87.5' - 90'	marcasite	0.10	22.2	111.1	72.2
DR-16	97.5' - 100'	pyrite	2.40	5.6	33.3	17.8
DR-16	97.5' - 100'	marcasite	0.60	66.6	288.9	155.5
DR-25	75' - 77.5'	pyrite	25.00	1.1	1955	22
DR-25	75' - 77.5'	marcasite	2.50	55.6	621.6	265.5
SS-31	NA	chalcopyrite	0.01	ND	ND	10
SS-37	NA	pyrite	0.02	7	14	11.7

Notes:

<sup>1</sup> Samples from 92.5' - 95' and 95' - 97.5' combined due to small sample volume

<sup>2</sup> Sample from 92.5' - 95' submitted instead of sample from 95' - 97.5' because no sample material available

<sup>3</sup> Originally TWN-16

<sup>4</sup> Originally TWN-19

<sup>5</sup> Originally TWN-22

NA = Not applicable: quality control sample

ND = Not determined

**TABLE 4**  
**Results of XRD and Sulfur Analysis**  
**in Weight Percent**

Mineral	Formula	MW-3A	MW-23	MW-24	MW-25	MW-26	MW-27	MW-28	MW-29	MW-30	MW-31	MW-32 (TW4-17)	SS-26
		Depth (feet)											
		89.5	108	118.5	65 - 67.5	90 - 92.5	80 - 82.5	88.5	102	65 - 67.5	95 - 97.5	105-107.5	NA
quartz	SiO <sub>2</sub>	79.7	96.2	88.4	90	86.9	95.4	90.1	95.8	87	91.7	94.1	39.2
K-feldspar	KAlSi <sub>3</sub> O <sub>8</sub>	ND	0.2	0.6	2.4	2.4	0.7	1.5	0.5	1.4	2	0.8	21.6
plagioclase	(Na,Ca)(Si,Al) <sub>4</sub> O <sub>8</sub>	ND	ND	ND	1.4	1.6	1.5	1.8	1.5	1.5	0.5	0.2	29
mica	KAl <sub>2</sub> (Si <sub>3</sub> Al)O <sub>10</sub> (OH) <sub>2</sub>	0.3	1.2	4.5	2.2	2	0.2	3	0.2	5.9	3.1	1.2	5.2
kaolinite	Al <sub>2</sub> Si <sub>2</sub> O <sub>5</sub> (OH) <sub>4</sub>	1.1	1	4.3	3.2	2.5	1.4	2.9	1.7	3.6	2.4	1.6	0.8
calcite	CaCO <sub>3</sub>	14	ND	ND	ND	3.9	ND	ND	ND	ND	ND	1.2	0.6
dolomite	CaMg(CO <sub>3</sub> ) <sub>2</sub>	4.1	ND	ND	ND	ND	ND	ND	ND	ND	ND	ND	ND
anhydrite	CaSO <sub>4</sub>	0.4	0.8	0.4	0.4	ND	ND	ND	ND	ND	ND	ND	ND
gypsum	CaSO <sub>4</sub> ·2H <sub>2</sub> O	ND	0.2	0.8	ND	ND	ND	0.3	ND	0.3	ND	ND	ND
iron	Fe	0.3	0.4	0.2	0.4	0.4	0.4	0.2	0.3	0.3	0.3	0.4	0.2
pyrite	FeS <sub>2</sub>	0.1	ND	0.8	ND	0.3	0.4	0.2	ND	ND	ND	0.5	ND
hematite	Fe <sub>2</sub> O <sub>3</sub>	ND	ND	ND	ND	ND	ND	ND	ND	ND	ND	ND	1.4
magnetite	Fe <sub>3</sub> O <sub>4</sub>	ND	ND	ND	ND	ND	ND	ND	ND	ND	ND	ND	2
Sulfur Determination													
Total S	S	0.14	0.14	0.63	0.05	0.13	0.15	0.04	0.03	0.02	0.02	0.26	0.02
equivalent FeS <sub>2</sub>	FeS <sub>2</sub>	0.3	0.3	1.2	0.1	0.2	0.3	0.1	0.1	<0.1	<0.1	0.5	<0.1

**Notes:**

NA = Not applicable: quality control sample

ND = Not Detected

**TABLE 5**  
**Summary of**  
**Pyrite in Drill Cuttings and Core**

Well	Pyrite Noted in Drill Logs	Pyrite Detected by Laboratory	°OOC for pH
MW-3A		X (Q)	X
<sup>a</sup> MW-16		NA	
<sup>a</sup> MW-17		NA	
<sup>a</sup> MW-18		NA	
<sup>a</sup> MW-19		NA	
<sup>a</sup> MW-20		NA	
<sup>a</sup> MW-21	X	NA	
<sup>a</sup> MW-22		NA	
MW-23		possible <sup>b</sup> (Q)	X
MW-24		X (Q)	X
MW-25	X	possible <sup>b</sup> (Q)	X
MW-26	X	X (Q)	X
MW-27	X	X (Q)	
MW-28		X (Q)	X
MW-29		possible <sup>b</sup> (Q)	X
MW-30	X	ND (Q)	
MW-31	X	ND (Q)	
MW-32	X	X (Q)	X
MW-33		NA	
MW-34	X	X (V)	
MW-35	X	NA	
MW-36	X	X (V)	
MW-37	X	X (V)	
Piez-2		NA	
Piez-4	X	NA	
Piez-5	X	NA	
DR-2	X	NA	
DR-5	X	NA	
DR-6	X	NA	
DR-7		NA	
DR-8		NA	
DR-9	X	X (V)	
DR-10		NA	
DR-11	X	NA	
DR-12	X	X (V)	
DR-13		NA	
DR-14	X	NA	
DR-15	X	NA	
DR-16	X	X (V)	
DR-17		NA	
DR-18	X	NA	
DR-19		NA	
DR-20	X	NA	
DR-21		NA	
DR-22		NA	
DR-23	X	NA	
DR-24	X	NA	
DR-25	X	X (V)	
TW4-1		NA	
TW4-2	X	NA	
TW4-3	X	NA	
TW4-4		NA	
TW4-5	X	NA	
TW4-6	X	NA	
TW4-7	X	NA	

**TABLE 5**  
**Summary of**  
**Pyrite in Drill Cuttings and Core**

Well	Pyrite Noted in Drill Logs	Pyrite Detected by Laboratory	°OOC for pH
TW4-8		NA	
TW4-9	X	NA	
TW4-10	X	NA	
TW4-11		NA	
TW4-12	X	NA	
TW4-13	X	NA	
TW4-14		NA	
TW4-15	X	NA	
TW4-16	X	X (V)	
TW4-17	X	NA	
TW4-18		NA	
TW4-19		NA	
TW4-20		NA	
TW4-21	X	NA	
TW4-22	X	X (V)	
TW4-23	X	NA	
TW4-24		NA	
TW4-25	X	NA	
TW4-26		NA	
TW4-27	X	NA	
TWN-1		NA	
TWN-2	X	NA	
TWN-3	X	NA	
TWN-4		NA	
TWN-5	X	X (V)	
TWN-6	X	NA	
TWN-7		NA	
TWN-8	X	X (V)	
TWN-9		NA	
TWN-10		NA	
TWN-11	X	NA	
TWN-12	X	NA	
TWN-13	X	NA	
TWN-14	X	NA	
TWN-15	X	NA	
TWN-16	X	X (V)	
TWN-17		NA	
TWN-18	X	NA	
TWN-19	X	X (V)	
AWN-X1		NA	
AWN-X2	X	X (V)	
AWN-X3		NA	

*Notes:*

<sup>a</sup> = only moderately detailed log available

<sup>b</sup> = detected iron and sulfur may indicate the presence of pyrite

Q = quantitative analysis by XRD

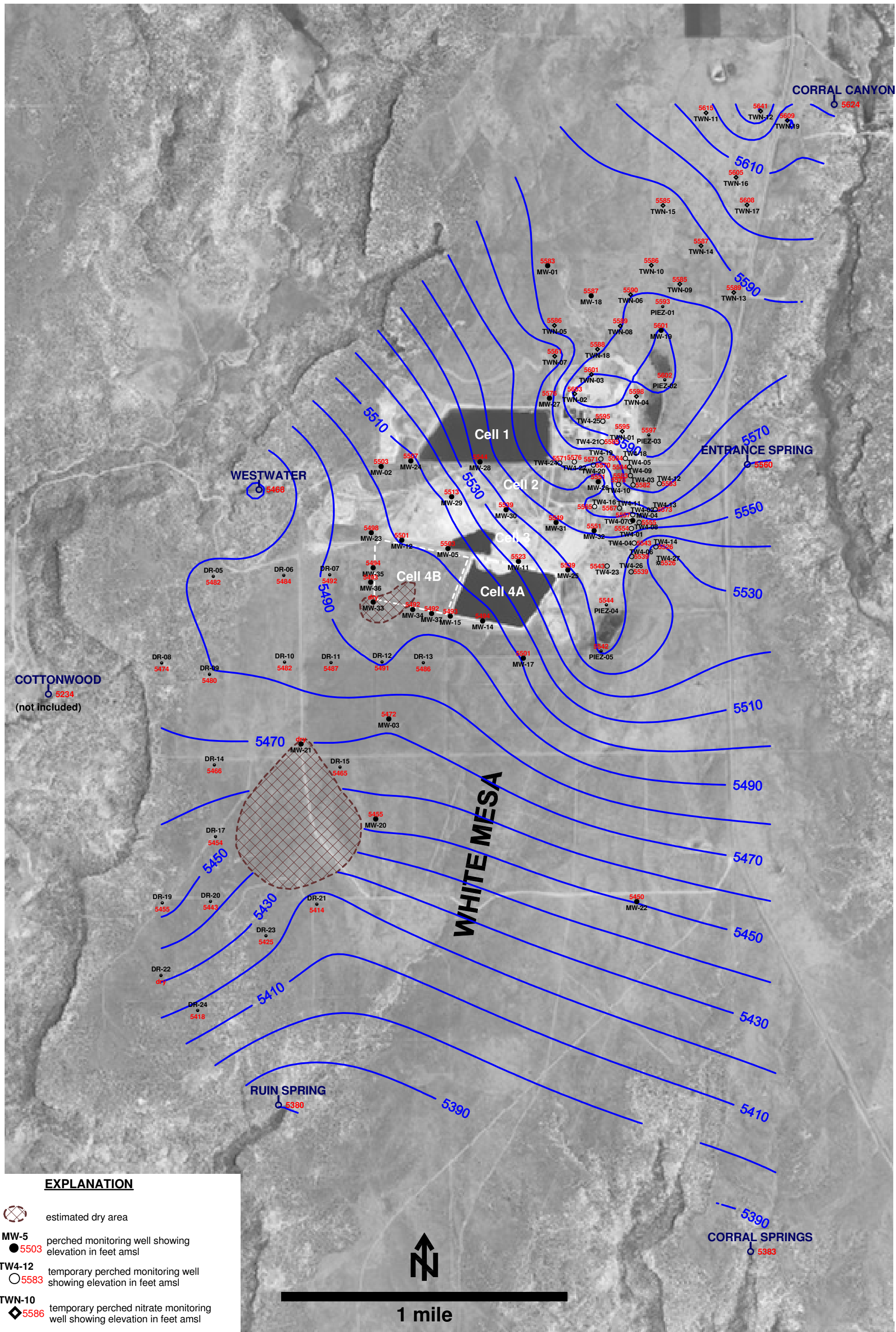
V = visual (microscopic) analysis

°OOC = out of compliance for pH

ND = not detected by laboratory

NA = not analyzed by laboratory

## **FIGURES**



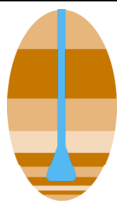
**EXPLANATION**

-  estimated dry area
- MW-5**  
 5503 perched monitoring well showing elevation in feet amsl
- TW4-12**  
 5583 temporary perched monitoring well showing elevation in feet amsl
- TWN-10**  
 5586 temporary perched nitrate monitoring well showing elevation in feet amsl
- PIEZ-1**  
 5593 perched piezometer showing elevation in feet amsl
- TW4-27**  
 5526 temporary perched monitoring well installed October, 2011 showing elevation in feet amsl
- RUIN SPRING**  
 5380 seep or spring showing elevation in feet amsl



1 mile

NOTE: MW-4, MW-26, TW4-4, TW4-19, and TW4-20 are pumping wells



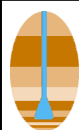
**HYDRO  
GEO  
CHEM, INC.**

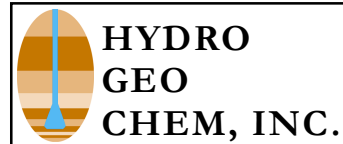
**KRIGED 3rd QUARTER, 2012 WATER LEVELS  
WHITE MESA SITE**

APPROVED	DATE	REFERENCE	FIGURE
SJS	11/19/12	H:\718000\pHdecrease/Uw\0912.srf	1

SYSTEM	SERIES	FORMATION AND MEMBERS	SYMBOL	THICKNESS Meters (Feet)	LITHOLOGY
QUAT.		Surficial deposits	Q	<12 (<40)	
CRET.	Upper	Mancos Shale	Km	0-9 (0-30)	Gray marine shale
		Dakota Sandstone	Kd	5-15 (15-50)	Thin discontinuous coal beds
	L.	Burro Canyon Formation	Kbc	24-36 (80-120)	Pebble conglomerate and sandstone
JURASSIC	Upper	Morrison F.m. Brushy Basin Member	Jmbb	>60 (>200)	Variegated mudstone, claystone, and sandstone  Commonly covered by landslides beneath canyon rims

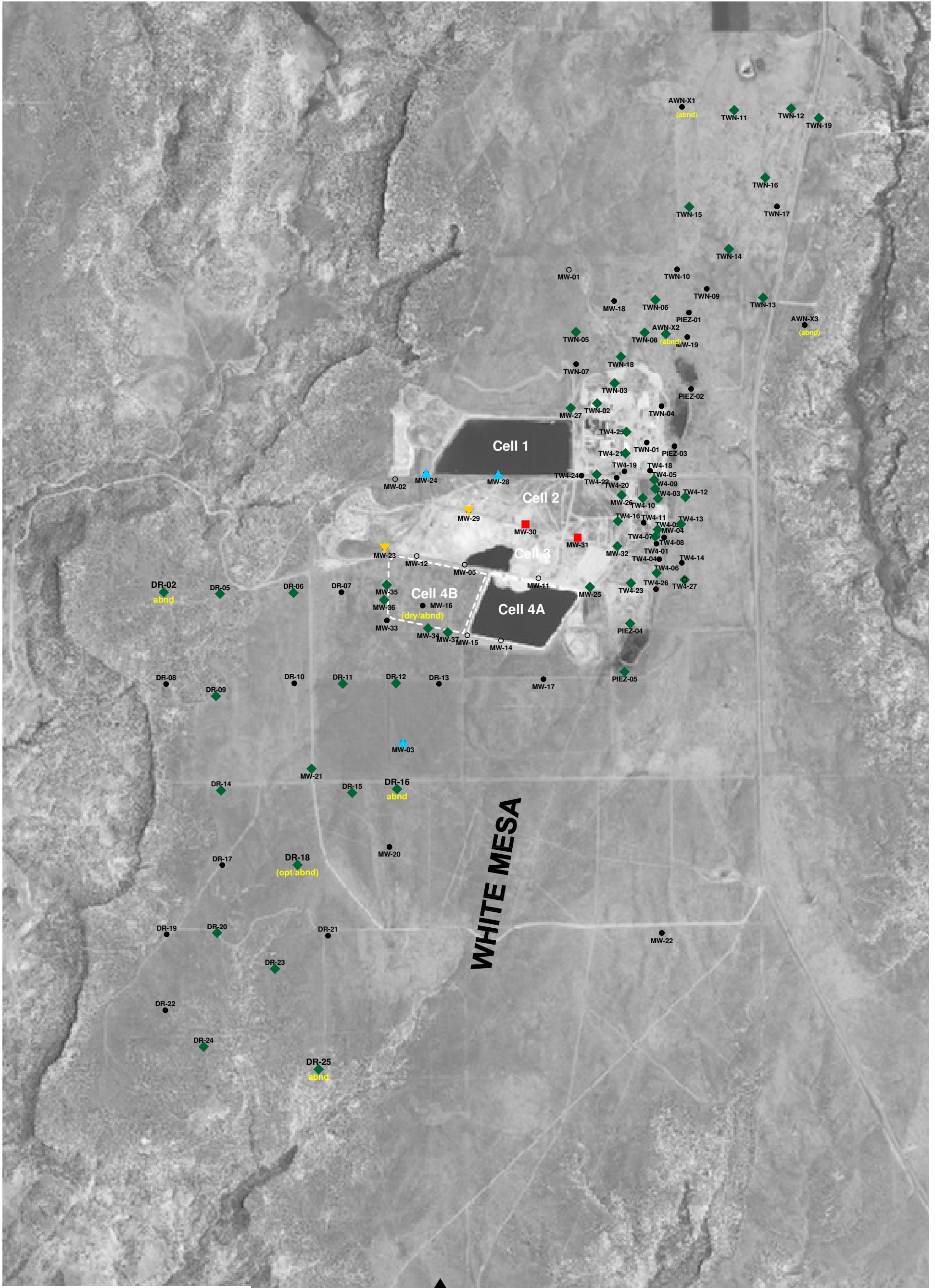
Modified from Doelling (2004).





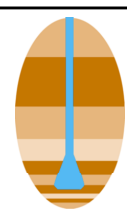
**EXTENT OF THE WESTERN INTERIOR SEA  
(CRETACEOUS)**

Approved <b>DRS</b>	Date <b>11/01/12</b>	File <b>K:\718000\Western Interior Sea.mxd</b>	Figure <b>3</b>
------------------------	-------------------------	---	--------------------



**EXPLANATION**

- MW-5 ○ perched boring (pyrite status unknown)
- MW-33 ● perched boring having detailed log showing no pyrite
- MW-25 ◆ perched boring showing pyrite in log and having a laboratory detection (if analyzed)
- MW-24 ▲ perched boring having pyrite detected via laboratory analysis only (not shown in log)
- MW-29 ▼ perched boring having a possible pyrite detection via laboratory analysis (but not in log)
- MW-30 ■ perched boring showing pyrite in log and having no laboratory detection



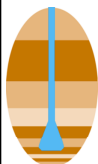
**HYDRO  
GEO  
CHEM, INC.**

**WHITE MESA SITE PLAN  
SHOWING PYRITE OCCURRENCE IN  
PERCHED BORINGS**

APPROVED	DATE	REFERENCE	H:718000/ pHdecrease//pyrite_occurrence_rev.srf	FIGURE
SJS	11/26/12			4

**APPENDIX A**

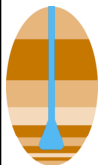
**PHOTOGRAPHS OF SAMPLES SUBMITTED FOR ANALYSIS**



HYDRO  
GEO  
CHEM, INC.

**PHOTO OF DR-SERIES SAMPLES  
(DR-9, DR-12, DR-16, and DR-25)**

APPROVED	DATE	REFERENCE	FIGURE
SJS	12/5/12	H:/718000/phdecrease/ 2012_existing_sample_collection/DRseries.srf	A.1



**HYDRO  
GEO  
CHEM, INC.**

**PHOTO OF MW-3A SAMPLE  
AND CORE BOX (80'- 90')**

APPROVED

SJS

DATE

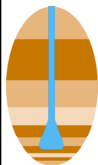
12/5/12

REFERENCE

H:/718000/phdecrease/  
2012\_existing\_sample\_collection/mw3a.srf

FIGURE

**A.2**



**HYDRO  
GEO  
CHEM, INC.**

**PHOTO OF MW-23 SAMPLE  
AND CORE BOX (100'-110')**

APPROVED

SJS

DATE

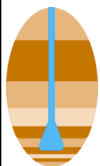
12/5/12

REFERENCE

H:/718000/phdecrease/  
2012\_existing\_sample\_collection/mw23.srf

FIGURE

**A.3**



**HYDRO  
GEO  
CHEM, INC.**

**PHOTO OF MW-24 SAMPLE  
AND CORE BOX (110'-120')**

APPROVED

SJS

DATE

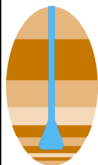
12/5/12

REFERENCE

H:/718000/phdecrease/  
2012\_existing\_sample\_collection/mw24B.srf

FIGURE

**A.4**



**HYDRO  
GEO  
CHEM, INC.**

**PHOTO OF MW-28 SAMPLE  
AND CORE BOX (80'- 90')**

APPROVED

SJS

DATE

12/5/12

REFERENCE

H:/718000/phdecrease/  
2012\_existing\_sample\_collection/mw28.srf

FIGURE

**A.5**



HYDRO  
GEO  
CHEM, INC.

**PHOTO OF MW-SERIES SAMPLES  
(MW-25, MW-29, MW-31, MW-36 [87.5],  
MW-27, MW-30, MW-34, MW-36 [112.5], MW-37)**

APPROVED

SJS

DATE

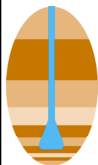
12/5/12

REFERENCE

H:/718000/phdecrease/  
2012\_existing\_sample\_collection/MWseries.srf

FIGURE

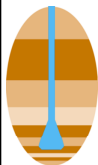
A.6



HYDRO  
GEO  
CHEM, INC.

**PHOTO OF SAMPLES SELECTED BY SCREENING  
(MW-29, MW-28, MW-24, MW-23, MW-3A)**

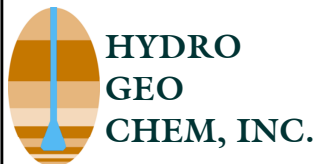
APPROVED SJS	DATE 12/5/12	REFERENCE H:/718000/phdecrease/ 2012_existing_sample_collection/screened.srf	FIGURE A.7
-----------------	-----------------	--	---------------



HYDRO  
GEO  
CHEM, INC.

**PHOTO OF TW4-SERIES SAMPLES  
(MW-26 [TW4-15] (90'-92.5', 92.5'-95', and 95'-97.5'),  
TW4-16, MW-32 [TW4-17], and TW4-22)**

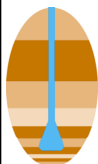
APPROVED	DATE	REFERENCE	FIGURE
SJS	12/5/12	H:/718000/phdecrease/ 2012_existing_sample_collection/TWNseries.srf	<b>A.8</b>



HYDRO  
GEO  
CHEM, INC.

**PHOTO OF TWN-SERIES SAMPLES  
(TWN-5 [110'-112.5' and 112.5'-115'],  
TWN-8, TWN-16, TWN-19)**

APPROVED SJS	DATE 12/5/12	REFERENCE H:/718000/phdecrease/ 2012_existing_sample_collection/TWNseries.srf	FIGURE A.9
-----------------	-----------------	---	---------------



HYDRO  
GEO  
CHEM, INC.

**PHOTO OF QUALITY CONTROL SAMPLES  
(SS-26 and SS-31)**

APPROVED

SJS

DATE

12/5/12

REFERENCE

H:/718000/phdecrease/  
2012\_existing\_sample\_collection/SSseries.srf

FIGURE

A.10

**APPENDIX B**

**LABORATORY ANALYTICAL REPORTS**

**P**

Pittsburgh

**M**

ineral &

**E**

nvironmental

**T**

echnology, Inc.

September 18, 2012

Mr. Daniel R. Simpson  
Hydro Geo Chem, Inc.  
51 W. Wetmore Road  
Suite 101  
Tucson, AZ 85705

Dear Mr. Simpson:

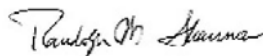
This report summarizes the results of quantitative x-ray diffraction (XRD) and total sulfur analysis of twelve samples and polished section preparation with optical microscopy analysis of eighteen samples associated with your Project No. 718000, Energy Fuels, White Mesa Mill, UT.

The samples were received at PMET's laboratory on August 21, 2012. The work was performed under your P.O. No. 718000 as communicated in your email of July 30, 2012.

The samples were received via FedEx accompanied by a PMET chain of custody record. Each sample was contained in a ziplock bag that was contained in an outer ziplock bag. One of the two bags was marked with the sample identification that corresponded to the sample listing in the chain of custody record which is shown on Pages 17-20. The identification was recorded in PMET's sample logbook under our RFA No. 6036 and the bags were labeled as shown in Table 1 on Page 2. The results of analysis are presented on the following pages.

Mr. Simpson, please contact me by email at [randys@pmet-inc.com](mailto:randys@pmet-inc.com) if you would like to discuss these results. Thank you for using PMET's laboratory services on this project.

Sincerely,



Randolph W. Shannon  
Laboratory Manager

RFA 6036

**700 Fifth Avenue  
New Brighton, PA  
15066  
(724) 843-5000  
FAX: (724) 843-5353  
[www.pmet-inc.com](http://www.pmet-inc.com)**

Table 1  
Sample Identification

PMET I.D.	08/17/12			As-received weight (g)
	HydroGeoChem Label	Type	Depth	
6036-1	MW-26 (TW4-15)	Drill Cuttings	92.5'	6.9
6036-2	MW-26 (TW4-15)	Drill Cuttings	95'	6.6
6036-3	MW-34	Drill Cuttings	67.5'	151.3
6036-4	MW-36	Drill Cuttings	87.5'	160.2
6036-5	MW-36	Drill Cuttings	112.5'	238.3
6036-6	MW-37	Drill Cuttings	110'	241.7
6036-7	TW-16	Drill Cuttings	92.5'	211.5
6036-8	TW-22	Drill Cuttings	90'	51.4
6036-9	TWN-5	Drill Cuttings	110'	145.0
6036-10	SS-31	Drill Cuttings	0' QA/QC	493.1
6036-11	TWN-5	Drill Cuttings	112.5'	185.3
6036-12	TWN-8	Drill Cuttings	117.5'	52.5
6036-13	TWN-16	Drill Cuttings	87.5'	143.3
6036-14	TWN-19	Drill Cuttings	82.5'	148.4
6036-15	DR-9	Drill Cuttings	105'	471.1
6036-16	DR-12	Drill Cuttings	87.5'	187.7
6036-17	DR-16	Drill Cuttings	97.5'	230.3
6036-18	DR-25	Drill Cuttings	75'	241.4
6036-19	MW-3A	Rock Core	89.5'	504.1
6036-20	MW-23	Rock Core	108'	309.5
6036-21	MW-24	Rock Core	118.5'	278.0
6036-22	MW-25	Drill Cuttings	65'	392.9
6036-23	MW-26	Drill Cuttings	90'	18.9
6036-24	MW-27	Drill Cuttings	80'	342.7
6036-25	MW-28	Rock Core	88.5'	402.4
6036-26	MW-29	Drill Cuttings	102'	274.6
6036-27	MW-30	Drill Cuttings	65'	36.3
6036-28	MW-31	Drill Cuttings	95'	307.7
6036-29	MW-32 (TW4-17)	Drill Cuttings	105'	25.2
6036-30	SS-26	Drill Cuttings	0' QA/QC	426.6

All samples were removed from their bags into labeled steel pans and dried in a muffle furnace at 60° C overnight.

Samples #1 and #2 were combined due to the lack of source material. Samples #1- #18 were stage crushed to 100% passing a 12 mesh sieve using a ceramic mortar and pestle, then riffle split to obtain an analytical aliquot. The split was embedded in epoxy and a polished section was obtained.

Samples 19-30 were crushed to 100% passing a 35 mesh sieve using a ring and puck mill, then riffle split to obtain an analytical aliquot. The split was pulverized to 100% passing a 325 mesh sieve and placed into labeled petri dishes.

All material remaining after obtaining the analytical aliquot was placed in labeled bags and retained for shipment back to Energy Fuels.

The seventeen polished sections of the first eighteen samples were examined for mineralogical composition by ore microscopic techniques with an emphasis on sulfide minerals. The polished sections were examined in detail employing standard reflected polarized light methods. Quantities (volume percent) of sulfide minerals were statistically estimated. Illustrative digital images were obtained from all polished sections and are shown in Figures 1-22 on Pages 6-16.

The examination of the polished sections shows that pyrite is the major sulfide ore mineral with associated marcasite. Both form the diagenetic cement between the grains of sandstone or occur as inclusion in quartz grains. Rare chalcopyrite inclusions occur in a few quartz grains (Figure 10).

Pyrite cemented sandstone probably forms thin beds or lenses in this formation. The pyrite usually forms a massive cement that makes it difficult to determine the mineral body size. It is also present as characteristic small cubes in the matrix between the sand grains, for which the size is determined (Figure 19). Marcasite is either massive or intergrown with pyrite or forms a separate rosette-like cluster of crystals as shown in Figure 21. Average iron sulfide content is 5.8 volume %. See Table 2 below for results of sulfide mode of occurrence.

The pulverized splits of samples #19 - #30 were scanned using a Bruker D500 X-ray Diffractometer from five to sixty-six degrees two theta. Cu K $\alpha$  x-rays were generated at 30 mA and 45 KV power. Diffracted x-rays were focused using a 0.15mm receiving slit and collected by a Solex solid state detector. The mineral phases were quantified using Bruker proprietary Rietveld whole pattern refinement software and the International Crystal Structure Database. Results are shown in Tables 3a and 3b below.

A small portion of the split was analyzed for total sulfur content using an induction furnace with an infrared sulfur oxide detector. The tests were run in duplicate and the average results along with an equivalent calculated pyrite are shown in Tables 3a and 3b below.

Table 2  
Sulfide Mineral Determination by Optical Microscopy  
Samples #1 - #18

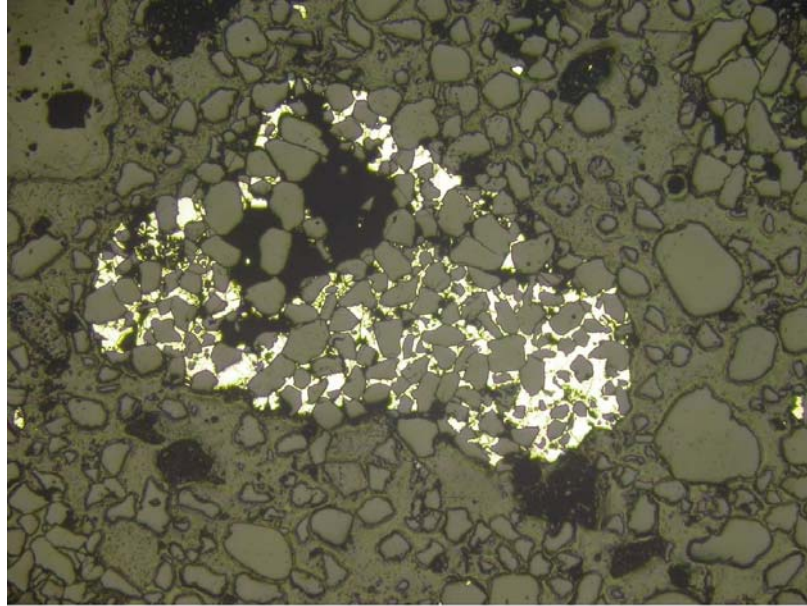
Sample #	Mineral	Vol. %	Size ( $\mu\text{m}$ )		
			Min.	Max.	Mean
1&2	pyrite	4.3	5.6	44.4	128.9
3	pyrite	0.3	1.1	177.8	71.1
4	pyrite	5.2	5.6	88.9	52.2
4	marcasite	0.5	22.2	488.8	121.2
5	pyrite	2.2	16.7	577.7	188.9
5	marcasite	0.2	22.2	333.3	177.8
6	pyrite	9.8	11.1	1666.5	131.1
7	pyrite	0.1	11.1	105.5	47.8
8	pyrite	0.3	5.6	66.7	26.7
9	pyrite	15.8	5.6	1377.6	208.9
10	chalcopyrite	0.01			10.0
11	pyrite	0.5	5.6	266.6	70.0
11	marcasite	0.5	22.2	55.6	36.7
11	chalcopyrite	0.02			6.0
12	pyrite	12.0	5.6	455.1	137.8
12	marcasite	0.6	66.6	288.9	155.5
13	pyrite	2.4	5.6	33.3	17.8
13	marcasite	0.6	66.6	288.9	155.5
14	pyrite	0.1	1.1	11.1	6.1
15	pyrite	17.0	2.2	677.7	136.7
16	pyrite	0.3	11.1	111.1	52.2
16	marcasite	0.1	22.2	111.1	72.2
17	pyrite	2.5	5.6	377.7	86.7
17	marcasite	0.1	33.3	133.3	66.7
18	pyrite	25.0	1.1	1955.0	22.0
18	marcasite	2.5	55.6	621.6	265.5

Table 3a  
Results of XRD and Sulfur Analysis  
Sample #19 - #24  
Weight %

Mineral	Formula	#19	#20	#21	#22	#23	#24
quartz	SiO <sub>2</sub>	79.7	96.2	88.4	90.0	86.9	95.4
K-feldspar	KAlSi <sub>3</sub> O <sub>8</sub>		0.2	0.6	2.4	2.4	0.7
plagioclase	(Na,Ca)(Si,Al) <sub>4</sub> O <sub>8</sub>				1.4	1.6	1.5
mica	KAl <sub>2</sub> (Si <sub>3</sub> Al)O <sub>10</sub> (OH) <sub>2</sub>	0.3	1.2	4.5	2.2	2.0	0.2
kaolinite	Al <sub>2</sub> Si <sub>2</sub> O <sub>5</sub> (OH) <sub>4</sub>	1.1	1.0	4.3	3.2	2.5	1.4
calcite	CaCO <sub>3</sub>	14.0				3.9	
dolomite	CaMg(CO <sub>3</sub> ) <sub>2</sub>	4.1					
anhydrite	CaSO <sub>4</sub>	0.4	0.8	0.4	0.4		
gypsum	CaSO <sub>4</sub> ·2H <sub>2</sub> O		0.2	0.8			
iron	Fe	0.3	0.4	0.2	0.4	0.4	0.4
pyrite	FeS <sub>2</sub>	0.1		0.8		0.3	0.4
<b>Sulfur Determination</b>							
Total S	S	0.14	0.14	0.63	0.05	0.13	0.15
equivalent FeS <sub>2</sub>	FeS <sub>2</sub>	0.3	0.3	1.2	0.1	0.2	0.3

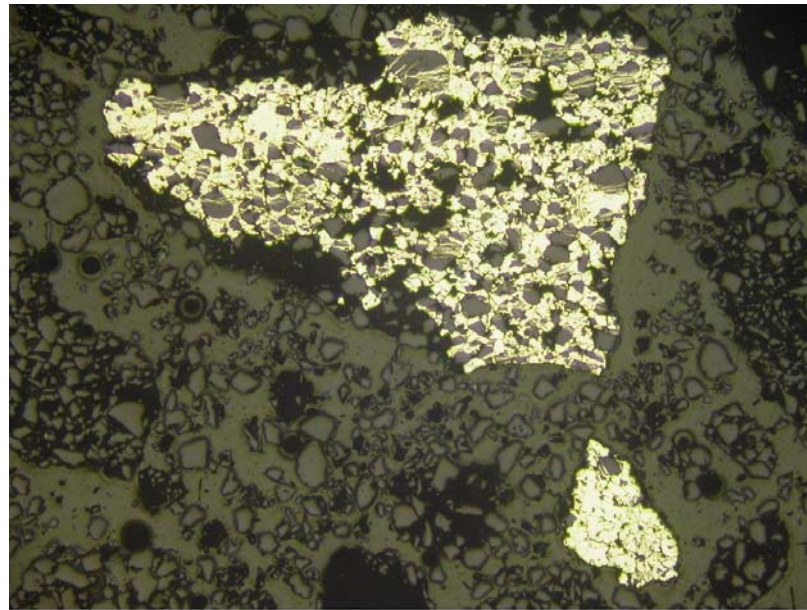
Table 3b  
Results of XRD and Sulfur Analysis  
Sample #25 - #30  
Weight %

Mineral	Formula	#25	#26	#27	#28	#29	#30
quartz	SiO <sub>2</sub>	90.1	95.8	87.0	91.7	94.1	39.2
K-feldspar	KAlSi <sub>3</sub> O <sub>8</sub>	1.5	0.5	1.4	2.0	0.8	21.6
plagioclase	(Na,Ca)(Si,Al) <sub>4</sub> O <sub>8</sub>	1.8	1.5	1.5	0.5	0.2	29.0
mica	KAl <sub>2</sub> (Si <sub>3</sub> Al)O <sub>10</sub> (OH) <sub>2</sub>	3.0	0.2	5.9	3.1	1.2	5.2
kaolinite	Al <sub>2</sub> Si <sub>2</sub> O <sub>5</sub> (OH) <sub>4</sub>	2.9	1.7	3.6	2.4	1.6	0.8
calcite	CaCO <sub>3</sub>					1.2	0.6
gypsum	CaSO <sub>4</sub> ·2H <sub>2</sub> O	0.3		0.3			
iron	Fe	0.2	0.3	0.3	0.3	0.4	0.2
pyrite	FeS <sub>2</sub>	0.2				0.5	
hematite	Fe <sub>2</sub> O <sub>3</sub>						1.4
magnetite	Fe <sub>3</sub> O <sub>4</sub>						2.0
<b>Sulfur Determination</b>							
Total S	S	0.04	0.03	0.02	0.02	0.26	0.02
equivalent FeS <sub>2</sub>	FeS <sub>2</sub>	0.1	0.1	<0.1	<0.1	0.5	<0.1



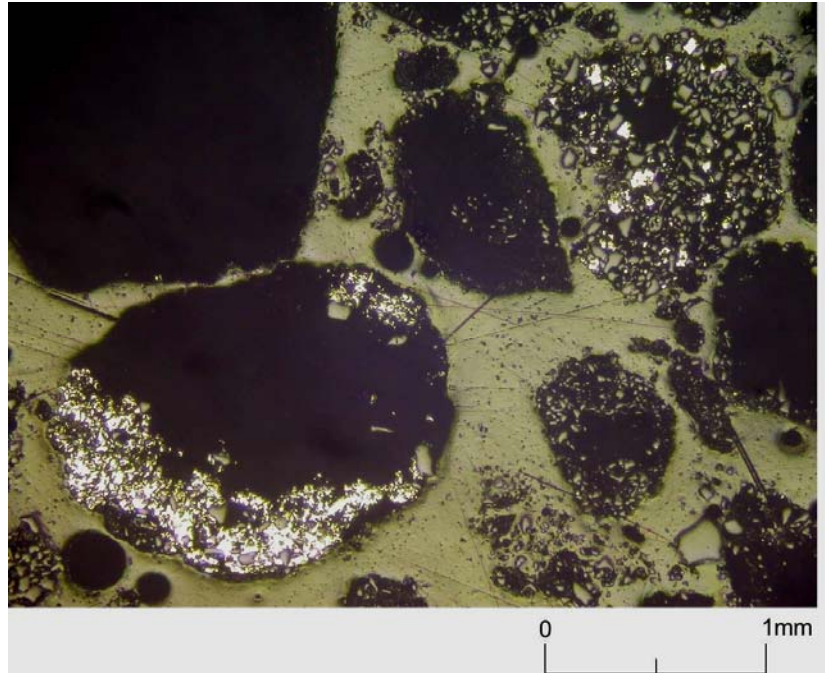
0 1mm

Composite sample #1 & #2  
Pyrite (yellow-white) cemented sandstone (tan)  
Figure 1



0 1mm

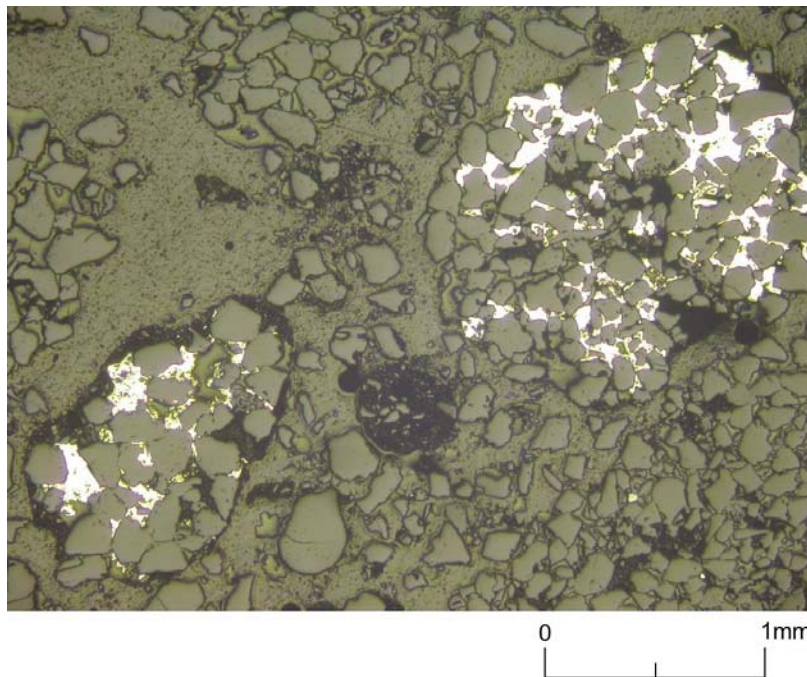
Sample #3  
Pyrite (yellow-white) cemented sandstone (tan), with  
smaller fragment of pyrite cement (lower right)  
Figure 2



Sample #4

Large fragment of small grained pyrite cement (white) (lower left)  
w/large breakout, pyrite cement in very fine sandstone (upper right)

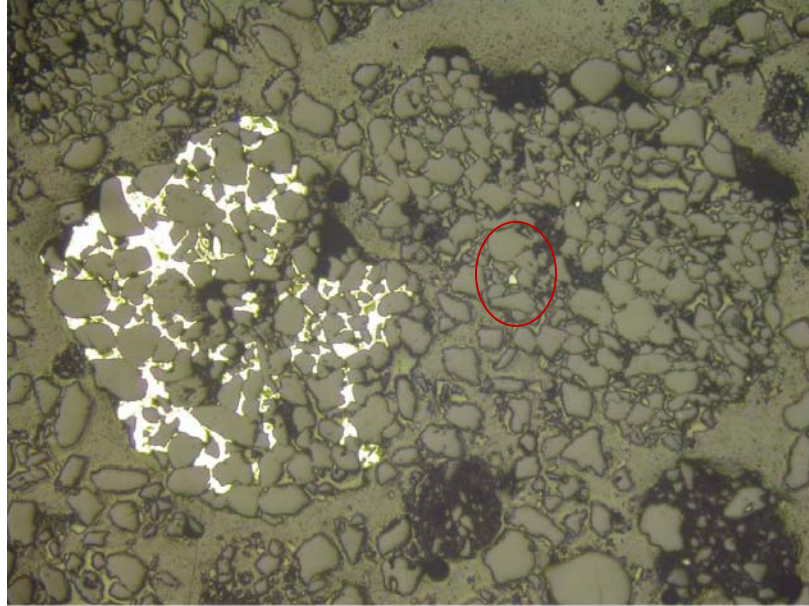
Figure 3



Sample #5

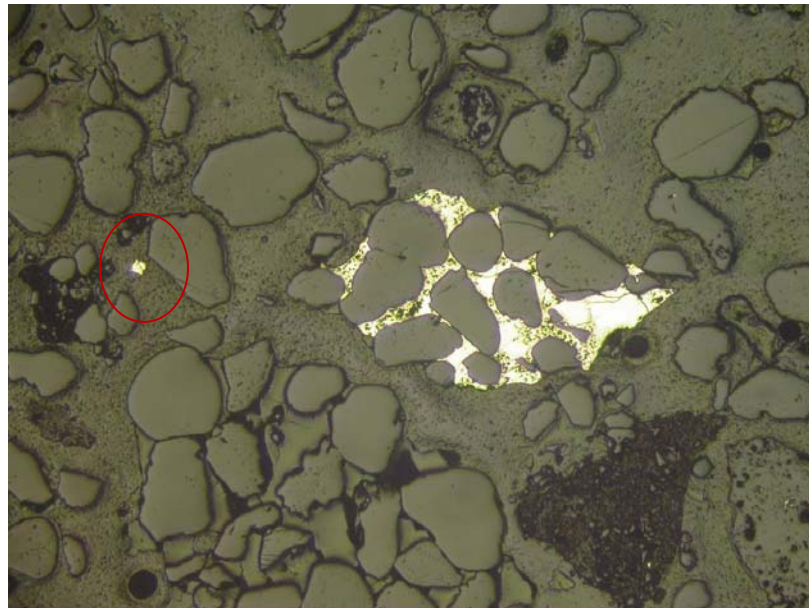
Pyrite (white) cement in very fine sandstone (lower left, upper right)

Figure 4



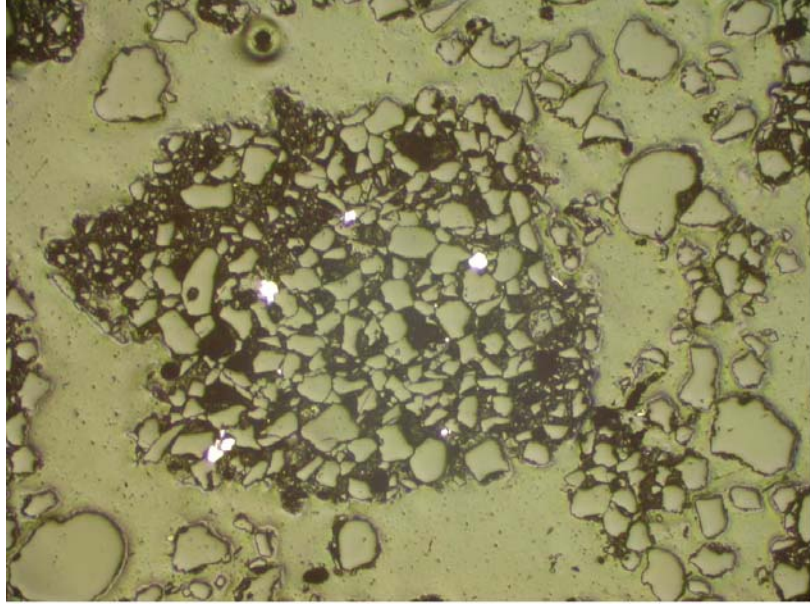
0 1mm

Sample #5  
Large sandstone fragment partially cemented by pyrite (white),  
single liberated pyrite grain (circled)  
Figure 5



0 1mm

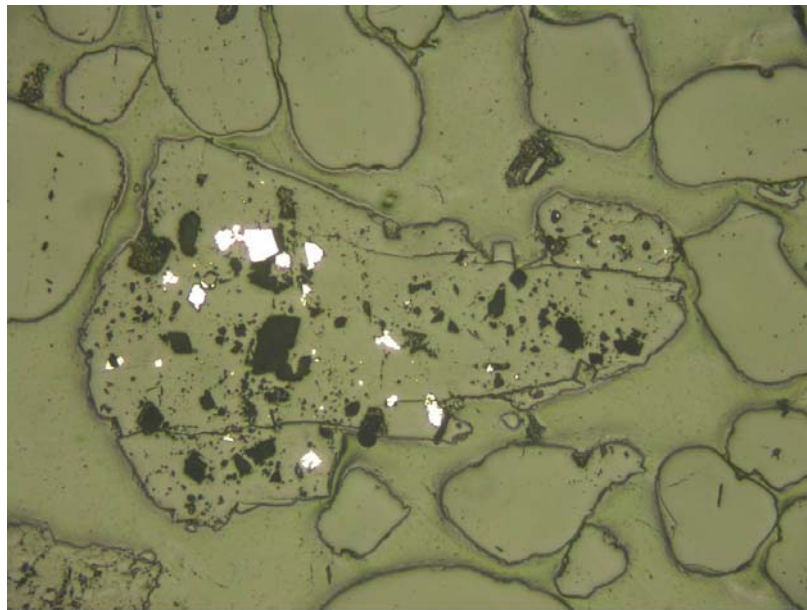
Sample #6  
Medium grained sandstone fragment with pyrite cement (white),  
single liberated pyrite grain (circled)  
Figure 6



Sample #7

Fine grained sandstone fragment with four pyrite (white) grains in the cement matrix

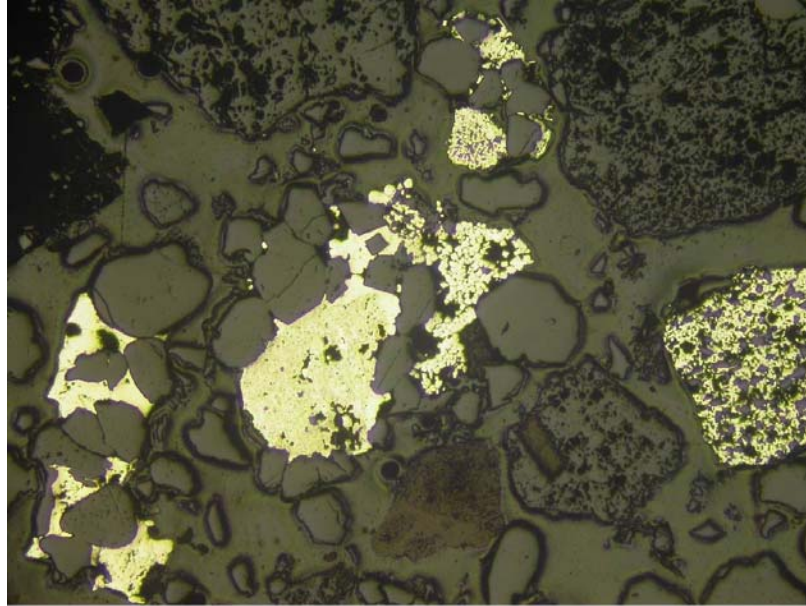
Figure 7



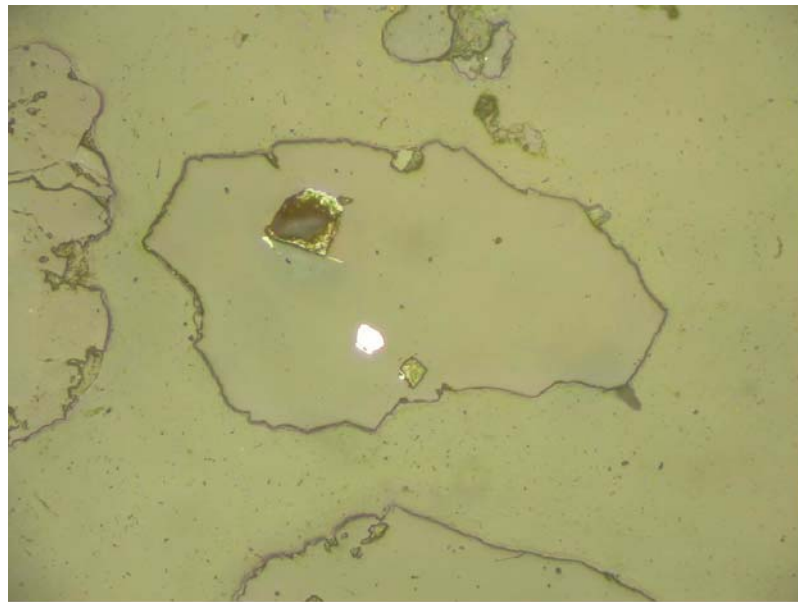
Sample #8

Locked original pyrite as mineral inclusions in a quartz sandstone grain

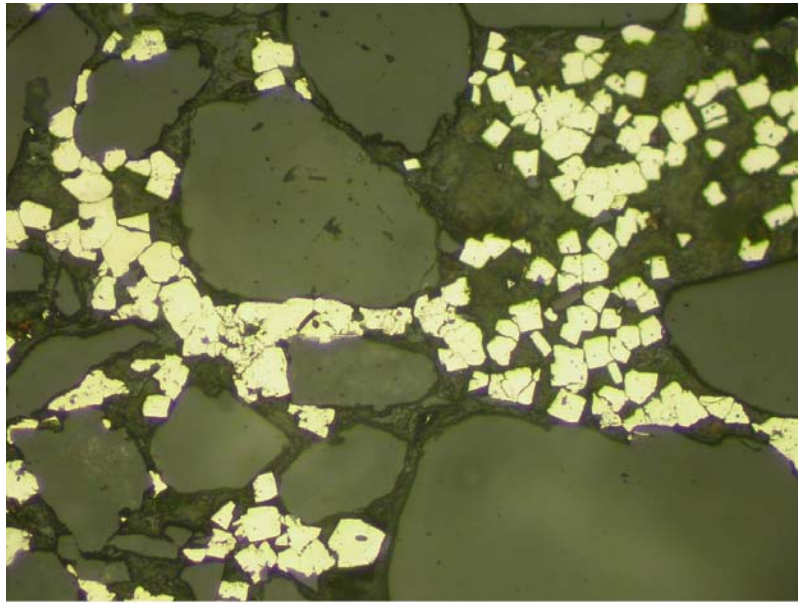
Figure 8



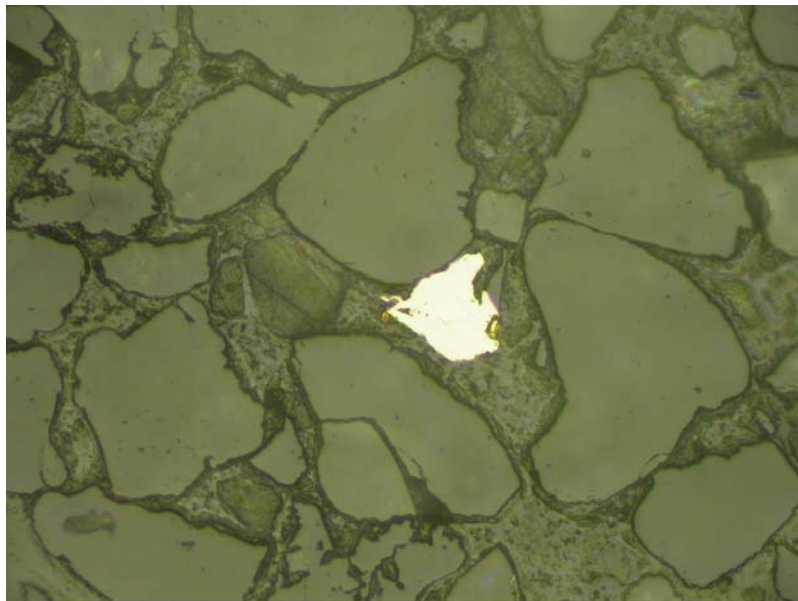
Sample #9  
Massive pyrite (yellow-white) cement  
Figure 9



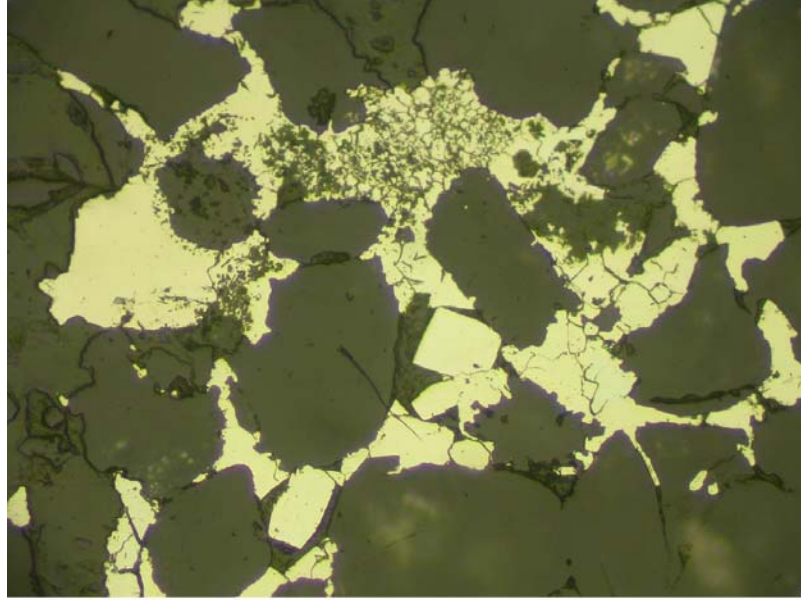
Sample #10  
Locked inclusion of original chalcopyrite in quartz grain  
(magnetite and ilmenite indicate volcanic origin)  
Figure 10



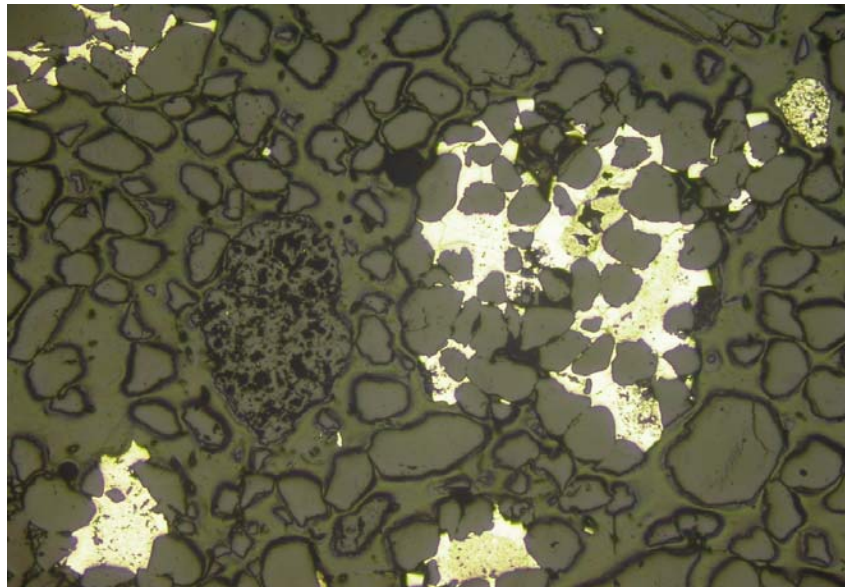
Sample #11  
Cubic euhedral pyrite crystals in matrix of sandstone cement  
Figure 11



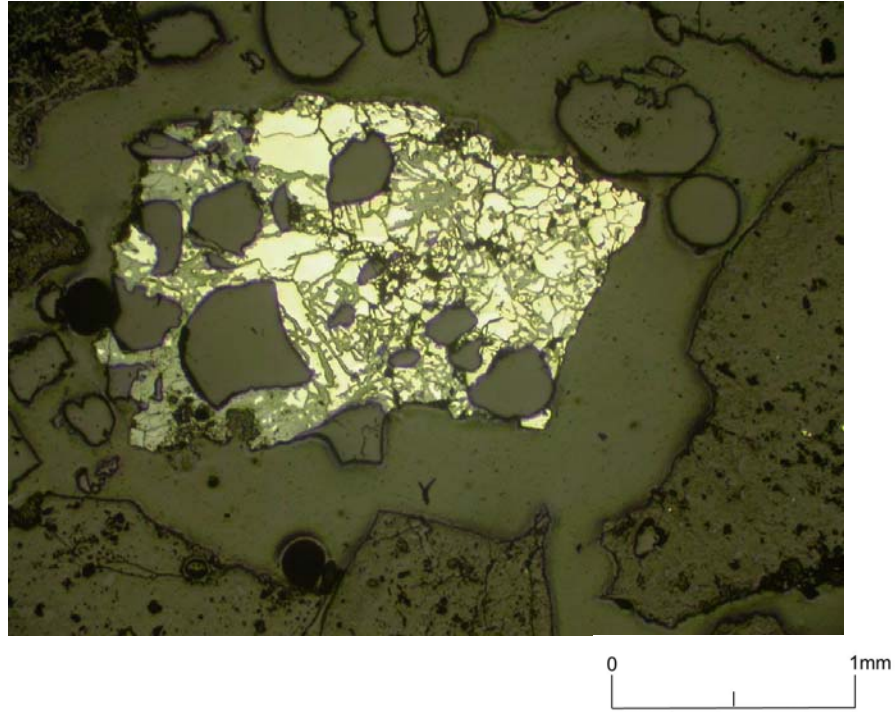
Sample #11  
Liberated grain of chalcopyrite  
Figure 12



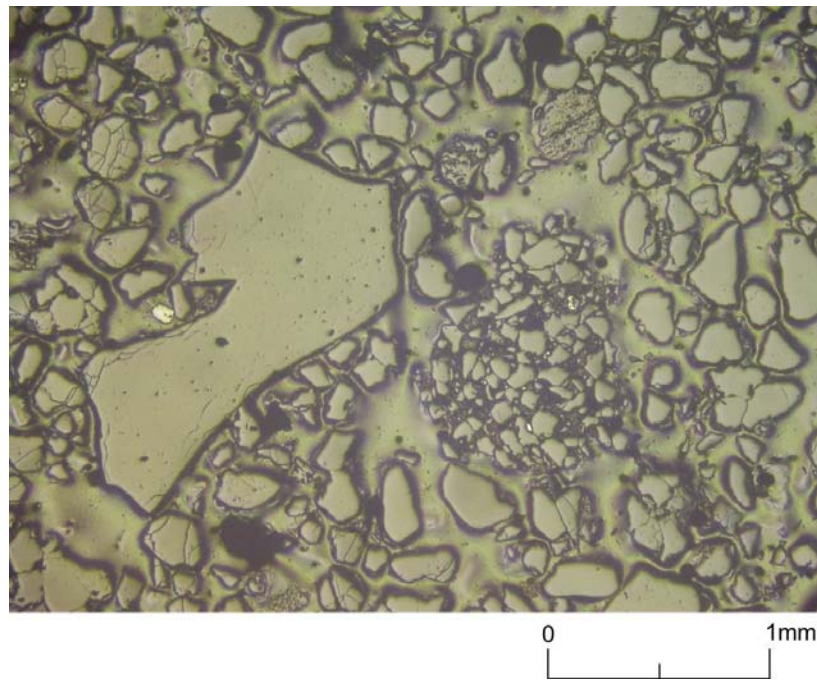
Sample #11  
Massive euhedral cubic pyrite (yellow) cements sandstone grains  
Figure 13



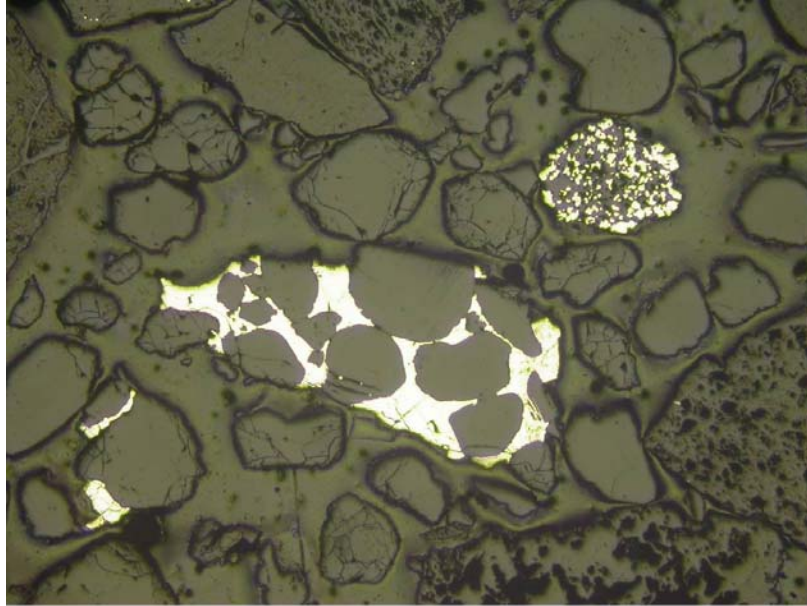
Sample #12  
Massive pyrite as cement between quartz grains,  
Some pyrite (yellow) apparently decomposing  
Figure 14



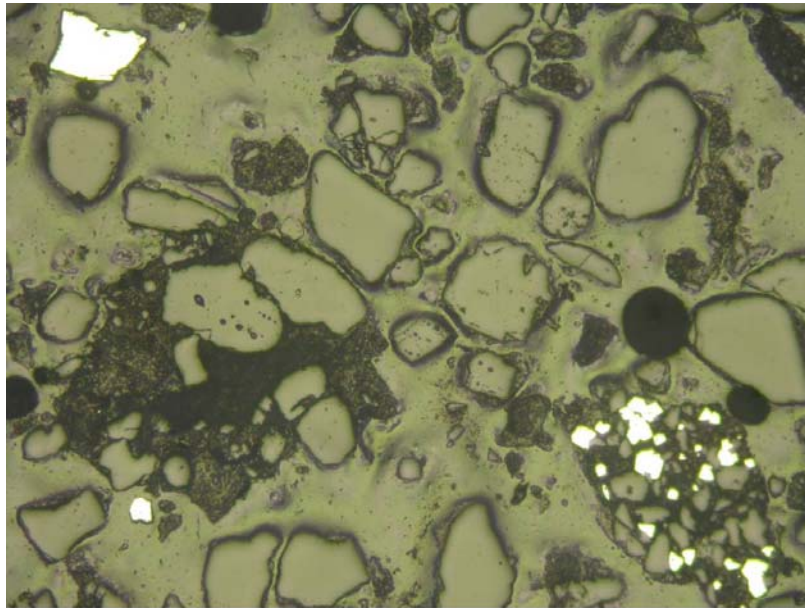
Sample #13  
Large sandstone fragment with pyrite and marcasite cement  
Figure 15



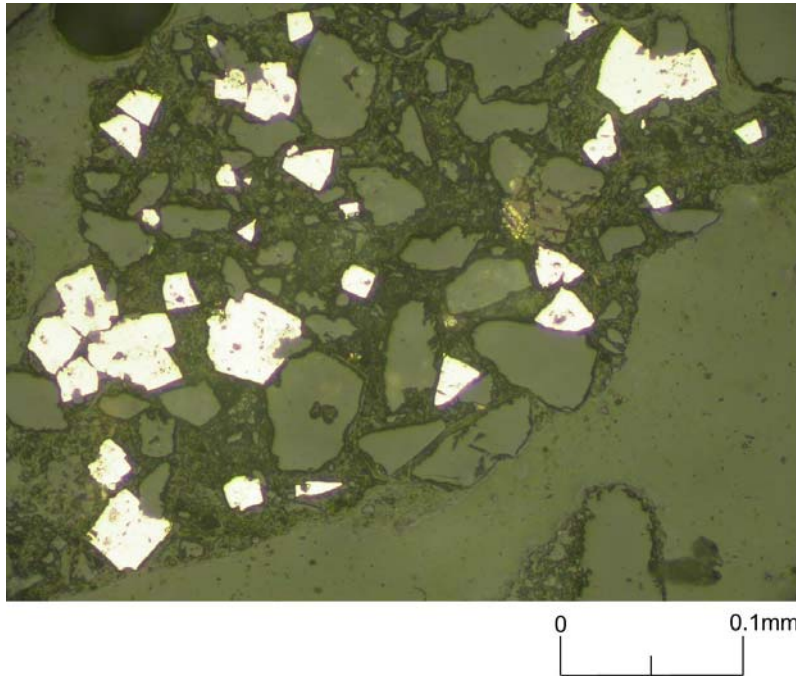
Sample #14  
No sulfides, small iron oxide particle (white) (left center)  
Figure 16



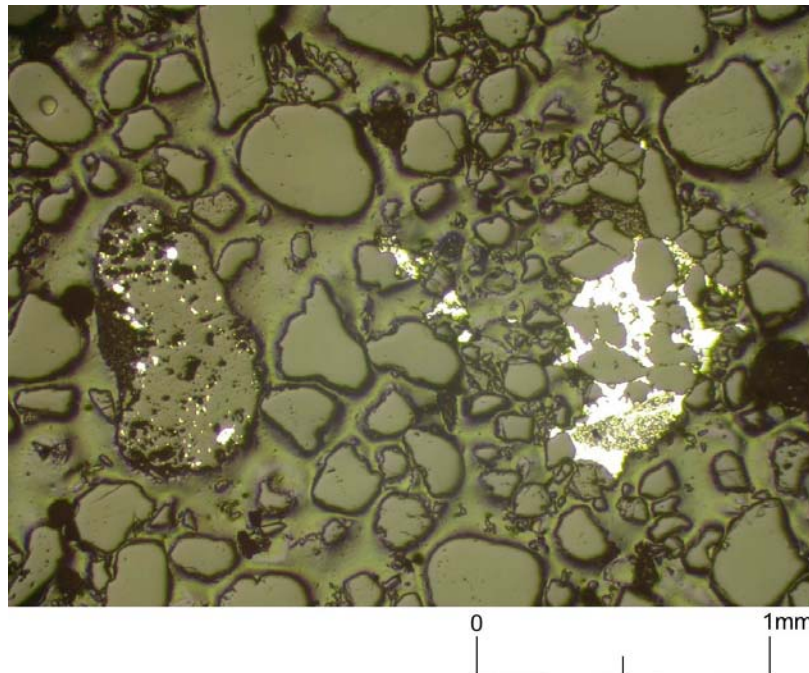
Sample #15  
Medium sandstone fragments with pyrite cement  
Figure 17



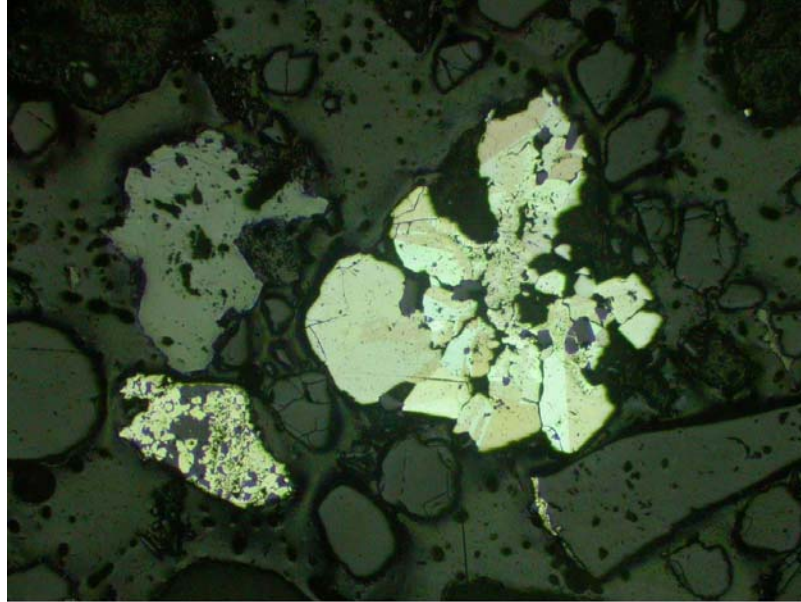
Sample #16  
Liberated pyrite (upper left), sandstone with some pyrite  
Cement (lower right)  
Figure 18



Sample #16  
Euhedral pyrite crystals in the matrix of a sandstone fragment  
Figure 19

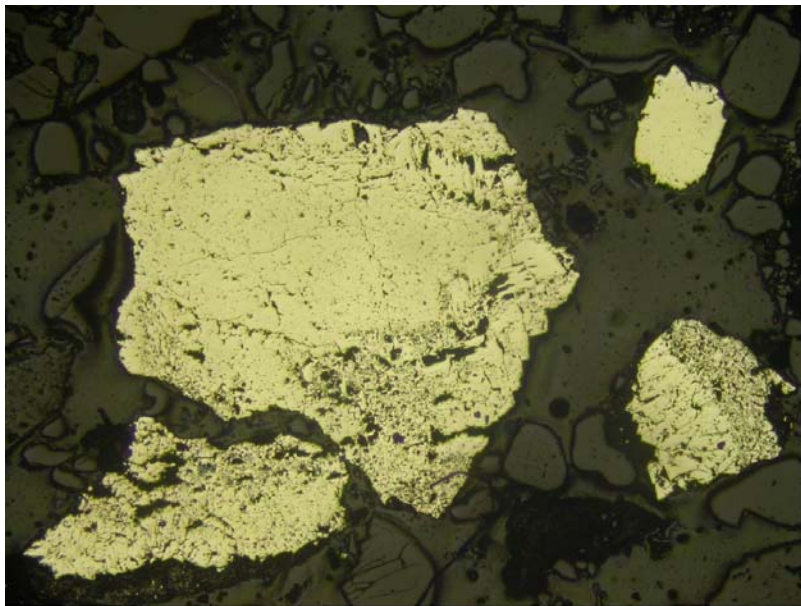


Sample #17  
Massive pyrite cement in sandstone fragment (right),  
original pyrite in quartz grain (left)  
Figure 20



0 1mm

Sample #18  
Rosette body of marcasite, pyrite matrix fragment (lower left)  
under cross polarized light  
Figure 21



0 1mm

Sample #18  
Large fragments of massive pyrite matrix  
Figure 22

RFI# 6036-1-Hum-18  
1 OF 2  
8-21-12

**CHAIN OF CUSTODY RECORD**

		700 Fifth Avenue New Brighton, PA 15066-1837 (724) 843-5000 FAX (724) 843-5353 Lab Manager: Randy Shannon randys@pmet-inc.com		Project Number <b>718000</b>		Project Name <b>ENERGY FUELS, WHITE MESA MILL, UTAH</b>	
PMET Sample ID		Date	Time	Comp.	Grab	No. Containers	Remarks
MW-26	08/17/12					1 BAG	DRILL CUTTINGS (92.5-95 FEET) AKA (TW4-15)
MW-26	08/17/12					1 BAG	DRILL CUTTINGS (95-97.5 FEET) AKA (TW4-15)
MW-34	08/17/12					1 BAG	DRILL CUTTINGS (67.5-70 FEET)
MW-36	08/17/12					1 BAG	DRILL CUTTINGS (87.5-90 FEET)
MW-36	08/17/12					1 BAG	DRILL CUTTINGS (112.5-115 FEET)
MW-37	08/17/12					1 BAG	DRILL CUTTINGS (110-112.5 FEET)
TW4-16	08/17/12					1 BAG	DRILL CUTTINGS (92.5-95 FEET)
TW4-22	08/17/12					1 BAG	DRILL CUTTINGS (90-92.5 FEET)
TWN-5	08/17/12					1 BAG	DRILL CUTTINGS (110-112.5 FEET)
SS-31	08/17/12					1 BAG	DRILL CUTTINGS (0-2.5 FEET) QA/QC SAMPLE
Relinquished by: (Signature)		Date	Time	Received by: (Signature)			
		8-17-12	14:00	 8-21-12			
Relinquished by: (Signature)		Date	Time	Received by: (Signature)			
Relinquished by: (Signature)		Date	Time	Received by: (Signature)			

2 OF 2

**CHAIN OF CUSTODY RECORD**

 <p>700 Fifth Avenue New Brighton, PA 15066-1837 (724) 843-5000 FAX (724) 843-5353 Lab Manager: Randy Shannon randys@pmet-inc.com</p>		<p>Project Number <b>718000</b></p>		<p>Project Name <b>ENERGY FUELS, WHITE MESA MILL, UTAH</b></p>		
<p>Remarks <b>Polished Section and Optical Microscopy</b></p>		<p>Sampler: (Signature) </p>		<p>Date <b>08/17/12</b></p>		
PMET Sample ID	Date	Time	Comp.	Grab	No. Containers	Remarks
TWN-5	08/17/12				1 BAG	DRILL CUTTINGS (112.5-115 FEET)
TWN-8	08/17/12				1 BAG	DRILL CUTTINGS (117.5-120 FEET)
TWN-16	08/17/12				1 BAG	DRILL CUTTINGS (87.5-90 FEET)
TWN-19	08/17/12				1 BAG	DRILL CUTTINGS (82.5-85 FEET)
DR-9	08/17/12				1 BAG	DRILL CUTTINGS (105-107.5 FEET)
DR-12	08/17/12				1 BAG	DRILL CUTTINGS (87.5-90 FEET)
DR-16	08/17/12				1 BAG	DRILL CUTTINGS (97.5-100 FEET)
DR-25	08/17/12				1 BAG	DRILL CUTTINGS (75-77.5 FEET)
XXXXX	XXXXX				XXXXX	XXXXXXXXXXXXXXXXXXXXXXXXXXXX
XXXXX	XXXXX				XXXXX	XXXXXXXXXXXXXXXXXXXXXXXXXXXX
Relinquished by: (Signature)		Date	8-17-12	Time	14:00	Received by: (Signature) 
Relinquished by: (Signature)		Date		Time		Received by: (Signature) <b>8-21-12</b>
Relinquished by: (Signature)		Date		Time		Received by: (Signature)
Relinquished by: (Signature)		Date		Time		Received by: (Signature)

lot 2  
 REF# 6036-19 thru 30  
 8-21-12

**CHAIN OF CUSTODY RECORD**

 700 Fifth Avenue New Brighton, PA 15066-1837 (724) 843-5000 FAX (724) 843-5353 Lab Manager: Randy Shannon randys@pmet-inc.com		Project Name <b>ENERGY FUELS, WHITE MESA MILL, UTAH</b>				
Project Number <b>718000</b>		Remarks <b>XRD and S (quantitative mineral phase analysis)</b>				
Sampler: (Signature) 		Date <b>08/17/12</b>				
PMET Sample ID	Date	Time	Comp.	Grab	No. Containers	Remarks
MW-3A	08/17/12				1 BAG	ROCK CORE (89.5 FEET)
MW-23	08/17/12				1 BAG	ROCK CORE (108 FEET)
MW-24	08/17/12				1 BAG	ROCK CORE (118.5 FEET)
MW-25	08/17/12				1 BAG	DRILL CUTTINGS (65-67.5 FEET)
MW-26	08/17/12				1 BAG	DRILL CUTTINGS (90-92.5 FEET) AKA (TW4-15)
MW-27	08/17/12				1 BAG	DRILL CUTTINGS (80-82.5 FEET)
MW-28	08/17/12				1 BAG	ROCK CORE (88.5 FEET)
MW-29	08/17/12				1 BAG	DRILL CUTTINGS (102-105 FEET)
MW-30	08/17/12				1 BAG	DRILL CUTTINGS (65-67.5 FEET)
MW-31	08/17/12				1 BAG	DRILL CUTTINGS (95-97.5 FEET)
Relinquished by: (Signature)	Date	Time	Received by: (Signature) 			
Relinquished by: (Signature)	8-17-12	14:00	Received by: (Signature) 			
Relinquished by: (Signature)	Date	Time	Received by: (Signature)			
Relinquished by: (Signature)	Date	Time	Received by: (Signature)			



**P**

Pittsburgh

**M**

ineral &

**E**

nvironmental

**T**

echnology, Inc.

October 30, 2012

Mr. Daniel R. Simpson  
Hydro Geo Chem, Inc.  
51 W. Wetmore Road  
Suite 101  
Tucson, AZ 85705

Dear Mr. Simpson:

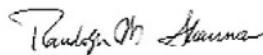
This report summarizes the results of polished section preparation with optical microscopic analysis of three samples associated with your Project No. 718000, Energy Fuels, White Mesa Mill, UT.

The samples were received at PMET's laboratory on October 10, 2012. The work was performed under your P.O. No. 718000 as communicated in your email of July 30, 2012.

The samples were received via FedEx accompanied by a PMET chain of custody record. Each sample was contained in a ziplock bag that was contained in an outer ziplock bag. One of the two bags was marked with the sample identification that corresponded to the sample listing in the chain of custody record which is shown on Page 9. The identification was recorded in PMET's sample logbook under our RFA No. 6056 and the bags were labeled as shown in Table 1 on Page 2. The results of analysis are presented on the following pages.

Mr. Simpson, please contact me by email at [randys@pmet-inc.com](mailto:randys@pmet-inc.com) if you would like to discuss these results. Thank you for using PMET's laboratory services on this project.

Sincerely,



Randolph W. Shannon  
Laboratory Manager

RFA 6056

**700 Fifth Avenue  
New Brighton, PA  
15066  
(724) 843-5000  
FAX: (724) 843-5353  
[www.pmet-inc.com](http://www.pmet-inc.com)**



Table 1  
Sample Identification

PMET I.D.	08/17/12			As-received weight (g)
	HydroGeoChem Label	Type	Depth	
6056-1	TWN-19	Drill Cuttings	87.5-90'	133
6056-2	TWN-22	Drill Cuttings	82.5-85'	146
6056-3	SS-37	Drill Cuttings	0-2.5'	337

All samples were removed from their bags into labeled steel pans and dried in a muffle furnace at 60° C overnight.

The samples were stage crushed to 100% passing a 12 mesh sieve using a ceramic mortar and pestle, then riffle split to obtain an analytical aliquot. The split was embedded in epoxy and a polished section was obtained.

All material remaining after obtaining the analytical aliquot was placed in labeled bags and retained for shipment back to Energy Fuels.

The polished sections were examined for mineralogical composition by ore microscopic techniques with an emphasis on sulfide minerals. The polished sections were examined in detail employing standard reflected polarized light methods. Quantities (volume percent) of sulfide minerals were statistically estimated. Illustrative digital images were obtained from all polished sections and are shown in Figures 1-9 on Pages 4-8. A 20X objective with 0.36 zoom was used yielding a scale of 1cm = 32 micrometers (shown in Figure 10).

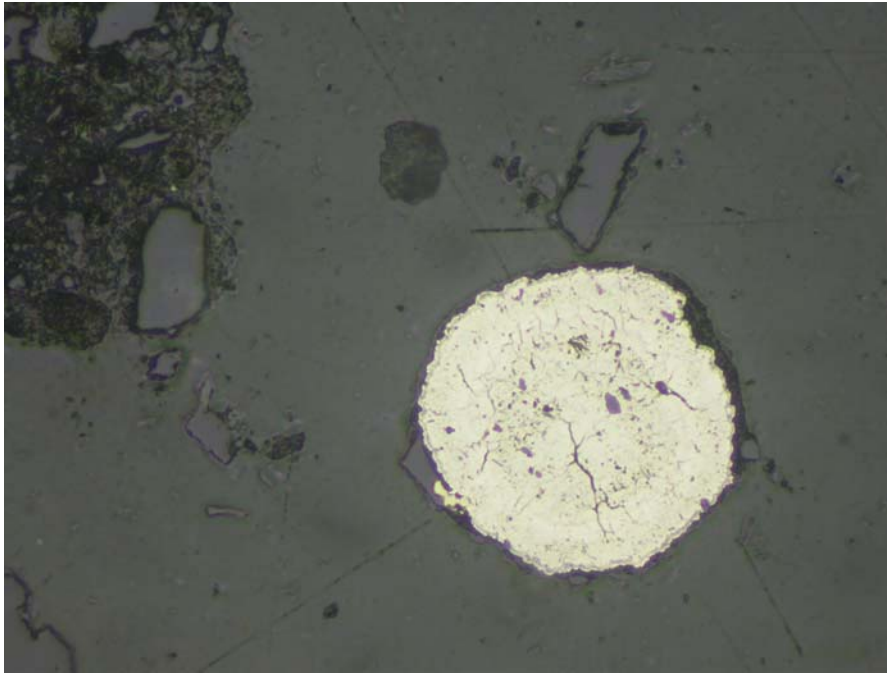
The examination of the polished sections shows that pyrite is the major sulfide ore mineral with associated marcasite. Both form the diagenetic cement between the grains of sandstone.

Pyrite cemented sandstone probably forms thin beds or lenses in this formation. The pyrite usually forms a massive cement that makes it difficult to determine the mineral body size. It is also present as characteristic small cubes in the matrix between the sand grains, for which the size is determined. Marcasite is uncommon, intergrown with pyrite, or forming radial crystal aggregates in spheres (one observation). See Table 2 below for results of sulfide mode of occurrence.

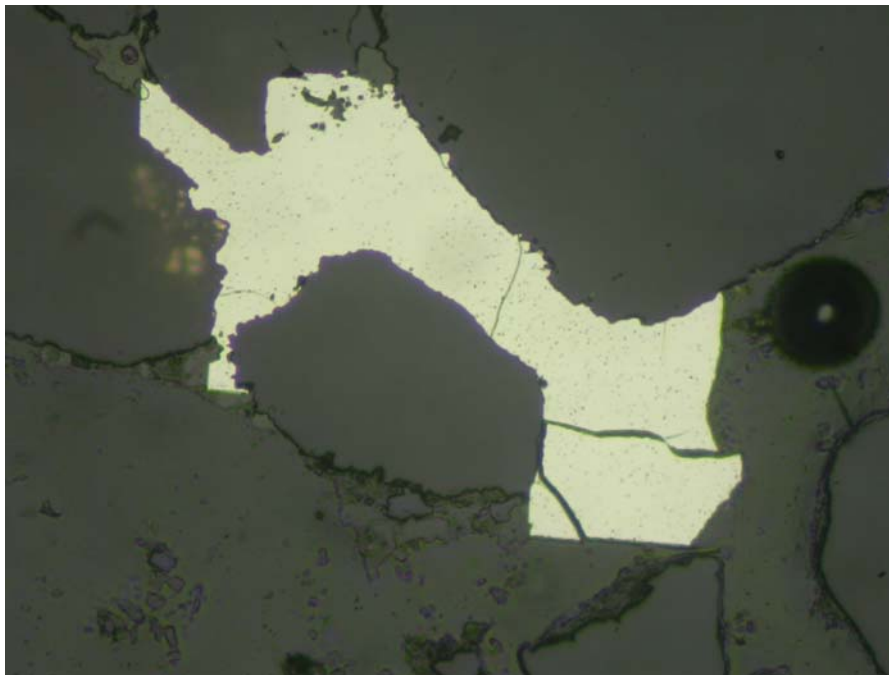
Sample #3 (SS-37) contained only one siltstone fragment with pyrite. This sample is essentially sulfide-free. It is characterized by oxidic ore minerals such as magnetite, hematite, rutile, ilmenite and volcanic rock particles besides quartz.

Table 2  
Sulfide Mineral Determination by Optical Microscopy  
Samples #1 - #3

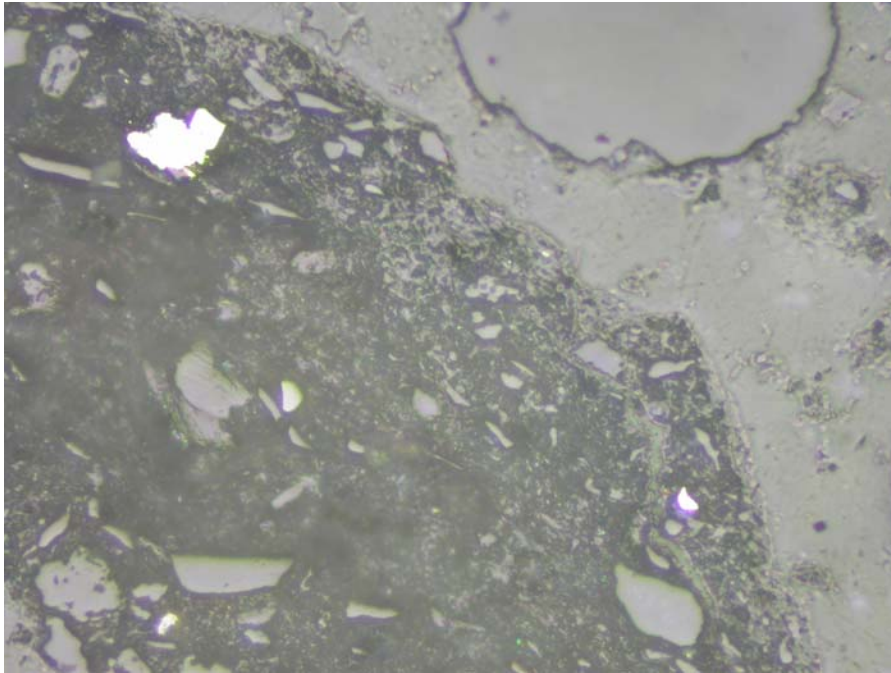
Sample #	Mineral	Vol. %	Size ( $\mu\text{m}$ )		
			Min.	Max.	Mean
1	pyrite	0.16	7.0	168.0	35.5
1	marcasite	0.05		129.5	
2	pyrite	1.18	3.5	434.0	42.1
2	marcasite	0.06	21.0	42.0	36.4
3	pyrite	0.02	7.0	14.0	11.7



Sample #1  
Composite marcasite sphere  
Figure 1

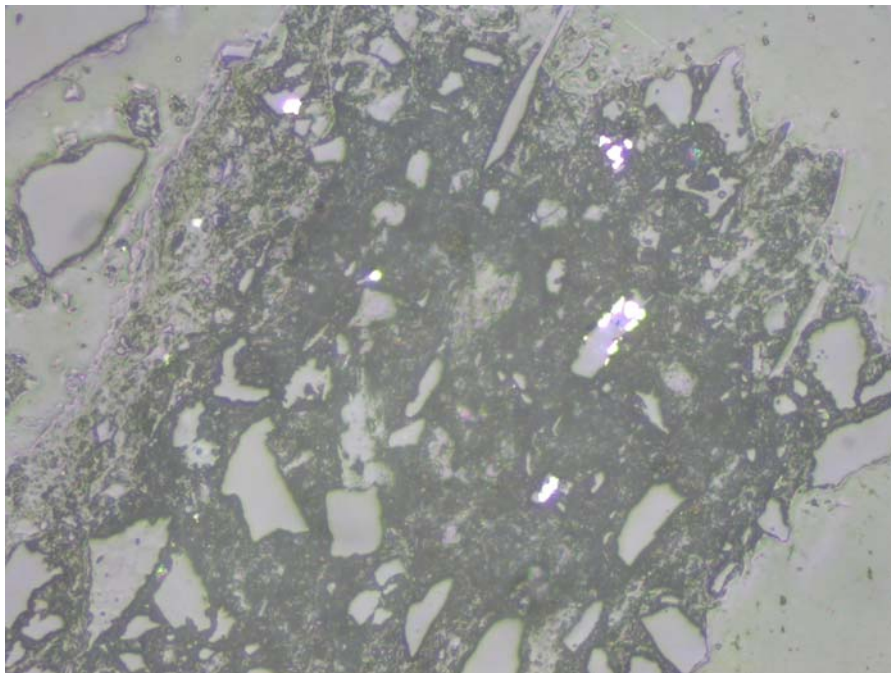


Sample #1  
Quartz grains cemented by massive pyrite  
Figure 2



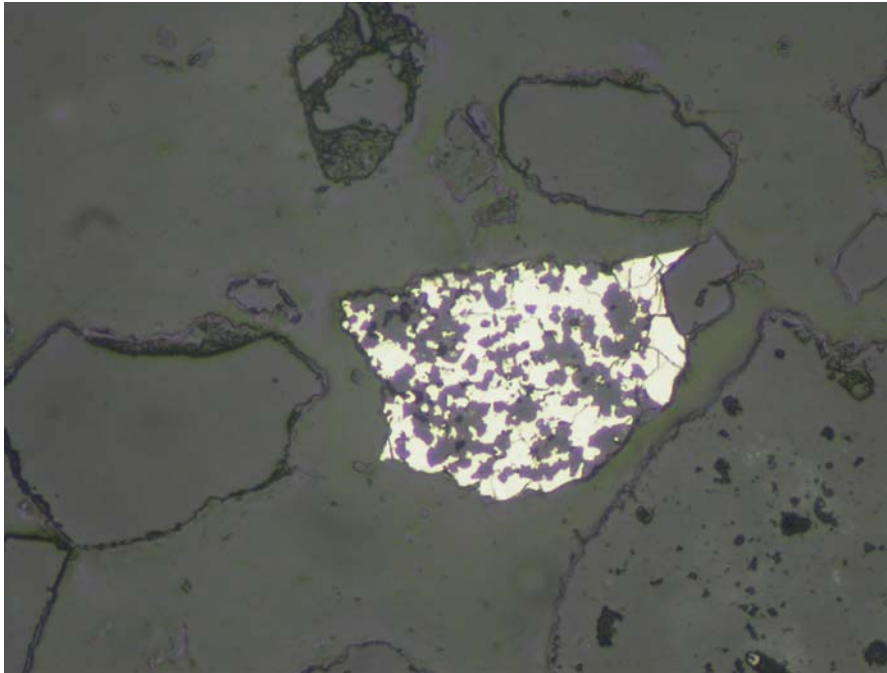
Sample #1  
Siltstone fragment with larger pyrite aggregate (upper left) and  
small pyrite grain (lower right)

Figure 3

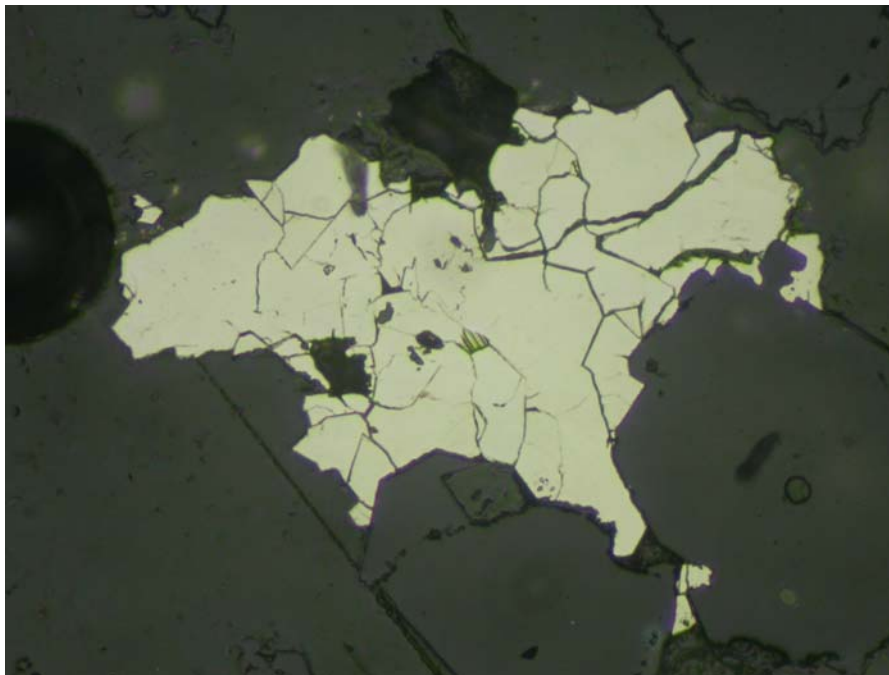


Sample #1  
Siltstone fragment with small white pyrite grains attached to quartz

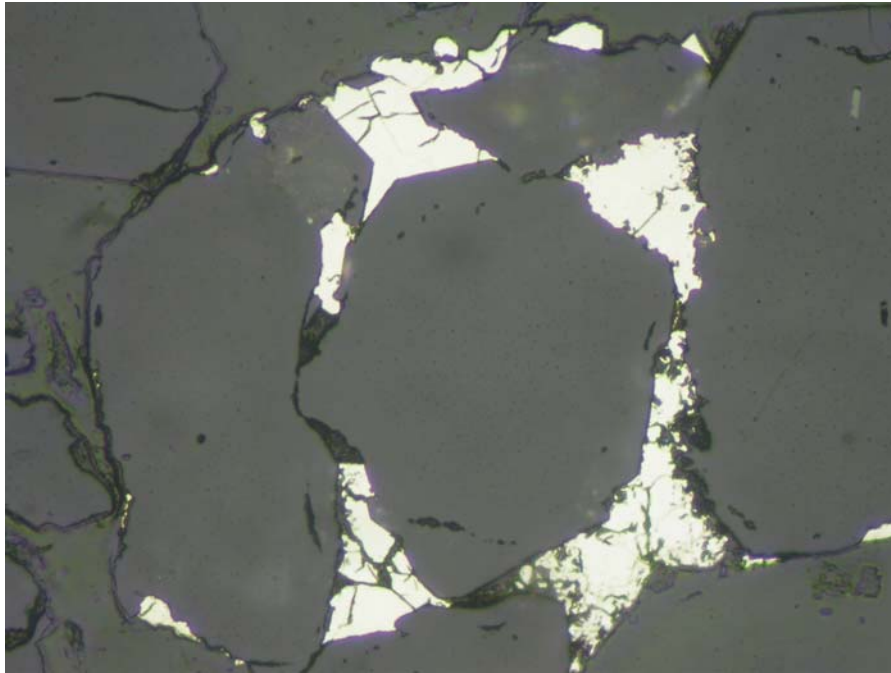
Figure 4



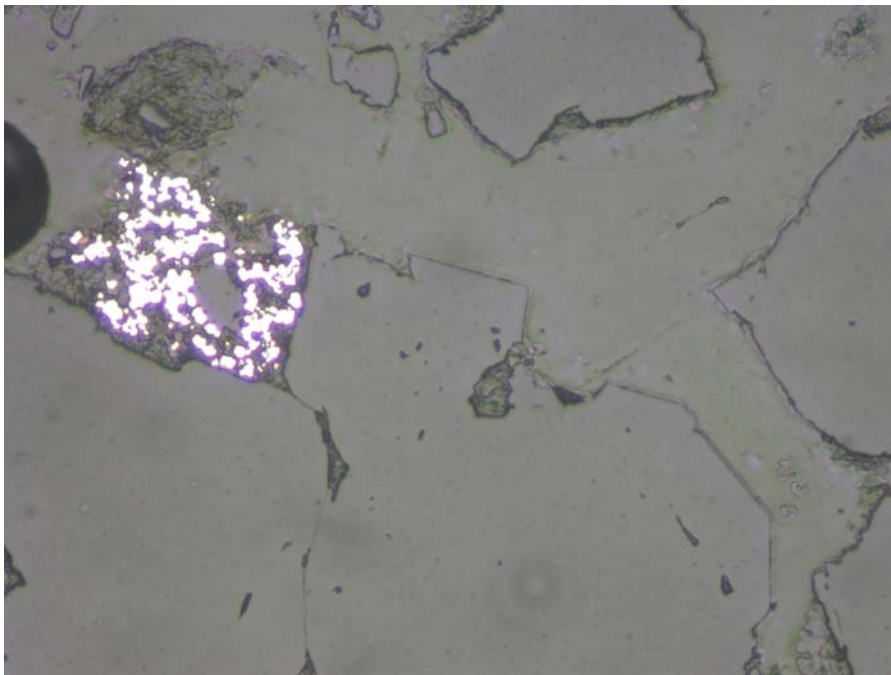
Sample #2  
Pyrite cement enclosing small quartz particles  
Figure 5



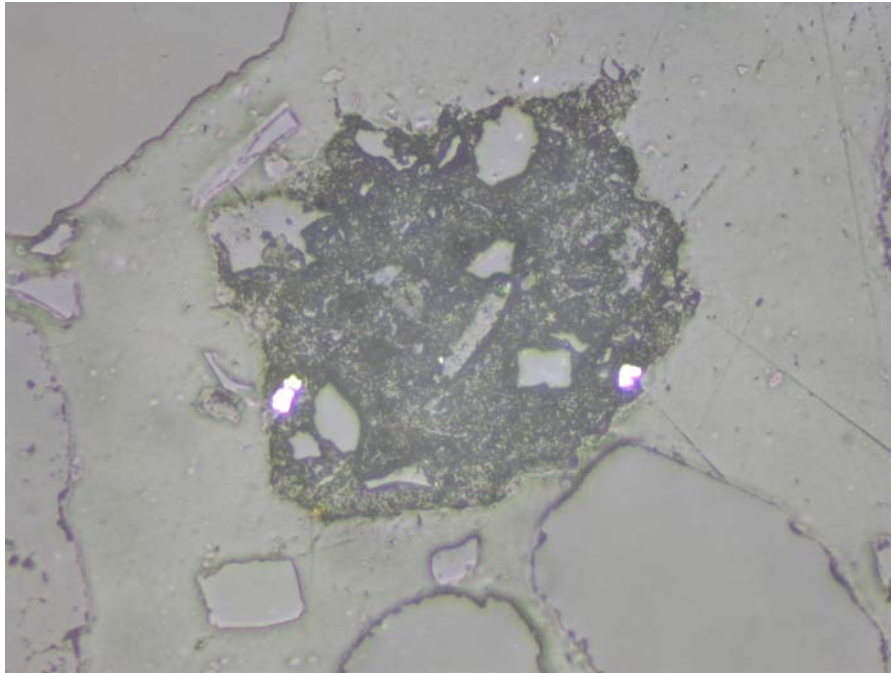
Sample #2  
Massive pyrite cement between quartz sandstone grains  
Figure 6



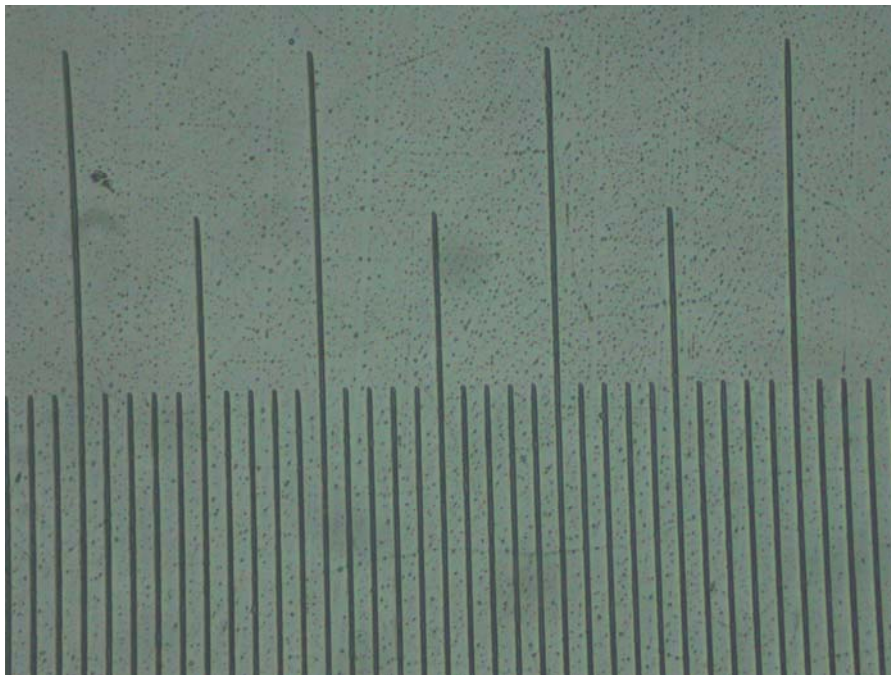
Sample #2  
Massive pyrite cement between quartz sandstone grains  
Figure 7



Sample #2  
Very small pyrite grains in the clay matrix between quartz  
sandstone grains  
Figure 8



Sample #3  
Only siltstone fragment shows two pyrite crystals  
Figure 9



Scale: 1cm = 32 microns  
Figure 10



**APPENDIX C**

**PHREEQC OUTPUT TABLES  
1 THROUGH 6**

**TABLE 1**  
**Initial Aqueous and Solid Phase Concentrations as**  
**Computed by PHREEQC for Anoxic Environment (MW-3A)**

INITIAL SOLUTION 1

-----Solution composition-----

Elements	Molality	Moles
Alkalinity	6.35E-03	1.14E-03
Ca	7.52E-03	1.35E-03
S(6)	3.56E-02	6.41E-03

-----Description of solution-----

pH = 6.850  
 pe = 4.000  
 Activity of water = 0.999  
 Ionic strength = 7.404e-02  
 Mass of water (kg) = 1.800e-01  
 Total carbon (mol/kg) = 8.028e-03  
 Total CO2 (mol/kg) = 8.028e-03  
 Temperature (deg C) = 20.000  
 Electrical balance (eq) = -1.127e-02  
 Percent error, 100\*(Cat-|An|)/(Cat+|An|) = -81.06  
 Iterations = 5  
 Total H = 1.998338e+01  
 Total O = 1.002081e+01

-----Distribution of species-----

Species	Molality	Log Activity	Log Molality	Log Activity	Gamma
H+	1.684E-07	1.413E-07	-6.774	-6.850	-0.076
OH-	6.002E-08	4.803E-08	-7.222	-7.319	-0.097
H2O	5.551E+01	9.992E-01	1.744	0.000	0.000
C(4)	8.028E-03				
HCO3-	6.225E-03	5.027E-03	-2.206	-2.299	-0.093
CO2	1.683E-03	1.712E-03	-2.774	-2.766	0.007
CaHCO3+	1.135E-04	9.084E-05	-3.945	-4.042	-0.097
CO3-2	3.523E-06	1.499E-06	-5.453	-5.824	-0.371
CaCO3	3.476E-06	3.536E-06	-5.459	-5.452	0.007
Ca	7.516E-03				
CaSO4	3.799E-03	3.865E-03	-2.420	-2.413	0.007
Ca+2	3.599E-03	1.542E-03	-2.444	-2.812	-0.368
CaHCO3+	1.135E-04	9.084E-05	-3.945	-4.042	-0.097
CaCO3	3.476E-06	3.536E-06	-5.459	-5.452	0.007
CaHSO4+	3.767E-09	3.014E-09	-8.424	-8.521	-0.097
CaOH+	2.263E-09	1.810E-09	-8.645	-8.742	-0.097
H(0)	2.922E-25				

Species	Molality	Log Activity	Log Molality	Log Activity	Gamma
H2	1.461E-25	1.486E-25	-24.835	-24.828	0.007
O(0)	0.000E+00				
O2	0.000E+00	0.000E+00	-44.373	-44.366	0.007
S(6)	3.563E-02				
SO4-2	3.183E-02	1.317E-02	-1.497	-1.880	-0.383
CaSO4	3.799E-03	3.865E-03	-2.420	-2.413	0.007
HSO4-	2.032E-07	1.626E-07	-6.692	-6.789	-0.097
CaHSO4+	3.767E-09	3.014E-09	-8.424	-8.521	-0.097

-----Saturation indices-----

Phase	SI Log	IAP Log	KT
Anhydrite	-0.35	-4.69	-4.34 CaSO4
Aragonite	-0.33	-8.64	-8.31 CaCO3
Calcite	-0.18	-8.64	-8.45 CaCO3
CO2(g)	-1.36	-2.77	-1.41 CO2
Fix_H+	-6.85	-6.85	0.00 H+
Gypsum	-0.11	-4.69	-4.58 CaSO4:2H2O
H2(g)	-21.70	-24.83	-3.13 H2
H2O(g)	-1.64	0.00	1.64 H2O
O2(g)	-41.51	-44.37	-2.85 O2
Portlandite	-12.30	10.89	23.19 Ca(OH)2

-----  
Beginning of batch-reaction calculations.  
-----

Reaction step 1.

Using solution 1.

Using pure phase assemblage 1.

-----Phase assemblage-----

Moles in Assemblage

Phase	SI Log	IAP Log	KT	Initial	Final	Delta
Fix_H+	-6.85	-6.85	0.00	1.000E+01	1.000E+01	1.357E-09
Gypsum	-0.11	-4.69	-4.58	0.000E+00	0.000E+00	0.000E+00
Hematite	-5.33	-8.95	-3.62	0.000E+00	0.000E+00	0.000E+00
Pyrite	0.00	-18.62	-18.62	8.400E-04	8.400E-04	-4.001E-10

-----Solution composition-----

Elements	Molality	Moles
C	8.028E-03	1.445E-03
Ca	7.516E-03	1.353E-03
Fe	2.223E-09	4.001E-10
S	3.563E-02	6.414E-03

-----Description of solution-----

pH = 6.850 Charge balance  
 pe = -2.514 Adjusted to redox equilibrium  
 Activity of water = 0.999  
 Ionic strength = 7.404e-02  
 Mass of water (kg) = 1.800e-01  
 Total alkalinity (eq/kg) = 6.352e-03  
 Total CO2 (mol/kg) = 8.028e-03  
 Temperature (deg C) = 20.000  
 Electrical balance (eq) = -1.127e-02  
 Percent error,  $100 \times (\text{Cat} - |\text{An}|) / (\text{Cat} + |\text{An}|) = -81.06$   
 Iterations = 19  
 Total H = 1.998338e+01  
 Total O = 1.002081e+01

-----Distribution of species-----

Species	Molality	Log Activity	Log Molality	Log Activity	Gamma
H+	1.684E-07	1.413E-07	-6.774	-6.850	-0.076
OH-	6.002E-08	4.803E-08	-7.222	-7.319	-0.097
H2O	5.551E+01	9.992E-01	1.744	0.000	0.000
C(-4)	4.162E-13				
CH4	4.162E-13	4.234E-13	-12.381	-12.373	0.007
C(4)	8.028E-03				
HCO3-	6.225E-03	5.027E-03	-2.206	-2.299	-0.093
CO2	1.683E-03	1.712E-03	-2.774	-2.766	0.007
CaHCO3+	1.135E-04	9.084E-05	-3.945	-4.042	-0.097
CO3-2	3.523E-06	1.499E-06	-5.453	-5.824	-0.371
CaCO3	3.476E-06	3.536E-06	-5.459	-5.452	0.007
FeHCO3+	2.684E-10	2.148E-10	-9.571	-9.668	-0.097
FeCO3	1.510E-11	1.536E-11	-10.821	-10.814	0.007
Ca	7.516E-03				
CaSO4	3.799E-03	3.865E-03	-2.420	-2.413	0.007
Ca+2	3.599E-03	1.542E-03	-2.444	-2.812	-0.368
CaHCO3+	1.135E-04	9.084E-05	-3.945	-4.042	-0.097
CaCO3	3.476E-06	3.536E-06	-5.459	-5.452	0.007
CaHSO4+	3.767E-09	3.014E-09	-8.424	-8.521	-0.097
CaOH+	2.263E-09	1.810E-09	-8.645	-8.742	-0.097
Fe(2)	2.223E-09				

Species	Molality	Log Activity	Log Molality	Log Activity	Gamma
Fe+2	1.042E-09	4.272E-10	-8.982	-9.369	-0.387
FeSO4	8.963E-10	9.118E-10	-9.048	-9.040	0.007
FeHCO3+	2.684E-10	2.148E-10	-9.571	-9.668	-0.097
FeCO3	1.510E-11	1.536E-11	-10.821	-10.814	0.007
FeOH+	8.167E-13	6.535E-13	-12.088	-12.185	-0.097
FeHSO4+	1.043E-15	8.349E-16	-14.982	-15.078	-0.097
Fe(OH)2	2.486E-17	2.528E-17	-16.605	-16.597	0.007
Fe(HS)2	4.480E-19	4.557E-19	-18.349	-18.341	0.007
Fe(OH)3-	7.900E-21	6.321E-21	-20.102	-20.199	-0.097
Fe(HS)3-	6.785E-26	5.429E-26	-25.168	-25.265	-0.097
Fe(3)	1.219E-17				
Fe(OH)2+	7.718E-18	6.175E-18	-17.113	-17.209	-0.097
Fe(OH)3	4.432E-18	4.509E-18	-17.353	-17.346	0.007
Fe(OH)4-	2.963E-20	2.371E-20	-19.528	-19.625	-0.097
FeOH+2	7.799E-21	3.197E-21	-20.108	-20.495	-0.387
FeSO4+	1.523E-23	1.219E-23	-22.817	-22.914	-0.097
Fe(SO4)2-	4.302E-24	3.443E-24	-23.366	-23.463	-0.097
Fe+3	7.023E-25	9.444E-26	-24.153	-25.025	-0.871
FeHSO4+2	1.131E-29	4.636E-30	-28.947	-29.334	-0.387
Fe2(OH)2+4	1.202E-38	3.395E-40	-37.920	-39.469	-1.549
Fe3(OH)4+5	0.000E+00	0.000E+00	-51.734	-54.155	-2.421
H(0)	3.123E-12				
H2	1.562E-12	1.588E-12	-11.806	-11.799	0.007
O(0)	0.000E+00				
O2	0.000E+00	0.000E+00	-70.431	-70.424	0.007
S(-2)	2.953E-09				
H2S	1.554E-09	1.581E-09	-8.808	-8.801	0.007
HS-	1.367E-09	1.094E-09	-8.864	-8.961	-0.097
S5-2	2.776E-12	1.506E-12	-11.557	-11.822	-0.266
S6-2	1.789E-12	1.019E-12	-11.747	-11.992	-0.245
S4-2	1.696E-12	8.685E-13	-11.771	-12.061	-0.291
S-2	1.611E-15	6.603E-16	-14.793	-15.180	-0.387
S3-2	6.280E-16	2.999E-16	-15.202	-15.523	-0.321
S2-2	3.687E-17	1.654E-17	-16.433	-16.781	-0.348
Fe(HS)2	4.480E-19	4.557E-19	-18.349	-18.341	0.007
Fe(HS)3-	6.785E-26	5.429E-26	-25.168	-25.265	-0.097
S(6)	3.563E-02				
SO4-2	3.183E-02	1.317E-02	-1.497	-1.880	-0.383
CaSO4	3.799E-03	3.865E-03	-2.420	-2.413	0.007
HSO4-	2.032E-07	1.626E-07	-6.692	-6.789	-0.097
CaHSO4+	3.767E-09	3.014E-09	-8.424	-8.521	-0.097
FeSO4	8.963E-10	9.118E-10	-9.048	-9.040	0.007
FeHSO4+	1.043E-15	8.349E-16	-14.982	-15.078	-0.097
FeSO4+	1.523E-23	1.219E-23	-22.817	-22.914	-0.097
Fe(SO4)2-	4.302E-24	3.443E-24	-23.366	-23.463	-0.097

Species	Molality	Log Activity	Log Molality	Log Activity	Gamma
FeHSO4+2	1.131E-29	4.636E-30	-28.947	-29.334	-0.387

-----Saturation indices-----

Phase	SI Log	IAP Log	KT
Anhydrite	-0.35	-4.69	-4.34 CaSO4
Aragonite	-0.33	-8.64	-8.31 CaCO3
Calcite	-0.18	-8.64	-8.45 CaCO3
CH4(g)	-9.56	-12.37	-2.82 CH4
CO2(g)	-1.36	-2.77	-1.41 CO2
Fe(OH)3(a)	-9.37	-4.48	4.89 Fe(OH)3
Fe3(OH)8	-24.84	-4.62	20.22 Fe3(OH)8
FeS(ppt)	-7.57	-11.48	-3.92 FeS
Fix_H+	-6.85	-6.85	0.00 H+
Goethite	-3.66	-4.48	-0.82 FeOOH
Greigite	-22.83	-67.86	-45.04 Fe3S4
Gypsum	-0.11	-4.69	-4.58 CaSO4:2H2O
H2(g)	-8.67	-11.80	-3.13 H2
H2O(g)	-1.64	0.00	1.64 H2O
H2S(g)	-7.86	-8.80	-0.94 H2S
Hematite	-5.33	-8.95	-3.62 Fe2O3
JarositeH	-39.89	-44.59	-4.70 (H3O)Fe3(SO4)2(OH)6
Mackinawite	-6.83	-11.48	-4.65 FeS
Maghemite	-15.34	-8.95	6.39 Fe2O3
Magnetite	-8.99	-4.62	4.37 Fe3O4
Melanterite	-8.98	-11.25	-2.27 FeSO4:7H2O
O2(g)	-67.57	-70.42	-2.85 O2
Portlandite	-12.30	10.89	23.19 Ca(OH)2
Pyrite	0.00	-18.62	-18.62 FeS2
Siderite	-4.33	-15.19	-10.86 FeCO3
Siderite(d)(3)	-4.74	-15.19	-10.45 FeCO3
Sulfur	-5.08	-20.21	-15.12 S

**TABLE 2**  
**Final Aqueous and Solid Phase Concentrations as Calculated**  
**by PHREEQC for 10 Liter Air Exposure (MW-3A)**

INITIAL SOLUTION 1

-----Solution composition-----

**Elements Molality Moles**

Alkalinity	6.355E-03	1.144E-03
Ca	1.196E-02	2.152E-03
S(6)	3.910E-02	7.039E-03

-----Description of solution-----

pH = 6.430  
pe = 4.000  
Activity of water = 0.999  
Ionic strength = 8.092e-02  
Mass of water (kg) = 1.800e-01  
Total carbon (mol/kg) = 1.071e-02  
Total CO2 (mol/kg) = 1.071e-02  
Temperature (deg C) = 20.000  
Electrical balance (eq) = -1.092e-02  
Percent error, 100\*(Cat-|An|)/(Cat+|An|) = -72.12  
Iterations = 7  
Total H = 1.998338e+01  
Total O = 1.002427e+01

-----Distribution of species-----

Species	Molality	Log Activity	Log Molality	Log Activity	Gamma
H+	4.448E-07	3.715E-07	-6.352	-6.430	-0.078
OH-	2.296E-08	1.826E-08	-7.639	-7.739	-0.100
H2O	5.551E+01	9.991E-01	1.744	0.000	0.000
C(4)	1.071E-02				
HCO3-	6.173E-03	4.954E-03	-2.209	-2.305	-0.096
CO2	4.356E-03	4.438E-03	-2.361	-2.353	0.008
CaHCO3+	1.762E-04	1.401E-04	-3.754	-3.854	-0.100
CaCO3	2.035E-06	2.073E-06	-5.691	-5.683	0.008
CO3-2	1.354E-06	5.615E-07	-5.868	-6.251	-0.382
Ca	1.196E-02				
CaSO4	6.004E-03	6.117E-03	-2.222	-2.213	0.008
Ca+2	5.774E-03	2.414E-03	-2.239	-2.617	-0.379
CaHCO3+	1.762E-04	1.401E-04	-3.754	-3.854	-0.100

Species	Molality	Log Activity	Log Molality	Log Activity	Gamma
CaCO3	2.035E-06	2.073E-06	-5.691	-5.683	0.008
CaHSO4+	1.578E-08	1.255E-08	-7.802	-7.901	-0.100
CaOH+	1.355E-09	1.077E-09	-8.868	-8.968	-0.100
H(0)	2.018E-24				
H2	1.009E-24	1.028E-24	-23.996	-23.988	0.008
O(0)	0.000E+00				
O2	0.000E+00	0.000E+00	-46.054	-46.046	0.008
S(6)	3.910E-02				
SO4-2	3.310E-02	1.332E-02	-1.480	-1.876	-0.395
CaSO4	6.004E-03	6.117E-03	-2.222	-2.213	0.008
HSO4-	5.438E-07	4.324E-07	-6.265	-6.364	-0.100
CaHSO4+	1.578E-08	1.255E-08	-7.802	-7.901	-0.100

-----Saturation indices-----

Phase	SI Log	IAP Log	Kt
Anhydrite	-0.15	-4.49	-4.34 CaSO4
Aragonite	-0.56	-8.87	-8.31 CaCO3
Calcite	-0.41	-8.87	-8.45 CaCO3
CO2(g)	-0.95	-2.35	-1.41 CO2
Fix_H+	-6.43	-6.43	0.00 H+
Gypsum	0.09	-4.49	-4.58 CaSO4:2H2O
H2(g)	-20.86	-23.99	-3.13 H2
H2O(g)	-1.64	0.00	1.64 H2O
O2(g)	-43.19	-46.05	-2.85 O2
Portlandite	-12.95	10.24	23.19 Ca(OH)2

-----  
Beginning of batch-reaction calculations.  
-----

Reaction step 1.

Using solution 1.

Using pure phase assemblage 1.

Using gas phase 1.

-----Gas phase-----

Total pressure: 0.0048 atmospheres  
Gas volume: 1.00e+01 liters

Moles in gas

Component	Log P	P	Initial	Final	Data
CO2(g)	-2.32	4.837E-03	1.663E-04	2.011E-03	1.844E-03
O2(g)	-66.4	4.001E-67	8.314E-02	0.000E+00	-8.314E-02

-----Phase assemblage-----

Moles in assemblage

Phase	SI Log	IAP Log	KT	Initial	Final	Data
Fix_H+	-6.43	-6.43	0.00	1.000E+01	9.672E+00	-3.285E-01
Gypsum	0.00	-4.58	-4.58	0.000E+00	4.381E-04	4.381E-04
Hematite	0.00	-3.62	-3.62	0.000E+00	1.367E-04	1.367E-04
Pyrite	0.00	-18.62	-18.62	8.400E-04	5.660E-04	-2.740E-04

-----Solution composition-----

**Elements Molality Moles**

C	4.550E-04	8.324E-05
Ca	9.369E-03	1.714E-03
Fe	3.278E-06	5.997E-07
S	3.907E-02	7.148E-03

-----Description of solution-----

pH = 6.430 Charge balance  
pe = -1.802 Adjusted to redox equilibrium  
Activity of water = 0.999  
Ionic strength = 7.736e-02  
Mass of water (kg) = 1.830e-01  
Total alkalinity (eq/kg) = 2.679e-04  
Total CO2 (mol/kg) = 4.550e-04  
Temperature (deg C) = 20.000  
Electrical balance (eq) = -1.092e-02  
Percent error,  $100 * (\text{Cat} - |\text{An}|) / (\text{Cat} + |\text{An}|) = -77.00$   
Iterations = 11  
Total H = 2.031008e+01  
Total O = 1.018382e+01

-----Distribution of species-----

Species	Molality	Log Activity	Log Molality	Log Activity	Gamma
H+	4.438E-07	3.715E-07	-6.353	-6.430	-0.077
OH-	2.289E-08	1.826E-08	-7.640	-7.739	-0.098
H2O	5.551E+01	9.993E-01	1.744	0.000	0.000
C(-4)	2.089E-16				
CH4	2.089E-16	2.127E-16	-15.680	-15.672	0.008
C(4)	4.550E-04				
HCO3-	2.628E-04	2.116E-04	-3.580	-3.675	-0.094
CO2	1.862E-04	1.895E-04	-3.730	-3.722	0.008
CaHCO3+	5.857E-06	4.672E-06	-5.232	-5.331	-0.098
CaCO3	6.792E-08	6.914E-08	-7.168	-7.160	0.008
CO3-2	5.709E-08	2.398E-08	-7.243	-7.620	-0.377
FeHCO3+	1.843E-08	1.470E-08	-7.734	-7.833	-0.098
FeCO3	3.927E-10	3.998E-10	-9.406	-9.398	0.008
Ca	9.369E-03				
CaSO4	4.911E-03	4.999E-03	-2.309	-2.301	0.008
Ca+2	4.452E-03	1.885E-03	-2.351	-2.725	-0.373
CaHCO3+	5.857E-06	4.672E-06	-5.232	-5.331	-0.098
CaCO3	6.792E-08	6.914E-08	-7.168	-7.160	0.008
CaHSO4+	1.286E-08	1.025E-08	-7.891	-7.989	-0.098
CaOH+	1.055E-09	8.412E-10	-8.977	-9.075	-0.098
Fe(2)	3.278E-06				
Fe+2	1.717E-06	6.949E-07	-5.765	-6.158	-0.393
FeSO4	1.542E-06	1.570E-06	-5.812	-5.804	0.008
FeHCO3+	1.843E-08	1.470E-08	-7.734	-7.833	-0.098
FeOH+	5.067E-10	4.042E-10	-9.295	-9.393	-0.098
FeCO3	3.927E-10	3.998E-10	-9.406	-9.398	0.008
FeHSO4+	4.740E-12	3.781E-12	-11.324	-11.422	-0.098
Fe(OH)2	5.840E-15	5.945E-15	-14.234	-14.226	0.008
Fe(OH)3-	7.085E-19	5.651E-19	-18.150	-18.248	-0.098
Fe(HS)2	1.162E-19	1.183E-19	-18.935	-18.927	0.008
Fe(HS)3-	2.232E-28	1.780E-28	-27.651	-27.750	-0.098
Fe(3)	1.147E-14				
Fe(OH)2+	9.399E-15	7.497E-15	-14.027	-14.125	-0.098
Fe(OH)3	2.044E-15	2.081E-15	-14.689	-14.682	0.008
FeOH+2	2.522E-17	1.021E-17	-16.598	-16.991	-0.393
Fe(OH)4-	5.217E-18	4.161E-18	-17.283	-17.381	-0.098
FeSO4+	1.358E-19	1.083E-19	-18.867	-18.965	-0.098
Fe(SO4)2-	4.061E-20	3.239E-20	-19.391	-19.490	-0.098
Fe+3	6.068E-21	7.930E-22	-20.217	-21.101	-0.884
FeHSO4+2	2.678E-25	1.084E-25	-24.572	-24.965	-0.393
Fe2(OH)2+4	1.289E-31	3.461E-33	-30.890	-32.461	-1.571
Fe3(OH)4+5	0.000E+00	0.000E+00	-41.607	-44.062	-2.455
H(0)	8.100E-13				

Species	Molality	Log Activity	Log Molality	Log Activity	Gamma
H2	4.050E-13	4.123E-13	-12.393	-12.385	0.008
O(0)	0.000E+00				
O2	0.000E+00	0.000E+00	-69.260	-69.252	0.008
S(-2)	6.909E-11				
H2S	5.161E-11	5.254E-11	-10.287	-10.280	0.008
HS-	1.733E-11	1.382E-11	-10.761	-10.859	-0.098
S5-2	1.342E-14	7.232E-15	-13.872	-14.141	-0.268
S6-2	8.639E-15	4.892E-15	-14.064	-14.310	-0.247
S4-2	8.209E-15	4.171E-15	-14.086	-14.380	-0.294
S-2	7.834E-18	3.171E-18	-17.106	-17.499	-0.393
S3-2	3.045E-18	1.440E-18	-17.516	-17.842	-0.325
S2-2	1.790E-19	7.943E-20	-18.747	-19.100	-0.353
Fe(HS)2	1.162E-19	1.183E-19	-18.935	-18.927	0.008
Fe(HS)3-	2.232E-28	1.780E-28	-27.651	-27.750	-0.098
S(6)	3.907E-02				
SO4-2	3.416E-02	1.394E-02	-1.466	-1.856	-0.389
CaSO4	4.911E-03	4.999E-03	-2.309	-2.301	0.008
FeSO4	1.542E-06	1.570E-06	-5.812	-5.804	0.008
HSO4-	5.674E-07	4.526E-07	-6.246	-6.344	-0.098
CaHSO4+	1.286E-08	1.025E-08	-7.891	-7.989	-0.098
FeHSO4+	4.740E-12	3.781E-12	-11.324	-11.422	-0.098
FeSO4+	1.358E-19	1.083E-19	-18.867	-18.965	-0.098
Fe(SO4)2-	4.061E-20	3.239E-20	-19.391	-19.490	-0.098
FeHSO4+2	2.678E-25	1.084E-25	-24.572	-24.965	-0.393

-----Saturation indices-----

Phase	SI Log	IAP Log	KT
Anhydrite	-0.24	-4.58	-4.34 CaSO4
Aragonite	-2.04	-10.34	-8.31 CaCO3
Calcite	-1.89	-10.34	-8.45 CaCO3
CH4(g)	-12.85	-15.67	-2.82 CH4
CO2(g)	-2.32	-3.72	-1.41 CO2
Fe(OH)3(a)	-6.70	-1.81	4.89 Fe(OH)3
Fe3(OH)8	-17.14	3.08	20.22 Fe3(OH)8
FeS(ppt)	-6.67	-10.59	-3.92 FeS
Fix_H+	-6.43	-6.43	0.00 H+
Goethite	-0.99	-1.81	-0.82 FeOOH
Greigite	-21.04	-66.08	-45.04 Fe3S4
Gypsum	0.00	-4.58	-4.58 CaSO4:2H2O
H2(g)	-9.26	-12.38	-3.13 H2
H2O(g)	-1.64	0.00	1.64 H2O
H2S(g)	-9.34	-10.28	-0.94 H2S

Phase	SI Log	IAP Log	KT
Hematite	0.00	-3.62	-3.62 Fe <sub>2</sub> O <sub>3</sub>
JarositeH	-30.17	-34.87	-4.70 (H <sub>3</sub> O)Fe <sub>3</sub> (SO <sub>4</sub> ) <sub>2</sub> (OH) <sub>6</sub>
Mackinawite	-5.94	-10.59	-4.65 FeS
Maghemite	-10.01	-3.62	6.39 Fe <sub>2</sub> O <sub>3</sub>
Magnetite	-1.29	3.08	4.37 Fe <sub>3</sub> O <sub>4</sub>
Melanterite	-5.74	-8.02	-2.27 FeSO <sub>4</sub> :7H <sub>2</sub> O
O <sub>2</sub> (g)	-66.40	-69.25	-2.85 O <sub>2</sub>
Portlandite	-13.05	10.13	23.19 Ca(OH) <sub>2</sub>
Pyrite	0.00	-18.62	-18.62 FeS <sub>2</sub>
Siderite	-2.92	-13.78	-10.86 FeCO <sub>3</sub>
Siderite(d)(3)	-3.33	-13.78	-10.45 FeCO <sub>3</sub>
Sulfur	-5.98	-21.10	-15.12 S

**TABLE 3**  
**Initial Aqueous and Solid Phase Concentrations as**  
**Computed by PHREEQC for Anoxic Environment (MW-24)**

Input file: C:\DOCUME~1\ADMINI~1\LOCALS~1\Temp\phrq0004.tmp  
Output file: C:\Program Files\Phreeqc\Examples\Denison -MW-24- pyrite, O2 - initial - v5.out  
Database file: C:\Program Files\Phreeqc\Databases\wateq4f.dat

-----  
Reading data base.  
-----

SOLUTION\_MASTER\_SPECIES  
SOLUTION\_SPECIES  
PHASES  
EXCHANGE\_MASTER\_SPECIES  
EXCHANGE\_SPECIES  
SURFACE\_MASTER\_SPECIES  
SURFACE\_SPECIES  
RATES  
END

-----  
Reading input data for simulation 1.  
-----

TITLE Modeling of Pyrite, O2 - MW-24 initial state - year 25  
SOLUTION 1  
temp 20  
water 0.18  
units mg/L  
Alkalinity 222 as HCO3-  
S(6) 2575. #2804. #2575.  
Ca 500.  
EQUILIBRIUM\_PHASES 1  
Calcite 0. 0.  
Aragonite 0. 0.  
Gypsum 0. 0.08372  
Hematite 0. 0.  
Goethite 0. 0.  
Diaspore 0. 0.  
Siderite 0. 0.0031  
Quartz 0. 26.520  
K-feldspar 0 0.03885  
Kmica 0. 0.2035  
Kaolinite 0. 0.300  
Anhydrite 0. 0.05294  
Pyrophyllite 0. 0.  
Pyrite 0. 0.012  
Fix\_H+ -7.37 #SO4-2 0.0045  
PHASES 1  
Fix\_H+  
H+ = H+  
log\_k 0  
K-feldspar  
KAISi3O8 + 8 H2O = K+ + Al(OH)4- + 3 H4SiO4

```

log_k -20.573
delta_h 30.820 kcal
HCO3-
H+ + CO3-2 = HCO3-
log_k 10.329
delta_h -3.561 kcal
GAS_PHASE 1
fixed_volume
volume 0.
temperature 20
O2(g) 0.2
CO2(g) 0.0004
END

```

```

-----
TITLE
-----

```

Modeling of Pyrite, O2 - MW-24 initial state - year 25

```

-----
Beginning of initial solution calculations.
-----

```

INITIAL SOLUTION 1

```

-----Solution composition-----

```

**Elements Molality Moles**

Alkalinity	3.65E-03	6.57E-04
Ca	1.25E-02	2.25E-03
S(6)	2.69E-02	4.84E-03

```

-----Description of solution-----

```

pH = 7.000  
pe = 4.000  
Activity of water = 0.999  
Ionic strength = 5.813e-02  
Mass of water (kg) = 1.800e-01  
Total carbon (mol/kg) = 4.327e-03  
Total CO2 (mol/kg) = 4.327e-03  
Temperature (deg C) = 20.000  
Electrical balance (eq) = -5.833e-03  
Percent error,  $100 * (\text{Cat} - |\text{An}|) / (\text{Cat} + |\text{An}|) = -54.06$   
Iterations = 6  
Total H = 1.998289e+01  
Total O = 1.001270e+01

-----Distribution of species-----

Species	Molality	Log Activity	Log Molality	Log Activity	Gamma
H+	1.178E-07	1.000E-07	-6.929	-7.000	-0.071
OH-	8.334E-08	6.785E-08	-7.079	-7.168	-0.089
H2O	5.551E+01	9.994E-01	1.744	0.000	0.000
C(4)	4.327E-03				
HCO3-	3.504E-03	2.879E-03	-2.455	-2.541	-0.085
CO2	6.848E-04	6.940E-04	-3.164	-3.159	0.006
CaHCO3+	1.293E-04	1.052E-04	-3.889	-3.978	-0.089
CaCO3	5.709E-06	5.786E-06	-5.243	-5.238	0.006
CO3-2	2.662E-06	1.212E-06	-5.575	-5.916	-0.341
Ca	1.252E-02				
Ca+2	6.820E-03	3.120E-03	-2.166	-2.506	-0.340
CaSO4	5.561E-03	5.636E-03	-2.255	-2.249	0.006
CaHCO3+	1.293E-04	1.052E-04	-3.889	-3.978	-0.089
CaCO3	5.709E-06	5.786E-06	-5.243	-5.238	0.006
CaOH+	6.356E-09	5.174E-09	-8.197	-8.286	-0.089
CaHSO4+	3.822E-09	3.112E-09	-8.418	-8.507	-0.089
H(0)	1.470E-25				
H2	7.348E-26	7.447E-26	-25.134	-25.128	0.006
O(0)	0.000E+00				
O2	0.000E+00	0.000E+00	-43.772	-43.766	0.006
S(6)	2.689E-02				
SO4-2	2.133E-02	9.495E-03	-1.671	-2.023	-0.352
CaSO4	5.561E-03	5.636E-03	-2.255	-2.249	0.006
HSO4-	1.019E-07	8.296E-08	-6.992	-7.081	-0.089
CaHSO4+	3.822E-09	3.112E-09	-8.418	-8.507	-0.089

-----Saturation indices-----

Phase	SI Log	IAP Log	KT
Anhydrite	-0.18	-4.53	-4.34 CaSO4
Aragonite	-0.12	-8.42	-8.31 CaCO3
Calcite	0.03	-8.42	-8.45 CaCO3
CO2(g)	-1.75	-3.16	-1.41 CO2
Fix_H+	-7.00	-7.00	0.00 H+
Gypsum	0.05	-4.53	-4.58 CaSO4:2H2O
H2(g)	-22.00	-25.13	-3.13 H2
H2O(g)	-1.64	0.00	1.64 H2O
HCO3-	-7.00	3.38	10.37 H+
O2(g)	-40.91	-43.77	-2.85 O2
Portlandite	-11.69	11.49	23.19 Ca(OH)2

-----  
Beginning of batch-reaction calculations.  
-----

Reaction step 1.

Using solution 1.

Using pure phase assemblage 1.

Using gas phase 1.

-----Gas phase-----

Total pressure: 0.0034 atmospheres

Gas volume: 0.00e+00 liters

Moles in gas

Component	log P	P	Initial	Final	Data
CO2(g)	-2.46	3.429E-03	0.000E+00	0.000E+00	0.000E+00
O2(g)	-67.49	3.263E-68	0.000E+00	0.000E+00	0.000E+00

-----Phase assemblage-----

Moles in assemblage

Phase	SI Log	IAP Log	KT	Initial	Final	Data
Anhydrite	-0.24	-4.58	-4.34	5.294E-02	0.000E+00	-5.294E-02
Aragonite	-0.15	-8.45	-8.31	0.000E+00	0.000E+00	0.000E+00
Calcite	0.00	-8.45	-8.45	0.000E+00	3.552E-03	3.552E-03
Diaspore	-0.04	7.15	7.19	0.000E+00	0.000E+00	0.000E+00
Fix_H+	-7.37	-7.37	0.00	1.000E+01	9.978E+00	-2.165E-02
Goethite	-0.99	-1.81	-0.82	0.000E+00	0.000E+00	0.000E+00
Gypsum	0.00	-4.58	-4.58	8.372E-02	1.334E-01	4.964E-02
Hematite	0.00	-3.62	-3.62	0.000E+00	7.250E-04	7.250E-04
K-feldspar	-3.09	-24.05	-20.96	3.885E-02	0.000E+00	-3.885E-02
Kaolinite	-1.69	6.19	7.88	3.000E-01	0.000E+00	-3.000E-01
Kmica	0.00	13.45	13.45	2.035E-01	2.422E-01	3.870E-02
Pyrite	0.00	-18.62	-18.62	1.200E-02	1.365E-02	1.650E-03
Pyrophyllite	0.00	-48.31	-48.31	0.000E+00	2.614E-01	2.614E-01
Quartz	0.00	-4.06	-4.06	2.652E+01	2.607E+01	-4.451E-01
Siderite	-2.80	-13.66	-10.86	3.100E-03	0.000E+00	-3.100E-03

-----Solution composition-----

**Elements Molality Moles**

Al	2.65E-09	4.88E-10
C	1.78E-03	3.27E-04
Ca	1.09E-02	2.00E-03

**Elements Molality Moles**

Fe	6.83E-08	1.26E-08
K	8.21E-04	1.51E-04
S	2.63E-02	4.84E-03
Si	8.71E-05	1.60E-05

## -----Description of solution-----

pH = 7.370 Charge balance  
 pe = -3.014 Adjusted to redox equilibrium  
 Activity of water = 0.999  
 Ionic strength = 5.576e-02  
 Mass of water (kg) = 1.838e-01  
 Total alkalinity (eq/kg) = 1.654e-03  
 Total CO2 (mol/kg) = 1.778e-03  
 Temperature (deg C) = 20.000  
 Electrical balance (eq) = -5.833e-03  
 Percent error,  $100 \cdot (\text{Cat} - |\text{An}|) / (\text{Cat} + |\text{An}|) = -55.69$   
 Iterations = 66  
 Total H = 2.040583e+01  
 Total O = 1.022312e+01

## -----Distribution of species-----

Species	Molality	Log Activity	Log Molality	Log Activity	Gamma
OH-	1.948E-07	1.591E-07	-6.710	-6.798	-0.088
H+	5.016E-08	4.266E-08	-7.300	-7.370	-0.070
H2O	5.551E+01	9.994E-01	1.744	0.000	0.000
Al	2.654E-09				
Al(OH)4-	2.577E-09	2.104E-09	-8.589	-8.677	-0.088
Al(OH)3	4.999E-11	5.064E-11	-10.301	-10.296	0.006
Al(OH)2+	2.629E-11	2.146E-11	-10.580	-10.668	-0.088
AlOH+2	4.123E-13	1.833E-13	-12.385	-12.737	-0.352
AlSO4+	3.817E-14	3.117E-14	-13.418	-13.506	-0.088
Al(SO4)2-	1.135E-14	9.264E-15	-13.945	-14.033	-0.088
Al+3	6.782E-15	1.094E-15	-14.169	-14.961	-0.792
AlHSO4+2	2.546E-22	1.132E-22	-21.594	-21.946	-0.352
C(-4)	2.239E-14				
CH4	2.239E-14	2.268E-14	-13.650	-13.644	0.006
C(4)	1.778E-03				
HCO3-	1.586E-03	1.307E-03	-2.800	-2.884	-0.084
CO2	1.327E-04	1.344E-04	-3.877	-3.872	0.006
CaHCO3+	5.118E-05	4.179E-05	-4.291	-4.379	-0.088
CaCO3	5.317E-06	5.386E-06	-5.274	-5.269	0.006
CO3-2	2.800E-06	1.290E-06	-5.553	-5.889	-0.337
FeHCO3+	2.743E-09	2.240E-09	-8.562	-8.650	-0.088
FeCO3	5.237E-10	5.304E-10	-9.281	-9.275	0.006

Species	Molality	Log Activity	Log Molality	Log Activity	Gamma
Ca	1.089E-02				
Ca+2	5.901E-03	2.729E-03	-2.229	-2.564	-0.335
CaSO4	4.934E-03	4.998E-03	-2.307	-2.301	0.006
CaHCO3+	5.118E-05	4.179E-05	-4.291	-4.379	-0.088
CaCO3	5.317E-06	5.386E-06	-5.274	-5.269	0.006
CaOH+	1.300E-08	1.061E-08	-7.886	-7.974	-0.088
CaHSO4+	1.441E-09	1.177E-09	-8.841	-8.929	-0.088
Fe(2)	6.832E-08				
Fe+2	3.856E-08	1.714E-08	-7.414	-7.766	-0.352
FeSO4	2.639E-08	2.673E-08	-7.579	-7.573	0.006
FeHCO3+	2.743E-09	2.240E-09	-8.562	-8.650	-0.088
FeCO3	5.237E-10	5.304E-10	-9.281	-9.275	0.006
FeOH+	1.063E-10	8.684E-11	-9.973	-10.061	-0.088
Fe(OH)2	1.098E-14	1.113E-14	-13.959	-13.954	0.006
FeHSO4+	9.052E-15	7.391E-15	-14.043	-14.131	-0.088
Fe(OH)3-	1.128E-17	9.213E-18	-16.948	-17.036	-0.088
Fe(HS)2	4.090E-19	4.142E-19	-18.388	-18.383	0.006
Fe(HS)3-	9.098E-27	7.428E-27	-26.041	-26.129	-0.088
Fe(3)	3.154E-15				
Fe(OH)3	2.055E-15	2.082E-15	-14.687	-14.682	0.006
Fe(OH)2+	1.054E-15	8.608E-16	-14.977	-15.065	-0.088
Fe(OH)4-	4.440E-17	3.625E-17	-16.353	-16.441	-0.088
FeOH+2	3.027E-19	1.346E-19	-18.519	-18.871	-0.352
FeSO4+	1.386E-22	1.131E-22	-21.858	-21.946	-0.088
Fe(SO4)2-	2.860E-23	2.335E-23	-22.544	-22.632	-0.088
Fe+3	7.439E-24	1.200E-24	-23.128	-23.921	-0.792
FeHSO4+2	2.925E-29	1.300E-29	-28.534	-28.886	-0.352
Fe2(OH)2+4	1.541E-35	6.013E-37	-34.812	-36.221	-1.409
Fe3(OH)4+5	0.000E+00	0.000E+00	-46.561	-48.762	-2.201
H(0)	2.851E-12				
H2	1.425E-12	1.444E-12	-11.846	-11.840	0.006
K	8.214E-04				
K+	7.740E-04	6.248E-04	-3.111	-3.204	-0.093
KSO4-	4.735E-05	3.866E-05	-4.325	-4.413	-0.088
O(0)	0.000E+00				
O2	0.000E+00	0.000E+00	-70.346	-70.341	0.006
S(-2)	2.877E-10				
HS-	2.017E-10	1.647E-10	-9.695	-9.783	-0.088
H2S	7.096E-11	7.188E-11	-10.149	-10.143	0.006
S5-2	1.327E-12	7.505E-13	-11.877	-12.125	-0.247
S6-2	8.604E-13	5.077E-13	-12.065	-12.294	-0.229
S4-2	8.043E-13	4.329E-13	-12.095	-12.364	-0.269
S-2	7.405E-16	3.291E-16	-15.130	-15.483	-0.352
S3-2	2.947E-16	1.495E-16	-15.531	-15.825	-0.295
S2-2	1.712E-17	8.244E-18	-16.766	-17.084	-0.317

Species	Molality	Log Activity	Log Molality	Log Activity	Gamma
Fe(HS)2	4.090E-19	4.142E-19	-18.388	-18.383	0.006
Fe(HS)3-	9.098E-27	7.428E-27	-26.041	-26.129	-0.088
S(6)	2.634E-02				
SO4-2	2.136E-02	9.624E-03	-1.670	-2.017	-0.346
CaSO4	4.934E-03	4.998E-03	-2.307	-2.301	0.006
KSO4-	4.735E-05	3.866E-05	-4.325	-4.413	-0.088
HSO4-	4.393E-08	3.587E-08	-7.357	-7.445	-0.088
FeSO4	2.639E-08	2.673E-08	-7.579	-7.573	0.006
CaHSO4+	1.441E-09	1.177E-09	-8.841	-8.929	-0.088
AlSO4+	3.817E-14	3.117E-14	-13.418	-13.506	-0.088
Al(SO4)2-	1.135E-14	9.264E-15	-13.945	-14.033	-0.088
FeHSO4+	9.052E-15	7.391E-15	-14.043	-14.131	-0.088
AlHSO4+2	2.546E-22	1.132E-22	-21.594	-21.946	-0.352
FeSO4+	1.386E-22	1.131E-22	-21.858	-21.946	-0.088
Fe(SO4)2-	2.860E-23	2.335E-23	-22.544	-22.632	-0.088
FeHSO4+2	2.925E-29	1.300E-29	-28.534	-28.886	-0.352
Si	8.713E-05				
H4SiO4	8.682E-05	8.794E-05	-4.061	-4.056	0.006
H3SiO4-	3.111E-07	2.540E-07	-6.507	-6.595	-0.088
H2SiO4-2	6.515E-13	2.896E-13	-12.186	-12.538	-0.352

-----Saturation indices-----

Phase	SI Log	IAP Log	KT
Adularia	-3.09	-24.05	-20.96 KAlSi3O8
Al(OH)3(a)	-3.98	7.15	11.13 Al(OH)3
AlumK	-16.94	-22.20	-5.26 KAl(SO4)2:12H2O
Alunite	-7.13	-7.90	-0.77 KAl3(SO4)2(OH)6
Anhydrite	-0.24	-4.58	-4.34 CaSO4
Annite	-1.71	-88.13	-86.43 KFe3AlSi3O10(OH)2
Anorthite	-8.17	-28.03	-19.86 CaAl2Si2O8
Aragonite	-0.15	-8.45	-8.31 CaCO3
Basaluminite	-10.86	11.84	22.70 Al4(OH)10SO4
Boehmite	-1.79	7.15	8.94 AlOOH
Calcite	0.00	-8.45	-8.45 CaCO3
CH4(g)	-10.83	-13.64	-2.82 CH4
Chalcedony	-0.44	-4.06	-3.61 SiO2
CO2(g)	-2.46	-3.87	-1.41 CO2
Cristobalite	-0.40	-4.06	-3.66 SiO2
Diaspore	-0.04	7.15	7.19 AlOOH
Fe(OH)3(a)	-6.70	-1.81	4.89 Fe(OH)3
Fe3(OH)8	-16.87	3.35	20.22 Fe3(OH)8

Phase	SI Log	IAP Log	KT
FeS(ppt)	-6.26	-10.18	-3.92 FeS
Fix_H+	-7.37	-7.37	0.00 H+
Gibbsite	-1.25	7.15	8.40 Al(OH) <sub>3</sub>
Goethite	-0.99	-1.81	-0.82 FeOOH
Greenalite	-8.00	12.81	20.81 Fe <sub>3</sub> Si <sub>2</sub> O <sub>5</sub> (OH) <sub>4</sub>
Greigite	-20.23	-65.26	-45.04 Fe <sub>3</sub> S <sub>4</sub>
Gypsum	0.00	-4.58	-4.58 CaSO <sub>4</sub> ·2H <sub>2</sub> O
H <sub>2</sub> (g)	-8.71	-11.84	-3.13 H <sub>2</sub>
H <sub>2</sub> O(g)	-1.64	0.00	1.64 H <sub>2</sub> O
H <sub>2</sub> S(g)	-9.20	-10.14	-0.94 H <sub>2</sub> S
Halloysite	-6.81	6.19	13.00 Al <sub>2</sub> Si <sub>2</sub> O <sub>5</sub> (OH) <sub>4</sub>
HCO <sub>3</sub> <sup>-</sup>	-7.37	3.01	10.37 H+
Hematite	0.00	-3.62	-3.62 Fe <sub>2</sub> O <sub>3</sub>
Jarosite-K	-25.96	-34.78	-8.82 KFe <sub>3</sub> (SO <sub>4</sub> ) <sub>2</sub> (OH) <sub>6</sub>
JarositeH	-34.25	-38.95	-4.70 (H <sub>3</sub> O)Fe <sub>3</sub> (SO <sub>4</sub> ) <sub>2</sub> (OH) <sub>6</sub>
Jurbanite	-6.38	-9.61	-3.23 AlOHSO <sub>4</sub>
K-feldspar	-3.09	-24.05	-20.96 KAISi <sub>3</sub> O <sub>8</sub>
Kaolinite	-1.69	6.19	7.88 Al <sub>2</sub> Si <sub>2</sub> O <sub>5</sub> (OH) <sub>4</sub>
Kmica	0.00	13.45	13.45 KAl <sub>3</sub> Si <sub>3</sub> O <sub>10</sub> (OH) <sub>2</sub>
Laumontite	-4.68	-36.14	-31.46 CaAl <sub>2</sub> Si <sub>4</sub> O <sub>12</sub> ·4H <sub>2</sub> O
Leonhardite	-1.40	-72.28	-70.88 Ca <sub>2</sub> Al <sub>4</sub> Si <sub>8</sub> O <sub>24</sub> ·7H <sub>2</sub> O
Mackinawite	-5.53	-10.18	-4.65 FeS
Maghemite	-10.01	-3.62	6.39 Fe <sub>2</sub> O <sub>3</sub>
Magnetite	-1.02	3.35	4.37 Fe <sub>3</sub> O <sub>4</sub>
Melanterite	-7.51	-9.78	-2.27 FeSO <sub>4</sub> ·7H <sub>2</sub> O
Montmorillonite-Ca	-4.51	-50.26	-45.76 Ca <sub>0.165</sub> Al <sub>2.33</sub> Si <sub>3.67</sub> O <sub>10</sub> (OH) <sub>2</sub>
O <sub>2</sub> (g)	-67.49	-70.34	-2.85 O <sub>2</sub>
Portlandite	-11.01	12.18	23.19 Ca(OH) <sub>2</sub>
Prehnite	-8.08	-19.91	-11.82 Ca <sub>2</sub> Al <sub>2</sub> Si <sub>3</sub> O <sub>10</sub> (OH) <sub>2</sub>
Pyrite	0.00	-18.62	-18.62 FeS <sub>2</sub>
Pyrophyllite	0.00	-48.31	-48.31 Al <sub>2</sub> Si <sub>4</sub> O <sub>10</sub> (OH) <sub>2</sub>
Quartz	0.00	-4.06	-4.06 SiO <sub>2</sub>
Siderite	-2.80	-13.66	-10.86 FeCO <sub>3</sub>
Siderite(d)(3)	-3.21	-13.66	-10.45 FeCO <sub>3</sub>
Silicagel	-0.98	-4.06	-3.07 SiO <sub>2</sub>
SiO <sub>2</sub> (a)	-1.30	-4.06	-2.75 SiO <sub>2</sub>
Sulfur	-6.39	-21.51	-15.12 S
Wairakite	-9.10	-36.14	-27.03 CaAl <sub>2</sub> Si <sub>4</sub> O <sub>12</sub> ·2H <sub>2</sub> O

**TABLE 4**  
**Final Aqueous and Solid Phase Concentrations as Calculated**  
**by PHREEQC for 10 Liter Air Exposure (MW-24)**

-----  
 Reading input data for simulation 1.  
 -----

TITLE Modeling of Pyrite, O2 - MW-24 final state - year 30  
 SOLUTION 1

temp 20  
 water 0.18  
 units mg/L

Alkalinity 222 as HCO3-  
 S(6) 2804. #2575.

Ca 500. # charge

EQUILIBRIUM\_PHASES 1

Calcite 0. 0.  
 Aragonite 0. 0.  
 Gypsum 0. 0.08372  
 Hematite 0. 0.  
 Goethite 0. 0.  
 Diaspore 0. 0.  
 Siderite 0. 0.0031  
 Quartz 0. 26.520  
 K-feldspar 0 0.03885  
 Kmica 0. 0.2035  
 Kaolinite 0. 0.300  
 Anhydrite 0. 0.05294  
 Pyrophyllite 0. 0.  
 Pyrite 0. 0.012  
 Fix\_H+ -6.20 #SO4-2 0.005257

PHASES 1

Fix\_H+  
 H+ = H+  
 log\_k 0  
 K-feldspar  
 $\text{KAISi3O8} + 8 \text{H2O} = \text{K}^+ + \text{Al(OH)4}^- + 3 \text{H4SiO4}$   
 log\_k -20.573  
 delta\_h 30.820 kcal

HCO3-

$\text{H}^+ + \text{CO3}^{2-} = \text{HCO3}^-$   
 log\_k 10.329  
 delta\_h -3.561 kcal

GAS\_PHASE 1

fixed\_volume  
 volume 10.  
 temperature 20  
 O2(g) 0.2  
 CO2(g) 0.0004

END

-----  
 TITLE  
 -----

Modeling of Pyrite, O2 - MW-24 final state - year 30

-----  
 Beginning of initial solution calculations.  
 -----

INITIAL SOLUTION 1

-----Solution composition-----

**Elements Molality Moles**

Alkalinity 3.651E-03 6.572E-04  
 Ca 1.252E-02 2.253E-03  
 S(6) 2.929E-02 5.273E-03

-----Description of solution-----

pH = 7.000  
 pe = 4.000  
 Activity of water = 0.999  
 Ionic strength = 6.219e-02  
 Mass of water (kg) = 1.800e-01  
 Total carbon (mol/kg) = 4.325e-03  
 Total CO2 (mol/kg) = 4.325e-03  
 Temperature (deg C) = 20.000  
 Electrical balance (eq) = -6.696e-03  
 Percent error, 100\*(Cat-|An|)/(Cat+|An|) = -58.11  
 Iterations = 6  
 Total H = 1.998289e+01  
 Total O = 1.001442e+01

-----Distribution of species-----

Species	Molality	Log Activity	Log Molality	Log Activity	Gamma
H+	1.182E-07	1.000E-07	-6.927	-7.000	-0.073
OH-	8.374E-08	6.785E-08	-7.077	-7.168	-0.091
H2O	5.551E+01	9.993E-01	1.744	0.000	0.000
C(4)	4.325E-03				
HCO3-	3.511E-03	2.871E-03	-2.455	-2.542	-0.087
CO2	6.823E-04	6.921E-04	-3.166	-3.160	0.006
CaHCO3+	1.239E-04	1.004E-04	-3.907	-3.998	-0.091
CaCO3	5.440E-06	5.518E-06	-5.264	-5.258	0.006
CO3-2	2.705E-06	1.209E-06	-5.568	-5.918	-0.350
Ca	1.252E-02				
Ca+2	6.641E-03	2.984E-03	-2.178	-2.525	-0.347
CaSO4	5.749E-03	5.831E-03	-2.240	-2.234	0.006
CaHCO3+	1.239E-04	1.004E-04	-3.907	-3.998	-0.091
CaCO3	5.440E-06	5.518E-06	-5.264	-5.258	0.006

Species	Molality	Log Activity	Log Molality	Log Activity	Gamma
CaOH+	6.107E-09	4.948E-09	-8.214	-8.306	-0.091
CaHSO4+	3.974E-09	3.219E-09	-8.401	-8.492	-0.091
H(0)	1.468E-25				
H2	7.341E-26	7.447E-26	-25.134	-25.128	0.006
O(0)	0.000E+00				
O2	0.000E+00	0.000E+00	-43.772	-43.766	0.006
S(6)	2.929E-02				
SO4-2	2.354E-02	1.027E-02	-1.628	-1.988	-0.360
CaSO4	5.749E-03	5.831E-03	-2.240	-2.234	0.006
HSO4-	1.108E-07	8.975E-08	-6.956	-7.047	-0.091
CaHSO4+	3.974E-09	3.219E-09	-8.401	-8.492	-0.091

-----Saturation indices-----

Phase	SI Log	IAP Log	KT
Anhydrite	-0.17	-4.51	-4.34 CaSO4
Aragonite	-0.14	-8.44	-8.31 CaCO3
Calcite	0.01	-8.44	-8.45 CaCO3
CO2(g)	-1.75	-3.16	-1.41 CO2
Fix_H+	-7.00	-7.00	0.00 H+
Gypsum	0.07	-4.51	-4.58 CaSO4:2H2O
H2(g)	-22.00	-25.13	-3.13 H2
H2O(g)	-1.64	0.00	1.64 H2O
HCO3-	-7.00	3.38	10.37 H+
O2(g)	-40.91	-43.77	-2.85 O2
Portlandite	-11.71	11.47	23.19 Ca(OH)2

-----  
Beginning of batch-reaction calculations.  
-----

Reaction step 1.

Using solution 1.

Using pure phase assemblage 1.

Using gas phase 1.

-----Gas phase-----

Total pressure: 0.0094 atmospheres  
 Gas volume: 1.00e+01 liters

Moles in gas

Component	Log P	P	Initial	Final	Data
CO2(g)	-2.03	9.429E-03	1.663E-04	3.920E-03	3.753E-03
O2(g)	-66.19	6.436E-67	8.314E-02	0.000E+00	-8.314E-02

-----Phase assemblage-----

Moles in assemblage

Phase	SI Log	IAP Log	KT	Initial	Final	Data
Anhydrite	-0.24	-4.58	-4.34	5.294E-02	0.000E+00	-5.294E-02
Aragonite	-2.14	-10.44	-8.31	0.000E+00	0.000E+00	0.000E+00
Calcite	-1.99	-10.44	-8.45	0.000E+00	0.000E+00	0.000E+00
Diaspore	-0.04	7.15	7.19	0.000E+00	0.000E+00	0.000E+00
Fix_H+	-6.20	-6.20	0.00	1.000E+01	9.682E+00	-3.184E-01
Goethite	-0.99	-1.81	-0.82	0.000E+00	0.000E+00	0.000E+00
Gypsum	0.00	-4.58	-4.58	8.372E-02	1.370E-01	5.331E-02
Hematite	0.00	-3.62	-3.62	0.000E+00	1.918E-03	1.918E-03
K-feldspar	-3.09	-24.05	-20.96	3.885E-02	0.000E+00	-3.885E-02
Kaolinite	-1.69	6.19	7.88	3.000E-01	0.000E+00	-3.000E-01
Kmica	0.00	13.45	13.45	2.035E-01	2.400E-01	3.650E-02
Pyrite	0.00	-18.62	-18.62	1.200E-02	1.126E-02	-7.378E-04
Pyrophyllite	0.00	-48.31	-48.31	0.000E+00	2.647E-01	2.647E-01
Quartz	0.00	-4.06	-4.06	2.652E+01	2.607E+01	-4.517E-01
Siderite	-2.68	-13.54	-10.86	3.100E-03	0.000E+00	-3.100E-03

-----Solution composition-----

**Elements Molality Moles**

Al	9.587E-10	1.786E-10
C	6.720E-04	1.252E-04
Ca	1.012E-02	1.886E-03
Fe	7.734E-06	1.441E-06
K	1.260E-02	2.349E-03
S	3.425E-02	6.381E-03
Si	8.643E-05	1.611E-05

-----Description of solution-----

pH = 6.200 Charge balance  
 pe = -1.520 Adjusted to redox equilibrium  
 Activity of water = 0.999  
 Ionic strength = 7.377e-02  
 Mass of water (kg) = 1.863e-01  
 Total alkalinity (eq/kg) = 3.072e-04  
 Total CO2 (mol/kg) = 6.720e-04  
 Temperature (deg C) = 20.000  
 Electrical balance (eq) = -6.696e-03  
 Percent error, 100\*(Cat-|An|)/(Cat+|An|) = -44.79  
 Iterations = 23  
 Total H = 2.068571e+01  
 Total O = 1.036869e+01

-----Distribution of species-----

Species	Molality	Log Activity	Log Molality	Log Activity	Gamma
H+	7.520E-07	6.310E-07	-6.124	-6.200	-0.076
OH-	1.343E-08	1.075E-08	-7.872	-7.969	-0.097
H2O	5.551E+01	9.991E-01	1.744	0.000	0.000
Al	9.587E-10				
Al(OH)2+	3.966E-10	3.175E-10	-9.402	-9.498	-0.097
Al(OH)4-	1.776E-10	1.422E-10	-9.750	-9.847	-0.097
AlSO4+	1.544E-10	1.236E-10	-9.811	-9.908	-0.097
AlOH+2	9.772E-11	4.010E-11	-10.010	-10.397	-0.387
Al(SO4)2-	5.620E-11	4.498E-11	-10.250	-10.347	-0.097
Al(OH)3	4.977E-11	5.063E-11	-10.303	-10.296	0.007
Al+3	2.628E-11	3.542E-12	-10.580	-11.451	-0.870
AlHSO4+2	1.617E-17	6.637E-18	-16.791	-17.178	-0.387
C(-4)	1.575E-16				
CH4	1.575E-16	1.602E-16	-15.803	-15.795	0.007
C(4)	6.720E-04				
CO2	3.633E-04	3.695E-04	-3.440	-3.432	0.007
HCO3-	3.006E-04	2.429E-04	-3.522	-3.615	-0.093
CaHCO3+	7.928E-06	6.345E-06	-5.101	-5.198	-0.097
CaCO3	5.436E-08	5.529E-08	-7.265	-7.257	0.007
FeHCO3+	5.400E-08	4.322E-08	-7.268	-7.364	-0.097
CO3-2	3.806E-08	1.621E-08	-7.420	-7.790	-0.371
FeCO3	6.804E-10	6.920E-10	-9.167	-9.160	0.007
Ca	1.012E-02				
Ca+2	5.199E-03	2.230E-03	-2.284	-2.652	-0.368
CaSO4	4.916E-03	5.001E-03	-2.308	-2.301	0.007
CaHCO3+	7.928E-06	6.345E-06	-5.101	-5.198	-0.097
CaCO3	5.436E-08	5.529E-08	-7.265	-7.257	0.007
CaHSO4+	2.176E-08	1.742E-08	-7.662	-7.759	-0.097

Species	Molality	Log Activity	Log Molality	Log Activity	Gamma
CaOH+	7.322E-10	5.860E-10	-9.135	-9.232	-0.097
Fe(2)	7.734E-06				
Fe+2	4.337E-06	1.780E-06	-5.363	-5.750	-0.387
FeSO4	3.341E-06	3.399E-06	-5.476	-5.469	0.007
FeHCO3+	5.400E-08	4.322E-08	-7.268	-7.364	-0.097
FeOH+	7.615E-10	6.095E-10	-9.118	-9.215	-0.097
FeCO3	6.804E-10	6.920E-10	-9.167	-9.160	0.007
FeHSO4+	1.737E-11	1.390E-11	-10.760	-10.857	-0.097
Fe(OH)2	5.189E-15	5.278E-15	-14.285	-14.278	0.007
Fe(OH)3-	3.691E-19	2.954E-19	-18.433	-18.530	-0.097
Fe(HS)2	9.168E-20	9.325E-20	-19.038	-19.030	0.007
Fe(HS)3-	9.727E-29	7.785E-29	-28.012	-28.109	-0.097
Fe(3)	1.803E-14				
Fe(OH)2+	1.591E-14	1.273E-14	-13.798	-13.895	-0.097
Fe(OH)3	2.046E-15	2.081E-15	-14.689	-14.682	0.007
FeOH+2	7.175E-17	2.944E-17	-16.144	-16.531	-0.387
Fe(OH)4-	3.060E-18	2.449E-18	-17.514	-17.611	-0.097
FeSO4+	5.605E-19	4.486E-19	-18.251	-18.348	-0.097
Fe(SO4)2-	1.417E-19	1.134E-19	-18.849	-18.945	-0.097
Fe+3	2.882E-20	3.885E-21	-19.540	-20.411	-0.870
FeHSO4+2	1.857E-24	7.623E-25	-23.731	-24.118	-0.387
Fe2(OH)2+4	1.015E-30	2.879E-32	-29.993	-31.541	-1.547
Fe3(OH)4+5	0.000E+00	0.000E+00	-40.494	-42.912	-2.418
H(0)	6.391E-13				
H2	3.195E-13	3.250E-13	-12.495	-12.488	0.007
K	1.260E-02				
K+	1.173E-02	9.241E-03	-1.931	-2.034	-0.104
KSO4-	8.749E-04	7.003E-04	-3.058	-3.155	-0.097
O(0)	0.000E+00				
O2	0.000E+00	0.000E+00	-69.053	-69.046	0.007
S(-2)	5.829E-11				
H2S	4.867E-11	4.950E-11	-10.313	-10.305	0.007
HS-	9.580E-12	7.667E-12	-11.019	-11.115	-0.097
S5-2	4.353E-15	2.362E-15	-14.361	-14.627	-0.265
S6-2	2.806E-15	1.598E-15	-14.552	-14.796	-0.244
S4-2	2.659E-15	1.363E-15	-14.575	-14.866	-0.290
S-2	2.525E-18	1.036E-18	-17.598	-17.985	-0.387
S3-2	9.845E-19	4.706E-19	-18.007	-18.327	-0.321
Fe(HS)2	9.168E-20	9.325E-20	-19.038	-19.030	0.007
S2-2	5.779E-20	2.595E-20	-19.238	-19.586	-0.348
Fe(HS)3-	9.727E-29	7.785E-29	-28.012	-28.109	-0.097
S(6)	3.425E-02				
SO4-2	2.845E-02	1.179E-02	-1.546	-1.929	-0.383
CaSO4	4.916E-03	5.001E-03	-2.308	-2.301	0.007
KSO4-	8.749E-04	7.003E-04	-3.058	-3.155	-0.097

Species	Molality	Log Activity	Log Molality	Log Activity	Gamma
FeSO4	3.341E-06	3.399E-06	-5.476	-5.469	0.007
HSO4-	8.117E-07	6.497E-07	-6.091	-6.187	-0.097
CaHSO4+	2.176E-08	1.742E-08	-7.662	-7.759	-0.097
AlSO4+	1.544E-10	1.236E-10	-9.811	-9.908	-0.097
Al(SO4)2-	5.620E-11	4.498E-11	-10.250	-10.347	-0.097
FeHSO4+	1.737E-11	1.390E-11	-10.760	-10.857	-0.097
AlHSO4+2	1.617E-17	6.637E-18	-16.791	-17.178	-0.387
FeSO4+	5.605E-19	4.486E-19	-18.251	-18.348	-0.097
Fe(SO4)2-	1.417E-19	1.134E-19	-18.849	-18.945	-0.097
FeHSO4+2	1.857E-24	7.623E-25	-23.731	-24.118	-0.387
Si	8.643E-05				
H4SiO4	8.641E-05	8.789E-05	-4.063	-4.056	0.007
H3SiO4-	2.144E-08	1.716E-08	-7.669	-7.765	-0.097
H2SiO4-2	3.224E-15	1.323E-15	-14.492	-14.878	-0.387

-----Saturation indices-----

Phase	SI Log	IAP Log	KT
Adularia	-3.09	-24.05	-20.96 KAlSi3O8
Al(OH)3(a)	-3.98	7.15	11.13 Al(OH)3
AlumK	-12.09	-17.35	-5.26 KAl(SO4)2:12H2O
Alunite	-2.27	-3.05	-0.77 KAl3(SO4)2(OH)6
Anhydrite	-0.24	-4.58	-4.34 CaSO4
Annite	-2.68	-89.11	-86.43 KFe3AlSi3O10(OH)2
Anorthite	-10.60	-30.46	-19.86 CaAl2Si2O8
Aragonite	-2.14	-10.44	-8.31 CaCO3
Basaluminite	-8.44	14.26	22.70 Al4(OH)10SO4
Boehmite	-1.79	7.15	8.94 AlOOH
Calcite	-1.99	-10.44	-8.45 CaCO3
CH4(g)	-12.98	-15.80	-2.82 CH4
Chalcedony	-0.44	-4.06	-3.61 SiO2
CO2(g)	-2.03	-3.43	-1.41 CO2
Cristobalite	-0.40	-4.06	-3.66 SiO2
Diaspore	-0.04	7.15	7.19 AlOOH
Fe(OH)3(a)	-6.70	-1.81	4.89 Fe(OH)3
Fe3(OH)8	-17.20	3.03	20.22 Fe3(OH)8
FeS(ppt)	-6.75	-10.67	-3.92 FeS
Fix_H+	-6.20	-6.20	0.00 H+
Gibbsite	-1.25	7.15	8.40 Al(OH)3
Goethite	-0.99	-1.81	-0.82 FeOOH
Greenalite	-8.97	11.84	20.81 Fe3Si2O5(OH)4
Greigite	-21.20	-66.23	-45.04 Fe3S4
Gypsum	0.00	-4.58	-4.58 CaSO4:2H2O

Phase	SI Log	IAP Log	KT
H2(g)	-9.36	-12.49	-3.13 H2
H2O(g)	-1.64	0.00	1.64 H2O
H2S(g)	-9.37	-10.31	-0.94 H2S
Halloysite	-6.81	6.19	13.00 Al2Si2O5(OH)4
HCO3-	-6.20	4.18	10.37 H+
Hematite	0.00	-3.62	-3.62 Fe2O3
Jarosite-K	-21.11	-29.93	-8.82 KFe3(SO4)2(OH)6
JarositeH	-29.39	-34.09	-4.70 (H3O)Fe3(SO4)2(OH)6
Jurbanite	-3.95	-7.18	-3.23 AlOHSO4
K-feldspar	-3.09	-24.05	-20.96 KAISi3O8
Kaolinite	-1.69	6.19	7.88 Al2Si2O5(OH)4
Kmica	0.00	13.45	13.45 KAl3Si3O10(OH)2
Laumontite	-7.11	-38.57	-31.46 CaAl2Si4O12:4H2O
Leonhardite	-6.25	-77.13	-70.88 Ca2Al4Si8O24:7H2O
Mackinawite	-6.02	-10.67	-4.65 FeS
Maghemite	-10.01	-3.62	6.39 Fe2O3
Magnetite	-1.34	3.03	4.37 Fe3O4
Melanterite	-5.41	-7.68	-2.27 FeSO4:7H2O
Montmorillonite-Ca	-4.91	-50.66	-45.76 Ca0.165Al2.33Si3.67O10(OH)2
O2(g)	-66.19	-69.05	-2.85 O2
Portlandite	-13.44	9.75	23.19 Ca(OH)2
Prehnite	-12.94	-24.76	-11.82 Ca2Al2Si3O10(OH)2
Pyrite	0.00	-18.62	-18.62 FeS2
Pyrophyllite	0.00	-48.31	-48.31 Al2Si4O10(OH)2
Quartz	0.00	-4.06	-4.06 SiO2
Siderite	-2.68	-13.54	-10.86 FeCO3
Siderite(d)(3)	-3.09	-13.54	-10.45 FeCO3
Silicagel	-0.98	-4.06	-3.07 SiO2
SiO2(a)	-1.30	-4.06	-2.75 SiO2
Sulfur	-5.90	-21.02	-15.12 S
Wairakite	-11.53	-38.57	-27.03 CaAl2Si4O12:2H2O

**TABLE 5**  
**Initial Aqueous and Solid Phase Concentrations as**  
**Computed by PHREEQC for Anoxic Environment (MW-27)**

Input file: C:\DOCUME~1\ADMINI~1\LOCALS~1\Temp\phrq0004.tmp  
Output file: C:\Program Files\Phreeqc\Examples\Denison -MW-27- Pyrite, O2 initial - v5.out  
Database file: C:\Program Files\Phreeqc\Databases\wateq4f.dat

-----  
Reading data base.  
-----

SOLUTION\_MASTER\_SPECIES  
SOLUTION\_SPECIES  
PHASES  
EXCHANGE\_MASTER\_SPECIES  
EXCHANGE\_SPECIES  
SURFACE\_MASTER\_SPECIES  
SURFACE\_SPECIES  
RATES  
END

-----  
Reading input data for simulation 1.  
-----

TITLE Modeling of Pyrite, O2 - MW-27 - initial state - year 25  
SOLUTION 1  
    temp 20  
pH 7.2  
    water 0.18  
units mg/L  
S(6) 390.  
Alkalinity 449. as HCO3-  
Ca 54.  
EQUILIBRIUM\_PHASES 1  
Calcite 0. 0.  
Gypsum 0. 0.  
Hematite 0. 0.  
Goethite 0. 0.  
Chalcedony 0. 0.  
Diaspore 0. 0.  
Pyrophyllite 0. 0.  
Quartz 0. 28.620  
K-feldspar 0. 0.0453  
Kmica 0 0.014  
Kaolinite 0. 0.09767  
Plagioclase 0. 0.1007  
Pyrite 0. 0.0039  
Siderite 0. 0.0002  
Fix\_H+ -7.2 #SO4-2 0.00073  
PHASES 1  
Fix\_H+  
H+ = H+  
log\_k 0  
HCO3-

```

H+ + CO3-2 = HCO3-
log_k      10.329
delta_h -3.561 kcal
K-feldspar
KAlSi3O8 + 8 H2O = K+ + Al(OH)4- + 3 H4SiO4
log_k     -20.573
delta_h 30.820 kcal
Plagioclase
Na0.62Ca0.38Al1.38Si2.62O8 + 5.52 H+ + 2.48H2O = 0.62Na+ + 0.38Ca+2 + 1.38Al+3 +
2.62H4SiO4
log_k 0.0
GAS_PHASE 1
temperature 20
fixed_volume
volume 0. # liters
O2(g) 0.20
CO2(g) 0.0004
END

```

```

-----
TITLE
-----

```

Modeling of Pyrite, O2 - MW-27 - initial state - year 25

```

-----
Beginning of initial solution calculations.
-----

```

INITIAL SOLUTION 1

```

-----Solution composition-----

```

**Elements Molality Moles**

```

Alkalinity  7.365E-03 1.326E-03
Ca          1.349E-03 2.427E-04
S(6)       4.064E-03 7.314E-04

```

```

-----Description of solution-----

```

```

pH = 7.200
pe = 4.000
Activity of water = 1.000
Ionic strength = 1.323e-02
Mass of water (kg) = 1.800e-01
Total carbon (mol/kg) = 8.342e-03
Total CO2 (mol/kg) = 8.342e-03
Temperature (deg C) = 20.000
Electrical balance (eq) = -2.303e-03
Percent error, 100*(Cat-|An|)/(Cat+|An|) = -75.72
Iterations = 5
Total H = 1.998356e+01
Total O = 9.998372e+00

```

-----Distribution of species-----

Species	Molality	Log Activity	Log Molality	Log Activity	Gamma
OH-	1.207E-07	1.076E-07	-6.918	-6.968	-0.050
H+	6.972E-08	6.310E-08	-7.157	-7.200	-0.043
H2O	5.551E+01	9.998E-01	1.744	0.000	0.000
C(4)	8.34E-03				
HCO3-	7.288E-03	6.521E-03	-2.137	-2.186	-0.048
CO2	9.885E-04	9.915E-04	-3.005	-3.004	0.001
CaHCO3+	5.483E-05	4.886E-05	-4.261	-4.311	-0.050
CO3-2	6.790E-06	4.353E-06	-5.168	-5.361	-0.193
CaCO3	4.245E-06	4.258E-06	-5.372	-5.371	0.001
Ca	1.35E-03				
Ca+2	9.981E-04	6.395E-04	-3.001	-3.194	-0.193
CaSO4	2.913E-04	2.922E-04	-3.536	-3.534	0.001
CaHCO3+	5.483E-05	4.886E-05	-4.261	-4.311	-0.050
CaCO3	4.245E-06	4.258E-06	-5.372	-5.371	0.001
CaOH+	1.887E-09	1.682E-09	-8.724	-8.774	-0.050
CaHSO4+	1.142E-10	1.018E-10	-9.942	-9.992	-0.050
H(0)	5.91E-26				
H2	2.956E-26	2.965E-26	-25.529	-25.528	0.001
O(0)	0.00E+00				
O2	0.000E+00	0.000E+00	-42.967	-42.965	0.001
S(6)	4.06E-03				
SO4-2	3.772E-03	2.402E-03	-2.423	-2.619	-0.196
CaSO4	2.913E-04	2.922E-04	-3.536	-3.534	0.001
HSO4-	1.486E-08	1.324E-08	-7.828	-7.878	-0.050
CaHSO4+	1.142E-10	1.018E-10	-9.942	-9.992	-0.050

-----Saturation indices-----

Phase	SI Log	IAP Log	KT
Anhydrite	-1.47	-5.81	-4.34 CaSO4
Aragonite	-0.25	-8.56	-8.31 CaCO3
Calcite	-0.10	-8.56	-8.45 CaCO3
CO2(g)	-1.60	-3.00	-1.41 CO2
Fix_H+	-7.20	-7.20	0.00 H+
Gypsum	-1.23	-5.81	-4.58 CaSO4:2H2O
H2(g)	-22.40	-25.53	-3.13 H2
H2O(g)	-1.64	0.00	1.64 H2O
HCO3-	-7.20	3.18	10.37 H+
O2(g)	-40.11	-42.97	-2.85 O2
Portlandite	-11.98	11.21	23.19 Ca(OH)2

-----  
Beginning of batch-reaction calculations.  
-----

Reaction step 1.

WARNING: Maximum iterations exceeded, 100

WARNING: Numerical method failed with this set of convergence parameters.

WARNING: Trying smaller step size, pe step size 10, 5 ...

Using solution 1.

Using pure phase assemblage 1.

Using gas phase 1.

-----Gas phase-----

Total pressure: 0.0283 atmospheres

Gas volume: 0.00e+00 liters

Moles in gas

Component	Log P	P	Initial	Final	Data
CO2(g)	-1.55	2.832E-02	0.000E+00	0.000E+00	0.000E+00
O2(g)	-67.63	2.345E-68	0.000E+00	0.000E+00	0.000E+00

-----Phase assemblage-----

Moles in assemblage

Phase	SI Log	IAP Log	KT	Initial	Final	Data
Calcite	-0.06	-8.52	-8.45	0.000E+00	0.000E+00	0.000E+00
Chalcedony	-0.44	-4.06	-3.61	0.000E+00	0.000E+00	0.000E+00
Diaspore	-0.04	7.15	7.19	0.000E+00	0.000E+00	0.000E+00
Fix_H+	-7.20	-7.20	0.00	1.000E+01	1.000E+01	2.577E-04
Goethite	-0.99	-1.81	-0.82	0.000E+00	0.000E+00	0.000E+00
Gypsum	-1.25	-5.83	-4.58	0.000E+00	0.000E+00	0.000E+00
Hematite	0.00	-3.62	-3.62	0.000E+00	1.019E-04	1.019E-04
K-feldspar	-3.09	-24.05	-20.96	4.530E-02	0.000E+00	-4.530E-02
Kaolinite	-1.69	6.19	7.88	9.767E-02	0.000E+00	-9.767E-02
Kmica	0.00	13.45	13.45	1.400E-02	5.911E-02	4.511E-02
Plagioclase	0.00	0.00	0.00	1.007E-01	1.007E-01	1.612E-10
Pyrite	0.00	-18.62	-18.62	3.900E-03	3.896E-03	-3.847E-06
Pyrophyllite	0.00	-48.31	-48.31	0.000E+00	5.266E-02	5.266E-02
Quartz	0.00	-4.06	-4.06	2.862E+01	2.861E+01	-1.473E-02
Siderite	-1.84	-12.70	-10.86	2.000E-04	0.000E+00	-2.000E-04

-----Solution composition-----

**Elements Molality Moles**

Al	1.690E-09	3.072E-10
C	9.362E-03	1.702E-03
Ca	1.336E-03	2.427E-04
Fe	1.194E-07	2.170E-08
K	1.059E-03	1.925E-04
Na	1.663E-13	3.023E-14
S	4.067E-03	7.391E-04
Si	8.791E-05	1.598E-05

-----Description of solution-----

pH = 7.200 Charge balance  
 pe = -2.880 Adjusted to redox equilibrium  
 Activity of water = 1.000  
 Ionic strength = 1.419e-02  
 Mass of water (kg) = 1.818e-01  
 Total alkalinity (eq/kg) = 8.269e-03  
 Total CO2 (mol/kg) = 9.362e-03  
 Temperature (deg C) = 20.000  
 Electrical balance (eq) = -2.303e-03  
 Percent error,  $100 \times (\text{Cat} - |\text{An}|) / (\text{Cat} + |\text{An}|) = -67.27$   
 Iterations = 49  
 Total H = 2.017845e+01  
 Total O = 1.009637e+01

-----Distribution of species-----

Species	Molality	Log Activity	Log Molality	Log Activity	Gamma
OH-	1.211E-07	1.076E-07	-\$6.917	-\$6.968	-\$0.052
H+	6.991E-08	6.310E-08	-\$7.155	-\$7.200	-\$0.045
H2O	5.551E+01	9.997E-01	\$1.744	\$0.000	\$0.000
Al	1.690E-09				
Al(OH)4-	1.603E-09	1.423E-09	-\$8.795	-\$8.847	-\$0.052
Al(OH)3	5.049E-11	5.066E-11	-\$10.297	-\$10.295	\$0.001
Al(OH)2+	3.575E-11	3.175E-11	-\$10.447	-\$10.498	-\$0.052
AlOH+2	6.447E-13	4.008E-13	-\$12.191	-\$12.397	-\$0.206
AlSO4+	2.793E-14	2.480E-14	-\$13.554	-\$13.606	-\$0.052
Al+3	1.031E-14	3.538E-15	-\$13.987	-\$14.451	-\$0.464
Al(SO4)2-	2.043E-15	1.814E-15	-\$14.690	-\$14.741	-\$0.052
AlHSO4+2	2.142E-22	1.332E-22	-\$21.669	-\$21.876	-\$0.206
C(-4)	3.618E-13				
CH4	3.618E-13	3.629E-13	-\$12.442	-\$12.440	\$0.001
C(4)	9.362E-03				
HCO3-	8.183E-03	7.299E-03	-\$2.087	-\$2.137	-\$0.050

Species	Molality	Log Activity	Log Molality	Log Activity	Gamma
CO2	1.106E-03	1.110E-03	-\$2.956	-\$2.955	\$0.001
CaHCO3+	6.026E-05	5.351E-05	-\$4.220	-\$4.272	-\$0.052
CO3-2	7.699E-06	4.872E-06	-\$5.114	-\$5.312	-\$0.199
CaCO3	4.648E-06	4.663E-06	-\$5.333	-\$5.331	\$0.001
FeHCO3+	3.346E-08	2.971E-08	-\$7.475	-\$7.527	-\$0.052
FeCO3	4.742E-09	4.758E-09	-\$8.324	-\$8.323	\$0.001
NaHCO3	5.960E-16	5.980E-16	-\$15.225	-\$15.223	\$0.001
NaCO3-	1.152E-17	1.023E-17	-\$16.939	-\$16.990	-\$0.052
Ca	1.336E-03				
Ca+2	9.896E-04	6.258E-04	-\$3.005	-\$3.204	-\$0.199
CaSO4	2.810E-04	2.819E-04	-\$3.551	-\$3.550	\$0.001
CaHCO3+	6.026E-05	5.351E-05	-\$4.220	-\$4.272	-\$0.052
CaCO3	4.648E-06	4.663E-06	-\$5.333	-\$5.331	\$0.001
CaOH+	1.853E-09	1.646E-09	-\$8.732	-\$8.784	-\$0.052
CaHSO4+	1.106E-10	9.821E-11	-\$9.956	-\$10.008	-\$0.052
Fe(2)	1.194E-07				
Fe+2	6.549E-08	4.071E-08	-\$7.184	-\$7.390	-\$0.206
FeHCO3+	3.346E-08	2.971E-08	-\$7.475	-\$7.527	-\$0.052
FeSO4	1.557E-08	1.562E-08	-\$7.808	-\$7.806	\$0.001
FeCO3	4.742E-09	4.758E-09	-\$8.324	-\$8.323	\$0.001
FeOH+	1.571E-10	1.395E-10	-\$9.804	-\$9.855	-\$0.052
Fe(OH)2	1.205E-14	1.209E-14	-\$13.919	-\$13.918	\$0.001
FeHSO4+	7.196E-15	6.390E-15	-\$14.143	-\$14.195	-\$0.052
Fe(OH)3-	7.624E-18	6.770E-18	-\$17.118	-\$17.169	-\$0.052
Fe(HS)2	4.872E-19	4.888E-19	-\$18.312	-\$18.311	\$0.001
Fe(HS)3-	6.958E-27	6.178E-27	-\$26.158	-\$26.209	-\$0.052
Fe(3)	3.538E-15				
Fe(OH)3	2.076E-15	2.083E-15	-\$14.683	-\$14.681	\$0.001
Fe(OH)2+	1.434E-15	1.273E-15	-\$14.843	-\$14.895	-\$0.052
Fe(OH)4-	2.763E-17	2.453E-17	-\$16.559	-\$16.610	-\$0.052
FeOH+2	4.735E-19	2.943E-19	-\$18.325	-\$18.531	-\$0.206
FeSO4+	1.014E-22	9.005E-23	-\$21.994	-\$22.046	-\$0.052
Fe+3	1.131E-23	3.881E-24	-\$22.947	-\$23.411	-\$0.464
Fe(SO4)2-	5.150E-24	4.573E-24	-\$23.288	-\$23.340	-\$0.052
FeHSO4+2	2.461E-29	1.530E-29	-\$28.609	-\$28.815	-\$0.206
Fe2(OH)2+4	1.926E-35	2.877E-36	-\$34.715	-\$35.541	-\$0.826
Fe3(OH)4+5	0.000E+00	0.000E+00	-\$46.622	-\$47.912	-\$1.290
H(0)	3.397E-12				
H2	1.698E-12	1.704E-12	-\$11.770	-\$11.769	\$0.001
K	1.059E-03				
K+	1.043E-03	9.241E-04	-\$2.982	-\$3.034	-\$0.053
KSO4-	1.585E-05	1.407E-05	-\$4.800	-\$4.852	-\$0.052
Na	1.663E-13				
Na+	1.638E-13	1.457E-13	-\$12.786	-\$12.837	-\$0.051
NaSO4-	1.885E-15	1.674E-15	-\$14.725	-\$14.776	-\$0.052

Species	Molality	Log Activity	Log Molality	Log Activity	Gamma
NaHCO3	5.960E-16	5.980E-16	-\$15.225	-\$15.223	\$0.001
NaCO3-	1.152E-17	1.023E-17	-\$16.939	-\$16.990	-\$0.052
O(0)	0.000E+00				
O2	0.000E+00	0.000E+00	-\$70.486	-\$70.484	\$0.001
S(-2)	2.113E-10				
HS-	1.307E-10	1.161E-10	-\$9.884	-\$9.935	-\$0.052
H2S	7.469E-11	7.493E-11	-\$10.127	-\$10.125	\$0.001
S5-2	5.216E-13	3.576E-13	-\$12.283	-\$12.447	-\$0.164
S6-2	3.462E-13	2.419E-13	-\$12.461	-\$12.616	-\$0.156
S4-2	3.073E-13	2.063E-13	-\$12.512	-\$12.686	-\$0.173
S-2	2.523E-16	1.568E-16	-\$15.598	-\$15.805	-\$0.206
S3-2	1.087E-16	7.124E-17	-\$15.964	-\$16.147	-\$0.183
S2-2	6.112E-18	3.928E-18	-\$17.214	-\$17.406	-\$0.192
Fe(HS)2	4.872E-19	4.888E-19	-\$18.312	-\$18.311	\$0.001
Fe(HS)3-	6.958E-27	6.178E-27	-\$26.158	-\$26.209	-\$0.052
S(6)	4.067E-03				
SO4-2	3.770E-03	2.368E-03	-\$2.424	-\$2.626	-\$0.202
CaSO4	2.810E-04	2.819E-04	-\$3.551	-\$3.550	\$0.001
KSO4-	1.585E-05	1.407E-05	-\$4.800	-\$4.852	-\$0.052
FeSO4	1.557E-08	1.562E-08	-\$7.808	-\$7.806	\$0.001
HSO4-	1.470E-08	1.305E-08	-\$7.833	-\$7.884	-\$0.052
CaHSO4+	1.106E-10	9.821E-11	-\$9.956	-\$10.008	-\$0.052
AlSO4+	2.793E-14	2.480E-14	-\$13.554	-\$13.606	-\$0.052
FeHSO4+	7.196E-15	6.390E-15	-\$14.143	-\$14.195	-\$0.052
Al(SO4)2-	2.043E-15	1.814E-15	-\$14.690	-\$14.741	-\$0.052
NaSO4-	1.885E-15	1.674E-15	-\$14.725	-\$14.776	-\$0.052
AlHSO4+2	2.142E-22	1.332E-22	-\$21.669	-\$21.876	-\$0.206
FeSO4+	1.014E-22	9.005E-23	-\$21.994	-\$22.046	-\$0.052
Fe(SO4)2-	5.150E-24	4.573E-24	-\$23.288	-\$23.340	-\$0.052
FeHSO4+2	2.461E-29	1.530E-29	-\$28.609	-\$28.815	-\$0.206
Si	8.791E-05				
H4SiO4	8.771E-05	8.800E-05	-\$4.057	-\$4.056	\$0.001
H3SiO4-	1.935E-07	1.718E-07	-\$6.713	-\$6.765	-\$0.052
H2SiO4-2	2.131E-13	1.325E-13	-\$12.672	-\$12.878	-\$0.206

-----Saturation indices-----

Phase	SI Log	IAP Log	KT
Adularia	-3.09	-24.05	-20.96 KAlSi3O8
Al(OH)3(a)	-3.98	7.15	11.13 Al(OH)3
Albite	-15.52	-33.85	-18.33 NaAlSi3O8
AlumK	-17.48	-22.74	-5.26 KAl(SO4)2:12H2O

Phase	SI Log	IAP Log	KT
Alunite	-7.67	-8.44	-0.77 KAl <sub>3</sub> (SO <sub>4</sub> ) <sub>2</sub> (OH) <sub>6</sub>
Analcime	-16.87	-29.79	-12.93 NaAlSi <sub>2</sub> O <sub>6</sub> :H <sub>2</sub> O
Anhydrite	-1.49	-5.83	-4.34 CaSO <sub>4</sub>
Annite	-1.60	-88.03	-86.43 KFe <sub>3</sub> AlSi <sub>3</sub> O <sub>10</sub> (OH) <sub>2</sub>
Anorthite	-9.15	-29.01	-19.86 CaAl <sub>2</sub> Si <sub>2</sub> O <sub>8</sub>
Aragonite	-0.21	-8.52	-8.31 CaCO <sub>3</sub>
Basaluminite	-11.13	11.57	22.70 Al <sub>4</sub> (OH) <sub>10</sub> SO <sub>4</sub>
Boehmite	-1.79	7.15	8.94 AlOOH
Calcite	-0.06	-8.52	-8.45 CaCO <sub>3</sub>
CH <sub>4</sub> (g)	-9.62	-12.44	-2.82 CH <sub>4</sub>
Chalcedony	-0.44	-4.06	-3.61 SiO <sub>2</sub>
CO <sub>2</sub> (g)	-1.55	-2.95	-1.41 CO <sub>2</sub>
Cristobalite	-0.40	-4.06	-3.66 SiO <sub>2</sub>
Diaspore	-0.04	7.15	7.19 AlOOH
Fe(OH) <sub>3</sub> (a)	-6.70	-1.81	4.89 Fe(OH) <sub>3</sub>
Fe <sub>3</sub> (OH) <sub>8</sub>	-16.84	3.39	20.22 Fe <sub>3</sub> (OH) <sub>8</sub>
FeS(ppt)	-6.21	-10.13	-3.92 FeS
Fix_H+	-7.20	-7.20	0.00 H <sup>+</sup>
Gibbsite	-1.25	7.15	8.40 Al(OH) <sub>3</sub>
Goethite	-0.99	-1.81	-0.82 FeOOH
Greenalite	-7.89	12.92	20.81 Fe <sub>3</sub> Si <sub>2</sub> O <sub>5</sub> (OH) <sub>4</sub>
Greigite	-20.12	-65.15	-45.04 Fe <sub>3</sub> S <sub>4</sub>
Gypsum	-1.25	-5.83	-4.58 CaSO <sub>4</sub> :2H <sub>2</sub> O
H <sub>2</sub> (g)	-8.64	-11.77	-3.13 H <sub>2</sub>
H <sub>2</sub> O(g)	-1.64	0.00	1.64 H <sub>2</sub> O
H <sub>2</sub> S(g)	-9.19	-10.13	-0.94 H <sub>2</sub> S
Halloysite	-6.81	6.19	13.00 Al <sub>2</sub> Si <sub>2</sub> O <sub>5</sub> (OH) <sub>4</sub>
HCO <sub>3</sub> <sup>-</sup>	-7.20	3.18	10.37 H <sup>+</sup>
Hematite	0.00	-3.62	-3.62 Fe <sub>2</sub> O <sub>3</sub>
Jarosite(ss)	-26.62	-36.45	-9.83 (K <sub>0.77</sub> Na <sub>0.03</sub> H <sub>0.2</sub> )Fe <sub>3</sub> (SO <sub>4</sub> ) <sub>2</sub> (OH) <sub>6</sub>
Jarosite-K	-26.50	-35.32	-8.82 KFe <sub>3</sub> (SO <sub>4</sub> ) <sub>2</sub> (OH) <sub>6</sub>
Jarosite-Na	-40.29	-45.12	-4.83 NaFe <sub>3</sub> (SO <sub>4</sub> ) <sub>2</sub> (OH) <sub>6</sub>
JarositeH	-34.78	-39.49	-4.70 (H <sub>3</sub> O)Fe <sub>3</sub> (SO <sub>4</sub> ) <sub>2</sub> (OH) <sub>6</sub>
Jurbanite	-6.65	-9.88	-3.23 AlOHSO <sub>4</sub>
K-feldspar	-3.09	-24.05	-20.96 KAlSi <sub>3</sub> O <sub>8</sub>
Kaolinite	-1.69	6.19	7.88 Al <sub>2</sub> Si <sub>2</sub> O <sub>5</sub> (OH) <sub>4</sub>
Kmica	0.00	13.45	13.45 KAl <sub>3</sub> Si <sub>3</sub> O <sub>10</sub> (OH) <sub>2</sub>
Laumontite	-5.66	-37.12	-31.46 CaAl <sub>2</sub> Si <sub>4</sub> O <sub>12</sub> :4H <sub>2</sub> O
Leonhardite	-3.35	-74.24	-70.88 Ca <sub>2</sub> Al <sub>4</sub> Si <sub>8</sub> O <sub>24</sub> :7H <sub>2</sub> O
Mackinawite	-5.48	-10.13	-4.65 FeS
Magadiite	-19.72	-34.02	-14.30 NaSi <sub>7</sub> O <sub>13</sub> (OH) <sub>3</sub> :3H <sub>2</sub> O
Maghemite	-10.01	-3.62	6.39 Fe <sub>2</sub> O <sub>3</sub>
Magnetite	-0.98	3.39	4.37 Fe <sub>3</sub> O <sub>4</sub>
Melanterite	-7.75	-10.02	-2.27 FeSO <sub>4</sub> :7H <sub>2</sub> O
Mirabilite	-26.95	-28.30	-1.35 Na <sub>2</sub> SO <sub>4</sub> :10H <sub>2</sub> O
Montmorillonite-Ca	-4.67	-50.42	-45.76 Ca <sub>0.165</sub> Al <sub>2.33</sub> Si <sub>3.67</sub> O <sub>10</sub> (OH) <sub>2</sub>

Phase	SI Log	IAP Log	KT
Nahcolite	-14.38	-14.97	-0.59 NaHCO <sub>3</sub>
Natron	-29.48	-30.99	-1.51 Na <sub>2</sub> CO <sub>3</sub> :10H <sub>2</sub> O
O <sub>2</sub> (g)	-67.63	-70.48	-2.85 O <sub>2</sub>
Phillipsite	-9.07	-28.95	-19.87 Na <sub>0.5</sub> K <sub>0.5</sub> AlSi <sub>3</sub> O <sub>8</sub> :H <sub>2</sub> O
Plagioclase	0.00	0.00	0.00 Na <sub>0.62</sub> Ca <sub>0.38</sub> Al <sub>1.38</sub> Si <sub>2.62</sub> O <sub>8</sub>
Portlandite	-11.99	11.20	23.19 Ca(OH) <sub>2</sub>
Prehnite	-10.04	-21.87	-11.82 Ca <sub>2</sub> Al <sub>2</sub> Si <sub>3</sub> O <sub>10</sub> (OH) <sub>2</sub>
Pyrite	0.00	-18.62	-18.62 FeS <sub>2</sub>
Pyrophyllite	0.00	-48.31	-48.31 Al <sub>2</sub> Si <sub>4</sub> O <sub>10</sub> (OH) <sub>2</sub>
Quartz	0.00	-4.06	-4.06 SiO <sub>2</sub>
Siderite	-1.84	-12.70	-10.86 FeCO <sub>3</sub>
Siderite(d)(3)	-2.25	-12.70	-10.45 FeCO <sub>3</sub>
Silicagel	-0.98	-4.06	-3.07 SiO <sub>2</sub>
SiO <sub>2</sub> (a)	-1.30	-4.06	-2.75 SiO <sub>2</sub>
Sulfur	-6.44	-21.56	-15.12 S
Thenardite	-28.13	-28.30	-0.17 Na <sub>2</sub> SO <sub>4</sub>
Thermonatrite	-31.15	-30.99	0.16 Na <sub>2</sub> CO <sub>3</sub> :H <sub>2</sub> O
Trona	-45.39	-45.96	-0.57 NaHCO <sub>3</sub> :Na <sub>2</sub> CO <sub>3</sub> :2H <sub>2</sub> O
Wairakite	-10.08	-37.12	-27.03 CaAl <sub>2</sub> Si <sub>4</sub> O <sub>12</sub> :2H <sub>2</sub> O

**TABLE 6**  
**Final Aqueous and Solid Phase Concentrations as Calculated**  
**by PHREEQC for 0.1 Liter Air Exposure (MW-27)**

Input file: C:\DOCUME~1\ADMINI~1\LOCALS~1\Temp\phrq0004.tmp  
 Output file: C:\Program Files\Phreeqc\Examples\Denison -MW-27- Pyrite, O2 - final - v5.out  
 Database file: C:\Program Files\Phreeqc\Databases\wateq4f.dat

-----  
 Reading data base.  
 -----

SOLUTION\_MASTER\_SPECIES  
 SOLUTION\_SPECIES  
 PHASES  
 EXCHANGE\_MASTER\_SPECIES  
 EXCHANGE\_SPECIES  
 SURFACE\_MASTER\_SPECIES  
 SURFACE\_SPECIES  
 RATES  
 END

-----  
 Reading input data for simulation 1.  
 -----

TITLE Modeling of Pyrite, O2 - MW-27 - final state  
 SOLUTION 1  
     temp 20  
 pH 6.8  
     water 0.18  
     units mg/L  
 Alkalinity 449 as HCO3-  
     S(6) 453.  
     Ca 177.  
 EQUILIBRIUM\_PHASES 1  
 Gypsum 0. 0.0  
 Hematite 0. 0.  
 Goethite 0. 0.  
 Chalcedony 0. 0.  
 Diaspore 0. 0.  
 Quartz 0. 28.620  
 K-feldspar 0. 0.0453  
 Kmica 0 0.014  
 Kaolinite 0. 0.09767  
 Plagioclase 0. 0.1007  
 Pyrite 0. 0.0039  
 Siderite 0. 0.0002  
 Fix\_H+ -6.8  
 PHASES 1  
 Fix\_H+  
 H+ = H+  
 log\_k 0  
 HCO3-  
     H+ + CO3-2 = HCO3-

```

log_k      10.329
delta_h -3.561 kcal
K-feldspar
KAlSi3O8 + 8 H2O = K+ + Al(OH)4- + 3 H4SiO4
log_k     -20.573
delta_h 30.820 kcal
Plagioclase
Na0.62Ca0.38Al1.38Si2.62O8 + 5.52 H+ + 2.48H2O = 0.62Na+ + 0.38Ca+2 + 1.38Al+3 +
2.62H4SiO4
log_k 0.0
GAS_PHASE 1
temperature 20
fixed_volume
volume 0.1 # liters
O2(g) 0.20
CO2(g) 0.0004
END

```

```

-----
TITLE
-----

```

Modeling of Pyrite, O2 - MW-27 - final state

```

-----
Beginning of initial solution calculations.
-----

```

INITIAL SOLUTION 1

-----Solution composition-----

**Elements Molality Moles**

Alkalinity	7.366E-03	1.326E-03
Ca	4.421E-03	7.958E-04
S(6)	4.721E-03	8.497E-04

-----Description of solution-----

```

pH = 6.800
pe = 4.000
Activity of water = 1.000
Ionic strength = 1.808e-02
Mass of water (kg) = 1.800e-01
Total carbon (mol/kg) = 9.765e-03
Total CO2 (mol/kg) = 9.765e-03
Temperature (deg C) = 20.000
Electrical balance (eq) = -1.434e-03
Percent error, 100*(Cat-|An|)/(Cat+|An|) = -36.61
Iterations = 6
Total H = 1.998356e+01
Total O = 9.999358e+00

```

-----Distribution of species-----

Species	Molality	Log Activity	Log Molality	Log Activity	Gamma
H+	1.773E-07	1.585E-07	-6.751	-6.800	-0.049
OH-	4.884E-08	4.282E-08	-7.311	-7.368	-0.057
H2O	5.551E+01	9.997E-01	1.744	0.000	0.000
C(4)	9.765E-03				
HCO3-	7.179E-03	6.327E-03	-2.144	-2.199	-0.055
CO2	2.407E-03	2.417E-03	-2.619	-2.617	0.002
CaHCO3+	1.714E-04	1.503E-04	-3.766	-3.823	-0.057
CaCO3	5.193E-06	5.214E-06	-5.285	-5.283	0.002
CO3-2	2.787E-06	1.681E-06	-5.555	-5.774	-0.219
Ca	4.421E-03				
Ca+2	3.362E-03	2.028E-03	-2.473	-2.693	-0.220
CaSO4	8.818E-04	8.855E-04	-3.055	-3.053	0.002
CaHCO3+	1.714E-04	1.503E-04	-3.766	-3.823	-0.057
CaCO3	5.193E-06	5.214E-06	-5.285	-5.283	0.002
CaOH+	2.421E-09	2.123E-09	-8.616	-8.673	-0.057
CaHSO4+	8.837E-10	7.748E-10	-9.054	-9.111	-0.057
H(0)	3.726E-25				
H2	1.863E-25	1.871E-25	-24.730	-24.728	0.002
O(0)	0.000E+00				
O2	0.000E+00	0.000E+00	-44.567	-44.565	0.002
S(6)	4.721E-03				
SO4-2	3.839E-03	2.295E-03	-2.416	-2.639	-0.223
CaSO4	8.818E-04	8.855E-04	-3.055	-3.053	0.002
HSO4-	3.625E-08	3.178E-08	-7.441	-7.498	-0.057
CaHSO4+	8.837E-10	7.748E-10	-9.054	-9.111	-0.057

-----Saturation indices-----

Phase	SI Log	IAP Log	KT
Anhydrite	-0.99	-5.33	-4.34 CaSO4
Aragonite	-0.16	-8.47	-8.31 CaCO3
Calcite	-0.01	-8.47	-8.45 CaCO3
CO2(g)	-1.21	-2.62	-1.41 CO2
Fix_H+	-6.80	-6.80	0.00 H+
Gypsum	-0.75	-5.33	-4.58 CaSO4:2H2O
H2(g)	-21.60	-24.73	-3.13 H2
H2O(g)	-1.64	0.00	1.64 H2O
HCO3-	-6.80	3.58	10.37 H+
O2(g)	-41.71	-44.57	-2.85 O2
Portlandite	-12.28	10.91	23.19 Ca(OH)2

-----  
Beginning of batch-reaction calculations.  
-----

Reaction step 1.

Using solution 1.

Using pure phase assemblage 1.

Using gas phase 1.

-----Gas phase-----

Total pressure: 0.0593 atmospheres

Gas volume: 1.00e-01 liters

Moles in gas

Component	Log P	P	Initial	Final	Delta
CO2(g)	-1.23	5.929E-02	1.663E-06	2.465E-04	2.448E-04
O2(g)	-67.17	6.816E-68	8.314E-04	0.000E+00	-8.314E-04

-----Phase assemblage-----

Moles in assemblage

Phase	SI Log	IAP Log	KT	Initial	Final	Delta
Chalcedony	-0.44	-4.06	-3.61	0.000E+00	0.000E+00	0.000E+00
Diaspore	0.00	7.19	7.19	0.000E+00	1.059E-01	1.059E-01
Fix_H+	-6.80	-6.80	0.00	1.000E+01	9.998E+00	-1.587E-03
Goethite	-0.99	-1.81	-0.82	0.000E+00	0.000E+00	0.000E+00
Gypsum	-0.70	-5.28	-4.58	0.000E+00	0.000E+00	0.000E+00
Hematite	0.00	-3.62	-3.62	0.000E+00	1.512E-04	1.512E-04
K-feldspar	-3.17	-24.12	-20.96	4.530E-02	0.000E+00	-4.530E-02
Kaolinite	-1.61	6.26	7.88	9.767E-02	0.000E+00	-9.767E-02
Kmica	0.00	13.45	13.45	1.400E-02	5.892E-02	4.492E-02
Plagioclase	0.00	0.00	0.00	1.007E-01	1.007E-01	-1.606E-13
Pyrite	0.00	-18.62	-18.62	3.900E-03	3.797E-03	-1.026E-04
Quartz	0.00	-4.06	-4.06	2.862E+01	2.882E+01	1.965E-01
Siderite	-1.64	-12.50	-10.86	2.000E-04	0.000E+00	-2.000E-04

-----Solution composition-----

**Elements Molality Moles**

Al	8.733E-10	1.587E-10
C	9.423E-03	1.713E-03
Ca	4.378E-03	7.958E-04
Fe	5.762E-07	1.047E-07
K	2.080E-03	3.781E-04

**Elements Molality Moles**

Na 5.480E-13 9.961E-14  
 S 5.804E-03 1.055E-03  
 Si 8.765E-05 1.593E-05

-----Description of solution-----

pH = 6.800 Charge balance  
 pe = -2.364 Adjusted to redox equilibrium  
 Activity of water = 1.000  
 Ionic strength = 2.059e-02  
 Mass of water (kg) = 1.818e-01  
 Total alkalinity (eq/kg) = 7.118e-03  
 Total CO2 (mol/kg) = 9.423e-03  
 Temperature (deg C) = 20.000  
 Electrical balance (eq) = -1.434e-03  
 Percent error, 100\*(Cat-|An|)/(Cat+|An|) = -31.32  
 Iterations = 13  
 Total H = 2.018011e+01  
 Total O = 1.009838e+01

-----Distribution of species-----

Species	Molality	Log Activity	Log Molality	Log Activity	Gamma
H+	1.782E-07	1.585E-07	-6.749	-6.800	-0.051
OH-	4.920E-08	4.282E-08	-7.308	-7.368	-0.060
H2O	5.551E+01	9.997E-01	1.744	0.000	0.000
Al	8.733E-10				
Al(OH)4-	7.122E-10	6.199E-10	-9.147	-9.208	-0.060
Al(OH)2+	1.002E-10	8.725E-11	-9.999	-10.059	-0.060
Al(OH)3	5.516E-11	5.542E-11	-10.258	-10.256	0.002
AlOH+2	4.820E-12	2.767E-12	-11.317	-11.558	-0.241
AlSO4+	5.790E-13	5.040E-13	-12.237	-12.298	-0.060
Al+3	2.139E-13	6.136E-14	-12.670	-13.212	-0.542
Al(SO4)2-	4.962E-14	4.319E-14	-13.304	-13.365	-0.060
AlHSO4+2	1.184E-20	6.799E-21	-19.927	-20.168	-0.241
C(-4)	8.950E-14				
CH4	8.950E-14	8.992E-14	-13.048	-13.046	0.002
C(4)	9.423E-03				
HCO3-	6.949E-03	6.083E-03	-2.158	-2.216	-0.058
CO2	2.312E-03	2.323E-03	-2.636	-2.634	0.002
CaHCO3+	1.549E-04	1.349E-04	-3.810	-3.870	-0.060
CaCO3	4.657E-06	4.679E-06	-5.332	-5.330	0.002
CO3-2	2.753E-06	1.616E-06	-5.560	-5.791	-0.231
FeHCO3+	1.375E-07	1.197E-07	-6.862	-6.922	-0.060
FeCO3	7.592E-09	7.628E-09	-8.120	-8.118	0.002

Species	Molality	Log Activity	Log Molality	Log Activity	Gamma
NaHCO3	1.600E-15	1.608E-15	-14.796	-14.794	0.002
NaCO3-	1.258E-17	1.095E-17	-16.900	-16.961	-0.060
Ca	4.378E-03				
Ca+2	3.224E-03	1.892E-03	-2.492	-2.723	-0.231
CaSO4	9.943E-04	9.991E-04	-3.002	-3.000	0.002
CaHCO3+	1.549E-04	1.349E-04	-3.810	-3.870	-0.060
CaCO3	4.657E-06	4.679E-06	-5.332	-5.330	0.002
CaOH+	2.276E-09	1.981E-09	-8.643	-8.703	-0.060
CaHSO4+	1.004E-09	8.742E-10	-8.998	-9.058	-0.060
Fe(2)	5.762E-07				
Fe+2	3.427E-07	1.967E-07	-6.465	-6.706	-0.241
FeHCO3+	1.375E-07	1.197E-07	-6.862	-6.922	-0.060
FeSO4	8.803E-08	8.845E-08	-7.055	-7.053	0.002
FeCO3	7.592E-09	7.628E-09	-8.120	-8.118	0.002
FeOH+	3.083E-10	2.684E-10	-9.511	-9.571	-0.060
FeHSO4+	1.044E-13	9.088E-14	-12.981	-13.042	-0.060
Fe(OH)2	9.214E-15	9.257E-15	-14.036	-14.034	0.002
Fe(OH)3-	2.371E-18	2.064E-18	-17.625	-17.685	-0.060
Fe(HS)2	2.853E-19	2.867E-19	-18.545	-18.543	0.002
Fe(HS)3-	1.450E-27	1.262E-27	-26.839	-26.899	-0.060
Fe(3)	5.762E-15				
Fe(OH)2+	3.675E-15	3.199E-15	-14.435	-14.495	-0.060
Fe(OH)3	2.072E-15	2.082E-15	-14.684	-14.681	0.002
Fe(OH)4-	1.122E-17	9.764E-18	-16.950	-17.010	-0.060
FeOH+2	3.235E-18	1.857E-18	-17.490	-17.731	-0.241
FeSO4+	1.921E-21	1.672E-21	-20.716	-20.777	-0.060
Fe+3	2.145E-22	6.152E-23	-21.669	-22.211	-0.542
Fe(SO4)2-	1.143E-22	9.952E-23	-21.942	-22.002	-0.060
FeHSO4+2	1.244E-27	7.138E-28	-26.905	-27.146	-0.241
Fe2(OH)2+4	1.055E-33	1.146E-34	-32.977	-33.941	-0.964
Fe3(OH)4+5	0.000E+00	0.000E+00	-44.406	-45.912	-1.507
H(0)	1.989E-12				
H2	9.946E-13	9.993E-13	-12.002	-12.000	0.002
K	2.080E-03				
K+	2.044E-03	1.772E-03	-2.690	-2.751	-0.062
KSO4-	3.632E-05	3.162E-05	-4.440	-4.500	-0.060
Na	5.480E-13				
Na+	5.391E-13	4.701E-13	-12.268	-12.328	-0.059
NaSO4-	7.272E-15	6.330E-15	-14.138	-14.199	-0.060
NaHCO3	1.600E-15	1.608E-15	-14.796	-14.794	0.002
NaCO3-	1.258E-17	1.095E-17	-16.900	-16.961	-0.060
O(0)	0.000E+00				
O2	0.000E+00	0.000E+00	-70.023	-70.021	0.002
S(-2)	1.126E-10				
H2S	6.526E-11	6.557E-11	-10.185	-10.183	0.002

Species	Molality	Log Activity	Log Molality	Log Activity	Gamma
HS-	4.645E-11	4.044E-11	-10.333	-10.393	-0.060
S5-2	7.601E-14	4.960E-14	-13.119	-13.305	-0.185
S6-2	5.019E-14	3.356E-14	-13.299	-13.474	-0.175
S4-2	4.505E-14	2.861E-14	-13.346	-13.544	-0.197
S-2	3.789E-17	2.175E-17	-16.421	-16.663	-0.241
S3-2	1.605E-17	9.880E-18	-16.795	-17.005	-0.211
S2-2	9.085E-19	5.448E-19	-18.042	-18.264	-0.222
Fe(HS)2	2.853E-19	2.867E-19	-18.545	-18.543	0.002
Fe(HS)3-	1.450E-27	1.262E-27	-26.839	-26.899	-0.060
S(6)	5.804E-03				
SO4-2	4.773E-03	2.775E-03	-2.321	-2.557	-0.236
CaSO4	9.943E-04	9.991E-04	-3.002	-3.000	0.002
KSO4-	3.632E-05	3.162E-05	-4.440	-4.500	-0.060
FeSO4	8.803E-08	8.845E-08	-7.055	-7.053	0.002
HSO4-	4.414E-08	3.842E-08	-7.355	-7.415	-0.060
CaHSO4+	1.004E-09	8.742E-10	-8.998	-9.058	-0.060
AlSO4+	5.790E-13	5.040E-13	-12.237	-12.298	-0.060
FeHSO4+	1.044E-13	9.088E-14	-12.981	-13.042	-0.060
Al(SO4)2-	4.962E-14	4.319E-14	-13.304	-13.365	-0.060
NaSO4-	7.272E-15	6.330E-15	-14.138	-14.199	-0.060
AlHSO4+2	1.184E-20	6.799E-21	-19.927	-20.168	-0.241
FeSO4+	1.921E-21	1.672E-21	-20.716	-20.777	-0.060
Fe(SO4)2-	1.143E-22	9.952E-23	-21.942	-22.002	-0.060
FeHSO4+2	1.244E-27	7.138E-28	-26.905	-27.146	-0.241
Si	8.765E-05				
H4SiO4	8.757E-05	8.798E-05	-4.058	-4.056	0.002
H3SiO4-	7.857E-08	6.839E-08	-7.105	-7.165	-0.060
H2SiO4-2	3.656E-14	2.099E-14	-13.437	-13.678	-0.241

-----Saturation indices-----

Phase	SI Log	IAP Log	KT
Adularia	-3.17	-24.12	-20.96 KAlSi3O8
Al(OH)3(a)	-3.94	7.19	11.13 Al(OH)3
Albite	-15.38	-33.70	-18.33 NaAlSi3O8
AlumK	-15.82	-21.08	-5.26 KAl(SO4)2:12H2O
Alunite	-5.93	-6.70	-0.77 KAl3(SO4)2(OH)6
Analcime	-16.72	-29.65	-12.93 NaAlSi2O6:H2O
Anhydrite	-0.94	-5.28	-4.34 CaSO4
Annite	-2.03	-88.45	-86.43 KFe3AlSi3O10(OH)2
Anorthite	-9.39	-29.25	-19.86 CaAl2Si2O8
Aragonite	-0.21	-8.51	-8.31 CaCO3

Phase	SI Log	IAP Log	KT
Basaluminite	-10.11	12.59	22.70 Al <sub>4</sub> (OH) <sub>10</sub> SO <sub>4</sub>
Boehmite	-1.75	7.19	8.94 AlOOH
Calcite	-0.06	-8.51	-8.45 CaCO <sub>3</sub>
CH <sub>4</sub> (g)	-10.23	-13.05	-2.82 CH <sub>4</sub>
Chalcedony	-0.44	-4.06	-3.61 SiO <sub>2</sub>
CO <sub>2</sub> (g)	-1.23	-2.63	-1.41 CO <sub>2</sub>
Cristobalite	-0.40	-4.06	-3.66 SiO <sub>2</sub>
Diaspore	0.00	7.19	7.19 AlOOH
Fe(OH) <sub>3</sub> (a)	-6.70	-1.81	4.89 Fe(OH) <sub>3</sub>
Fe <sub>3</sub> (OH) <sub>8</sub>	-16.95	3.27	20.22 Fe <sub>3</sub> (OH) <sub>8</sub>
FeS(ppt)	-6.38	-10.30	-3.92 FeS
Fix_H+	-6.80	-6.80	0.00 H <sup>+</sup>
Gibbsite	-1.21	7.19	8.40 Al(OH) <sub>3</sub>
Goethite	-0.99	-1.81	-0.82 FeOOH
Greenalite	-8.24	12.57	20.81 Fe <sub>3</sub> Si <sub>2</sub> O <sub>5</sub> (OH) <sub>4</sub>
Greigite	-20.47	-65.50	-45.04 Fe <sub>3</sub> S <sub>4</sub>
Gypsum	-0.70	-5.28	-4.58 CaSO <sub>4</sub> :2H <sub>2</sub> O
H <sub>2</sub> (g)	-8.87	-12.00	-3.13 H <sub>2</sub>
H <sub>2</sub> O(g)	-1.64	0.00	1.64 H <sub>2</sub> O
H <sub>2</sub> S(g)	-9.24	-10.18	-0.94 H <sub>2</sub> S
Halloysite	-6.73	6.26	13.00 Al <sub>2</sub> Si <sub>2</sub> O <sub>5</sub> (OH) <sub>4</sub>
HCO <sub>3</sub> <sup>-</sup>	-6.80	3.58	10.37 H <sup>+</sup>
Hematite	0.00	-3.62	-3.62 Fe <sub>2</sub> O <sub>3</sub>
Jarosite(ss)	-24.97	-34.80	-9.83 (K <sub>0.77</sub> Na <sub>0.03</sub> H <sub>0.2</sub> )Fe <sub>3</sub> (SO <sub>4</sub> ) <sub>2</sub> (OH) <sub>6</sub>
Jarosite-K	-24.88	-33.70	-8.82 KFe <sub>3</sub> (SO <sub>4</sub> ) <sub>2</sub> (OH) <sub>6</sub>
Jarosite-Na	-38.45	-43.28	-4.83 NaFe <sub>3</sub> (SO <sub>4</sub> ) <sub>2</sub> (OH) <sub>6</sub>
JarositeH	-33.05	-37.75	-4.70 (H <sub>3</sub> O)Fe <sub>3</sub> (SO <sub>4</sub> ) <sub>2</sub> (OH) <sub>6</sub>
Jurbanite	-5.74	-8.97	-3.23 AlOHSO <sub>4</sub>
K-feldspar	-3.17	-24.12	-20.96 KAISi <sub>3</sub> O <sub>8</sub>
Kaolinite	-1.61	6.26	7.88 Al <sub>2</sub> Si <sub>2</sub> O <sub>5</sub> (OH) <sub>4</sub>
Kmica	0.00	13.45	13.45 KAl <sub>3</sub> Si <sub>3</sub> O <sub>10</sub> (OH) <sub>2</sub>
Laumontite	-5.90	-37.36	-31.46 CaAl <sub>2</sub> Si <sub>4</sub> O <sub>12</sub> :4H <sub>2</sub> O
Leonhardite	-3.84	-74.72	-70.88 Ca <sub>2</sub> Al <sub>4</sub> Si <sub>8</sub> O <sub>24</sub> :7H <sub>2</sub> O
Mackinawite	-5.65	-10.30	-4.65 FeS
Magadiite	-19.62	-33.92	-14.30 NaSi <sub>7</sub> O <sub>13</sub> (OH) <sub>3</sub> :3H <sub>2</sub> O
Maghemite	-10.01	-3.62	6.39 Fe <sub>2</sub> O <sub>3</sub>
Magnetite	-1.10	3.27	4.37 Fe <sub>3</sub> O <sub>4</sub>
Melanterite	-6.99	-9.26	-2.27 FeSO <sub>4</sub> :7H <sub>2</sub> O
Mirabilite	-25.86	-27.21	-1.35 Na <sub>2</sub> SO <sub>4</sub> :10H <sub>2</sub> O
Montmorillonite-Ca	-4.63	-50.39	-45.76 Ca <sub>0.165</sub> Al <sub>2.33</sub> Si <sub>3.67</sub> O <sub>10</sub> (OH) <sub>2</sub>
Nahcolite	-13.95	-14.54	-0.59 NaHCO <sub>3</sub>
Natron	-28.94	-30.45	-1.51 Na <sub>2</sub> CO <sub>3</sub> :10H <sub>2</sub> O
O <sub>2</sub> (g)	-67.17	-70.02	-2.85 O <sub>2</sub>
Phillipsite	-9.04	-28.91	-19.87 Na <sub>0.5</sub> K <sub>0.5</sub> AlSi <sub>3</sub> O <sub>8</sub> :H <sub>2</sub> O
Plagioclase	0.00	0.00	0.00 Na <sub>0.62</sub> Ca <sub>0.38</sub> Al <sub>1.38</sub> Si <sub>2.62</sub> O <sub>8</sub>
Portlandite	-12.31	10.88	23.19 Ca(OH) <sub>2</sub>

Phase	SI Log	IAP Log	KT
Prehnite	-10.60	-22.43	-11.82 Ca <sub>2</sub> Al <sub>2</sub> Si <sub>3</sub> O <sub>10</sub> (OH) <sub>2</sub>
Pyrite	0.00	-18.62	-18.62 FeS <sub>2</sub>
Pyrophyllite	0.08	-48.24	-48.31 Al <sub>2</sub> Si <sub>4</sub> O <sub>10</sub> (OH) <sub>2</sub>
Quartz	0.00	-4.06	-4.06 SiO <sub>2</sub>
Siderite	-1.64	-12.50	-10.86 FeCO <sub>3</sub>
Siderite(d)(3)	-2.05	-12.50	-10.45 FeCO <sub>3</sub>
Silicagel	-0.98	-4.06	-3.07 SiO <sub>2</sub>
SiO <sub>2</sub> (a)	-1.30	-4.06	-2.75 SiO <sub>2</sub>
Sulfur	-6.27	-21.39	-15.12 S
Thenardite	-27.04	-27.21	-0.17 Na <sub>2</sub> SO <sub>4</sub>
Thermonatrite	-30.61	-30.45	0.16 Na <sub>2</sub> CO <sub>3</sub> :H <sub>2</sub> O
Trona	-44.42	-44.99	-0.57 NaHCO <sub>3</sub> :Na <sub>2</sub> CO <sub>3</sub> :2H <sub>2</sub> O
Wairakite	-10.32	-37.36	-27.03 CaAl <sub>2</sub> Si <sub>4</sub> O <sub>12</sub> :2H <sub>2</sub> O